UNIVERSITY OF Southampton

University of Southampton Research Repository
ePrints Soton

Copyright © and Moral Rights for this thesis are retained by the author and/or other copyright owners. A copy can be downloaded for personal non-commercial research or study, without prior permission or charge. This thesis cannot be reproduced or quoted extensively from without first obtaining permission in writing from the copyright holder/s. The content must not be changed in any way or sold commercially in any format or medium without the formal permission of the copyright holders.

When referring to this work, full bibliographic details including the author, title, awarding institution and date of the thesis must be given e.g.

AUTHOR (year of submission) "Full thesis title", University of Southampton, name of the University School or Department, PhD Thesis, pagination

http://eprints.soton.ac.uk

UNIVERSITY OF SOUTHAMPTON

FACULTY OF ENGINEERING, SCIENCE & MATHEMATICS

OPTOELECTRONICS RESEARCH CENTRE

ADVANCED HIGH-POWER PULSED FIBRE LASER SYSTEMS AND THEIR APPLICATIONS

by

Pascal Dupriez

Thesis submitted for the degree of Doctor of Philosophy

June 2007

University of Southampton

ABSTRACT

FACULTY OF ENGINEERING AND APPLIED SCIENCE
OPTOELECTRONICS RESEARCH CENTRE

Doctor of Philosophy

ADVANCED HIGH-POWER PULSED FIBRE LASER SYSTEMS AND THEIR APPLICATIONS

by Pascal Dupriez

In this thesis, I report experimental studies towards power scaling of ultrashort fibre-based sources designed for applications including high average power femtosecond pulse generation and nonlinear frequency conversion. While the power produced by rare-earth doped fibre lasers operating in continuous-wave has dramatically increased within a few years to exceed the kilowatt level, pulsed fibre sources have been limited to tens of watts due to the onset of nonlinearities in fibre amplifiers. Therefore the aim is to manage fibre nonlinearities to achieve specific output properties at high average power. An innovative aspect of this work lies in the remarkable combination of telecom-grade semiconductor laser sources and high-power Yb-doped fibre amplifier technologies to produce short pulses at very high average power.

Direct amplification of ultrashort pulses presents attractive properties including asymptotic evolution towards a parabolic pulse shape with a perfectly linear chirp. This thesis describes nonlinear fibre amplification of pulses of different duration produced by passively mode-locked VECSELs operating at a repetition rate of approximately 1 GHz. A first fibre MOPA seeded by 4.6 ps led to a SPM-dominated regime of amplification up to 200 W with subsequent pulse compression down to a duration of 430 fs. The development of another fibre MOPA, seeded by pulses with a duration of 0.5 ps allowed generation of parabolic pulses. This resulted in high quality pulse compression down to a pulse width of 170 fs at an average power of 53 W. These results represented the highest power demonstrated by a fibre source producing femtosecond range pulse width.

Further power scaling was demonstrated by amplifying longer 16-20 ps pulses produced by a laser diode gain-switched at 1 GHz and emitting at 1060 nm. This experimental study aims at increasing the average power while maintaining high beam quality and minimizing SPM induced spectral broadening. I demonstrated fibre sources generating 125 W in a diffraction limited output beam and 321 W with slightly multimode output beam. In both cases the output linewidth was maintained below the acceptance bandwidth of conventional nonlinear crystals for applications such as harmonic generation. The latest demonstration represents the highest power achieved by a pulsed fibre based source.

Efficient frequency conversion imposes additional requirements on the design of a high-power fibre MOPA. Consequently an improved fibre source including a selectable repetition rate provided by the gain-switched laser diode was realised. As a result 175 W of average power was produced in a linearly polarised, diffraction limited output beam with a narrow linewidth. This source was then employed to generate 80 W of average power in the green via single-pass frequency-doubling corresponding to nearly 50% conversion efficiency. This is the highest power produced by a frequency-doubled fibre-based source.

Fibre nonlinear effects are often detrimental to the performance of fibre systems but can also provide an attractive tool to generate new useful wavelengths. The final part of this thesis describes efficient white light generation produced by a microstructure fibre pumped by the previously described green fibre source. Furthermore, I investigated a novel fibre source configuration for guide star application. The source I developed produced 1 W at 589 nm through frequency doubling of 1178 nm radiation produced by pulsed Raman amplification in an Yb-doped fibre amplifier.

Acknowledgements

First of all, I would like to thank my supervisor Professor Johan Nilsson for his support, encouragement and patience, and Dr Yoonchan Jeong for the useful discussions we had and for sharing his remarkable skills and experience in high-power fibre lasers.

I am also very grateful to Professor David Richardson who, despite his busy schedule, was always available to provide constructive feedback and inspiration. Moreover, I would like to thank Dr Jayanta Sahu for the stimulating discussions and for fabricating most of ytterbium doped fibres used in this work. My expression of gratitude also goes to my co-workers in the high-power fibre laser group: Christophe Codemard, Daniel Soh, Carl Farrel and Dr Valery Philipov.

In addition, I would like to thank Dr Andrew Malinowski and Andy Piper for developing the gain-switched laser diode systems and for sharing their equipment with me. As far as the equipment was concerned, I am also thankful to Dr Morten Ibsen for making fibre-Bragg gratings used for various experiments and Professor Anne Tropper for making available the VECSELs. Through this collaboration, I acknowledge the contribution of Hannah Forman who developed VECSELs and helped making numerous measurements on the high-power systems, and Keith Wilcox who realised the femtosecond VECSEL. I would like to thank Dr Christophe Finot for useful discussions on ultrashort pulses and other interesting topics. I also thank Francesco Poletti and Dr Peter Horak for numerical modelling and their valuable feedback that led to the interpretation of the RGB generation observed at the output of microstructured fibres. Furthermore, I thank Marco Petrovich who fabricated the photonic bandgap fibres.

Eve Smith has made my life easier at the ORC, providing outstanding administrative support from the time before joining the ORC to the end of the PhD.

I also thank Dr Philippe de Sandro, from Coractive for supplying high-quality commercial large core ytterbium doped fibres and Dr John Clowes, from Fianium Ltd. who managed to find some time to proof-read this thesis.

Finally, special thanks go to Aline, who was understanding and a very good support during the challenging final days of the PhD.

List of Contents

List of Figures

List of Abbreviations

ASE	Amplified Spontaneous Emission
CFBG	Chirped Fibre Bragg Grating
CPA	Chirped Pulse Amplification
CRFL	Cascaded Raman Fibre Laser
CW	Continuous-Wave
DCF	Double-Clad Fibre
DFB	Distributed Feedback
DPSS	Diode Pumped Solid-State
EDFA	Erbium Doped Fibre Amplifier
FBG	Fibre Bragg Grating
FEM	Finite Element Method
FM	Fundamental Mode
FP	Fabry-Pérot
FWHM	Full Width Half Maximum
FWM	Four-Wave Mixing
HOM	Higher Order Mode
LBO	Lithium Triborate
LMA	Large Mode Area
MCVD	Modified Chemical Vapour Deposition
ML	Mode-Locked
MOPA	Master Oscillator - Power Amplifier
NA	Numerical Aperture
NLSE	Nonlinear Schrödinger Equation
OPO	Optical Parametric Oscillator
ORC	Optoelectronics Research Centre
PBGF	Photonic Bandgap Fibre
PM	Polarisation Maintaining
PPKTP	Periodically Poled KTP
RE	Rare-Earth
RGB	Red Green Blue
SESAM	Semiconductor Saturable Absorber Mirror
SHG	Second-Harmonic Generation
SMSR	Side Mode Suppression Ratio
SPM	Self-Phase Modulation

SRS	Stimulated Raman Scattering
SS	Self-Similar
TBP	Time-Bandwidth Product
TFB	Tapered Fibre Bundle
TOD	Third Order Dispersion
UV	Ultra-Violet
VECSEL	Vertical-External-Cavity Surface-Emitting Semiconductor Laser
XPM	Cross-Phase Modulation
YDF	Ytterbium Doped Fibre
YDFA	Ytterbium Doped Fibre Amplifier
YDFL	Ytterbium Doped Fibre Laser

DECLARATION OF AUTHORSHIP

I, **Pascal Dupriez** , declare that the thesis entitled *Advanced High-Power Pulsed Fibre Laser Systems and Their Applications* and the work presented in the thesis are both my own, and have been generated by me as the result of my own original research. I confirm that:

- this work was done wholly or mainly while in candidature for a research degree at this University;
- where any part of this thesis has previously been submitted for a degree or any other qualification at this University or any other institution, this has been clearly stated;
- where I have consulted the published work of others, this is always clearly attributed;
- where I have quoted from the work of others, the source is always given. With the exception of such quotations, this thesis is entirely my own work;
- I have acknowledged all main sources of help;
- where the thesis is based on work done by myself jointly with others, I have made clear exactly what was done by others and what I have contributed myself;
- parts of this work have been published (see list of publications);

Signed: .....

Date: .....28/06/2007.....

Chapter 1 Introduction

Advances towards practical high-power ultrafast fibre-based sources and their power scaling are reported in this thesis. The aim of this research is to apply attractive features of such sources such as high brightness and high peak power for frequency conversion in fibres and nonlinear crystals.

1.1 Motivations

High-power laser systems capable of producing ultrashort pulses find use in a wide variety of scientific and industrial applications such as harmonic generation, pumping of OPOs, laser displays, laser marking and micromachining. Over many years of development aiming for high-power, high-brightness and high efficiency, conventional ultrafast solid-state lasers have established themselves as the sources of choice for these applications. However their common rod geometry suffers from thermo-optical problems at high-power preventing simple power scaling with high beam quality. Special geometries of the gain media have been introduced to overcome this limitation such as thin-disc [1] and fibre configurations. Despite excellent thermal properties and similarly to traditional lasers, thin-disc based systems are very complex incorporating a large number of optical components arranged in free-space. Opposite to bulk lasers, rare-earth doped fibre lasers involve mainly fibre components and have strong potential for compactness and robustness. For this reason, the development of high-power ultrafast fibre based sources is of great research interest.

An additional key aspect of RE doped fibres is the high beam quality inherent to the tight beam confinement in the thin gain medium. The introduction of cladding-pumped technology combined with the rapid progress in high brightness pump laser diodes have enabled a tremendous increase in output power produced by fibre sources based on various RE dopants (i.e erbium, erbium/ytterbium, neodymium and thulium). This rate of progress was even more pronounced in the case of Yb-based fibre systems due to the outstanding properties of Yb-doped fibres. YDFs offer a very simple two level energy system and a low quantum defect making them highly efficient and resulting in reduced heat generation. While their broad

absorption spectrum implies higher flexibility in pump sources, their broad emission spectrum suits amplification of ultrashort optical pulses. The work presented in this thesis is mainly interested in cladding-pumped Yb-doped fibre technology applied to the amplification of picosecond and sub-picosecond pulses.

Although the long length and tight beam confinement make RE-doped fibres suitable for high-power amplification they dramatically reduce nonlinear thresholds. Therefore achieving high peak power associated with high-power ultrashort pulses and high beam quality constitutes a major challenge. Techniques such as chirped pulse amplification adopted from solid-state lasers were introduced to reduce peak power in the fibre amplifier and consequently minimize nonlinear effects. This method is well suited for achieving high-energy pulses but typically involves a complex optical arrangement. In practice direct amplification appears more practical for scaling average power because of its simplicity. This implies adequate management of nonlinearities in the fibre amplifier as a function of output specifications required for the application. Minimising these effects is often critical for applications such as nonlinear frequency conversion. Nevertheless nonlinearities can also be very attractive for the generation of high-power pulses and their subsequent compression. In fibre-based ultrafast systems, nonlinear effects can be controlled by adjusting, if possible, pulse parameters and fibre dimensions such as core size and fibre length. However most seed sources operate with fixed pulse parameters and fibre dimensions not only define nonlinear threshold but also dictate the beam quality and efficiency of the system. These challenges are a key aspect of this thesis.

1.2 State of the art of high-power ultrashort fibre sources before this work

Prior to the work presented herein, the rapid technological developments in fibre laser technology have led to the experimental demonstration of kilowatt average power from a single fibre by Y. Jeong et al. at the ORC, University of Southampton in August 2003 [2]. However the average power produced by ultrafast fibre sources from direct amplification of picosecond pulses has been restricted to 50 W for ps pulses [3] and 17 W for compressed fs pulses [4]. Most fibre systems relied on amplification of a solid-state mode-locked laser with limited pulse parameters. Power increase was therefore mostly determined by the ability of the YDF to reduce nonlinearities and these results were enabled by the emergence of fibres with larger highly doped cores with reduced fibre length. Alternatively some fibre-based

systems have been designed to provide selectable pulse parameters for applications such as frequency doubling to the green but with output powers not exceeding 10 W [5]. Whereas bulk solid state systems may perform better in different operating regimes, they are less attractive than fibre-based systems for reasons of efficiency, reliability, and compactness.

1.3 Thesis synopsis

In this thesis, ultrafast fibre sources are power scaled to very high average power by mitigating fibre nonlinearities not only by adequate choice of fibre characteristics but also by employing high-speed semiconductor lasers as seed sources for the systems. Indeed these seed lasers offer higher repetition rates than conventional seed sources, meaning that after amplification, average power can be scaled accordingly before the onset of nonlinearities. A key attraction of one of the seed sources resides in the selectable repetition rate which constitutes an ideal tool for controlling levels of nonlinear effects in the fibre amplifier. The unique combination of well controlled ultrafast semiconductor lasers and well designed high-power YDFAs led to the realisation of picosecond and femtosecond sources with average powers exceeding the hundred watts levels. Owing to the high degree of control of the pulse parameters provided by the system, optimal frequency conversion efficiency could be achieved leading to the development of a high-power picosecond green laser. This source was then utilised to pump a highly nonlinear fibre for efficient generation of white light. In addition, the versatility of the Yb based fibre source allowed investigation on the development of a laser guide star system based on picosecond pulses. In this case, the source was designed to pump a signal via stimulated Raman scattering and subsequently frequency-doubling resulted in pulsed laser radiation at 589 nm. These experimental realisations represent the core of this PhD thesis whose organisation is presented in the following.

Beginning with a brief description of RE doped fibre technology and its revolutionary capabilities, Chapter 2 reviews some of the basic theories useful to understand amplification in fibre amplifiers. This chapter also describes the various nonlinearities encountered by short pulses propagating in an optical fibre. Chapter 3 presents an experimental study on direct fibre amplification of a passively mode-locked optically-pumped VECSEL with GHz repetition rate through a chain of amplifiers. The aim of this chapter is the production of clean femtosecond pulses with very high average power after nonlinear fibre amplification. Chapter 4 describes fibre amplification of longer picosecond pulses produced by a gain-switched laser diode with selectable repetition rate. These longer pulses allow for further power scaling and nonlinear effects are analysed for various Yb-doped fibre amplifiers. Chapter 5 introduces

design considerations for efficient frequency-doubling of an ultrafast fibre source and presents application of the previously described source configuration for efficient high-power second-harmonic generation at 530 nm. This thesis is extended to Chapter 6 with demonstrations reporting on application of high-power picosecond fibre for exciting nonlinear effects in fibres for the generation of unconventional visible wavelengths. In the first part of Chapter 6, the high-power green source is a pump source to investigate white light generation in secondary cores of a microstructured fibre. In the second part, generation of radiation at 589 nm is investigated in a system based on the combination of Raman fibre amplification pumped by intense picosecond pulses and frequency-doubling in a nonlinear crystal. Finally, conclusions and future work are discussed in Chapter 7.

References

1. A. Giesen, H. Hugel, A. Voss, K. Wittig, U. Braucli and H. Opower, "Scalable concept for diode-pumped high power solid-state lasers," Appl. Phys. B **58** 365–372 (1994).
2. Y. Jeong, J. K. Sahu, D. N. Payne, and J. Nilsson, "Ytterbium-doped large-core fibre laser with 1 kW of continuous-wave output power," Electron. Lett. 40, 470-471 (2004).
3. J. Limpert, A. Liem, T. Gabler, H. Zellmer, A. Tünnermann, S. Unger, S. Jetschke, and H. -R. Müller, "High-average-power picosecond Yb-doped fiber amplifier," Opt. Lett. **26**, 1849-1851 (2001).
4. J. Limpert, T. Schreiber, T. Clausnitzer, K. Zöllner, H. Fuchs, E. Kley, H. Zellmer, and A. Tünnermann, "High-power femtosecond Yb-doped fiber amplifier," Opt. Express **10**, 628-638 (2002).
5. S. V. Popov, S. V. Chernikov, J. R. Taylor, "6-W Average power green light generation using seeded high power ytterbium fibre amplifier and periodically poled KTP," Opt. Comm. **174**, 231 (2000).

Chapter 2 Pulse propagation in high-power fibre amplifiers

The work presented in this thesis is dominated by Yb-doped fibres used for amplification of short pulses. Therefore in section 2.1, the main properties of ytterbium ions incorporated in a silica fibre and the technology involved in the development of high-power fibre lasers and amplifiers will be described. Afterwards the background required to understand amplification of a signal in a doped fibre will be reviewed. Various limiting factors arising in fibre systems associated with the constant increase of average power are also briefly described. Finally, section 2.2 presents the basics to pulse propagation in optical fibres including brief descriptions of dispersion and nonlinear effects which are typical of such a regime.

2.1 Ytterbium doped fibre lasers and amplifiers

2.1.1 Introduction

The first rare-earth doped fibre laser was demonstrated in the 1960's when C. J. Koester and E. Snitzer realised a flash-lamp pumped neodymium doped fibre laser [1, 2]. With the development of semiconductor pump lasers and the demonstration of low-loss RE-doped silica fibre fabricated with the now widely available MCVD process in 1985 [3], fibre lasers have become potential replacements for conventional "bulk" solid-state lasers in many applications.

Indeed glass fibre lasers offer many advantages over their crystal counterparts. Since fibres are flexible, compact and robust devices can be produced. The output beam quality is predominantly determined by the waveguide properties of the rare-earth doped core, which can be designed to emit a diffraction limited beam suitable for many applications. Furthermore the combination of low background loss and tight beam confinement make fibre-based devices highly efficient with very low lasing threshold and high slope efficiency. The excellent thermal management when operating at higher power adds to the benefits of fibre

lasers. Indeed the long length, small transverse dimension and large outer surface area of the active fibre allow more effective heat dissipation with lower heat-sinking requirements than with bulk lasers [4].

Another attractive feature of RE-doped fibre lasers is their high gain over the wide bandwidth that is characteristic for a glass host. Although the crystalline hosts benefits conventional bulk solid-state lasers in terms of thermo-mechanical properties and gain efficiency, they normally have narrow emission linewidths, limiting the range of operating wavelengths and hence their versatility. By contrast, the much broader emission linewidths make glass-based fibre lasers highly suitable for operation over a wide spectral range and hence for wavelength tunability, which opens up for a wider range of applications. While crystalline gain media other than RE-doped ones can have broader bandwidth, for example Ti-doped sapphire, these are difficult to combine with high gain and high-power operation because of their limited length (in bulk format). Furthermore their threshold is quite high, typically on the watt-scale, because of the relatively large pumped volume even for centimetre-long gain media.

For many years, intensive research in the expanding field of fibre lasers and amplifiers has led to the development of various types of fibre-based devices, including continuous-wave, narrow linewidth, Q-switched, and mode-locked fibre lasers. In addition, their operating wavelength ranges from the ultraviolet to the infrared spectrum. Fibre lasers and especially amplifiers have revolutionised optical telecommunications, expanding the transmission range and its bandwidth rapidly and seamlessly. They are attracting much interest in many other applications as well, such as industrial (e.g. material processing), aerospace (e.g. Lidar), military defence (e.g. range finding) and medicine.

2.1.2 Ytterbium doped fibre technology for high-power

The revolutionary capabilities of fibre-based sources have only become apparent with the tremendous and rapid technological developments of recent years. These include the development of pump laser diodes with increased brightness, the realization of new efficient RE-doped fibres, and the development of new pumping techniques and high-power components.

High-power fibre lasers

The rapid technological developments have not only increased the output power over recent years but have also enabled the development of fibre lasers with various configurations and

various operating conditions. For instance the most basic fibre laser is composed of a piece of RE-doped fibre pumped by laser diodes where the cavity consists of a flat cleave and an external reflector as shown in Fig. 2.1. This type of laser configuration is designed for CW operation and is capable of producing several kW of output power. The same type of fibre laser can be either Q-switched or mode-locked by inserting a modulator in the cavity. An all-fibre format is also possible thanks to the development of high-power fibre pigtailed components such as modulators, isolators, fibre Bragg gratings and pump combiners.

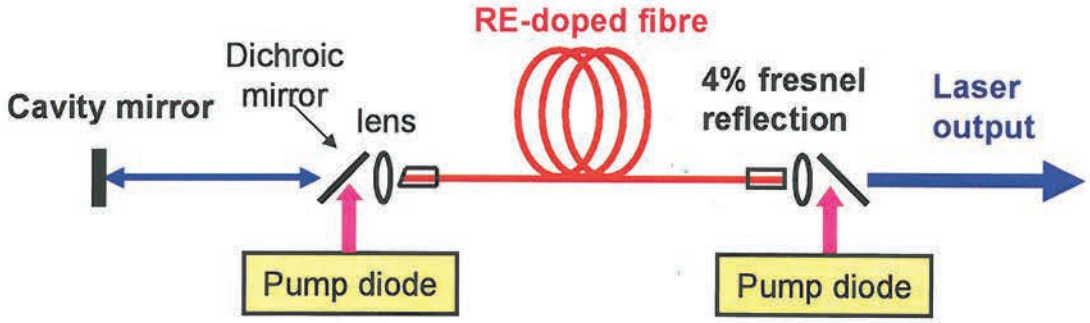

Fig. 2.1. Basic configuration of a diode-pumped fibre laser.

A key attraction of rare-earth doped fibres is the very high gain they can reach. Combined with their other attractive features, the high gain allows high-power fibre amplifiers to be used in MOPA configuration in which a low-power seed can be amplified by a cascade of fibre amplifiers to a suitable high power level as depicted in Fig. 2.2. In contrast to high-power laser systems, advanced telecom-grade low-power fibre components can be used to precisely customize the seed characteristics. The high-gain amplifier cascade can then boost the signal to very high powers, with high fidelity to the characteristics of the seed. This high degree of control makes fibre MOPAs very attractive for the realization of high-power single-frequency or pulsed sources with precise specifications.

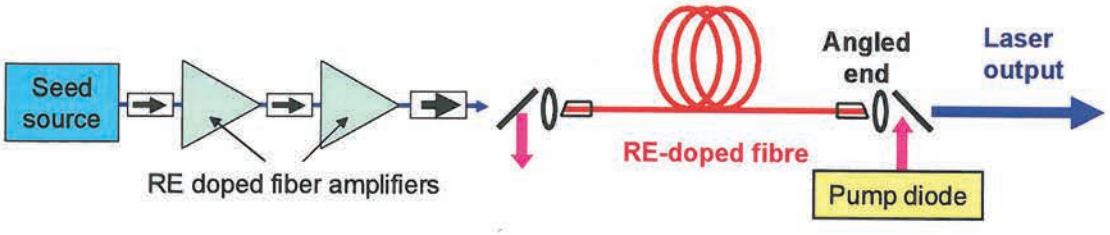

Fig. 2.2. Schematic representation of a fibre MOPA configuration including a seed source whose signal power is highly increased after propagation through 3 stages of amplification

The work presented here is based on Yb doped fibre MOPA sources seeded by low-power pulsed semiconductor lasers. A MOPA is often designed to reduce distortions and maintain the optical properties of the seed up to very high power. However in some cases such as ultrashort pulse generation, fibre amplifiers can be designed to induce nonlinearities to achieve temporal compression and hence improve the seed optical characteristics as will be described in Chapter 3.

Properties of ytterbium ion in a glass host

The first realisation of an EDFA in 1985 by D. N. Payne and his group [3] at the University of Southampton has triggered rapid technological progress to satisfy the main application in the field of optical communications. Through these developments, it also appeared that EDFAs were highly suitable to amplify short pulses to produce high peak power. This regime then becomes useful for other applications where power considerations prevail over wavelength of operation. Therefore other rare-earth dopants emitting at other wavelengths could be considered as candidate for the development of high-power fibre amplifiers. Indeed optical fibres can be doped by various rare-earth dopants including erbium, ytterbium, thulium and neodymium but only few candidates can meet the requirements for high-power operations.

Nd^{3+} ions initially attracted great interest due to their advantageous four-level transitions. Nevertheless this interest rapidly shifted towards Yb^{3+} ions due to several attractive features. Thus, the work presented here concentrates exclusively on ytterbium ions due to their outstanding properties for high-power operation in a fibre format. They are highly compatible with a silica host, an ideal material for fibre production. The spectroscopic properties of Yb^{3+} ions are very simple compared to other rare-earth ions. Their energy level structure consists of two manifolds; the ground manifold $^2F_{7/2}$ with four Stark levels labelled (d)-(g) in Fig. 2.3(a) and the excited manifold $^2F_{5/2}$ with three Stark levels labelled (a)-(c). This configuration prevents any excited state absorption for the pump and signal wavelengths. Furthermore since other levels of excited state configurations are in the ultraviolet, multiphoton relaxation and concentration quenching are not present. Thus high doping levels are possible for achieving high-gain in a very short length, and in particular absorption levels required for high power cladding-pumped operation.

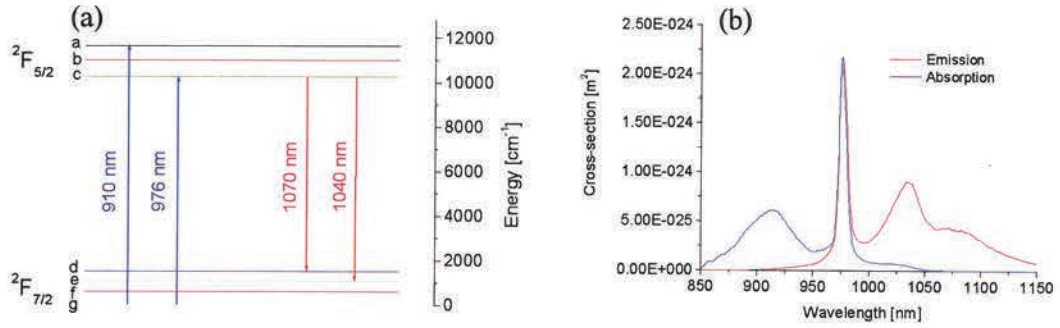

Fig. 2.3. (a) Energy level structure of Yb^{3+} ions in silica. (b) Absorption and emission cross-section of Yb^{3+} ions in an aluminosilicate glass.

Fig. 2.3(b) shows the absorption and emission cross-sections of Yb in an aluminosilicate glass, commonly used host for high-power RE doped fibres. The absorption and emission spectra vary slightly with the host glass composition. Due to strong absorption bands around 976 nm and 910 nm, Yb-doped systems can be pumped by commercially available telecom-grade high-power laser diodes. This proximity between the pump and signal wavelengths results in a low quantum defects, lower than for neodymium-based systems. This quantum defect can reach 8% for a signal wavelength of 1060 nm when pumped at 975 nm and slope efficiencies of 80% are commonly demonstrated. In addition the cross-sections indicate that amplification is possible over a wide spectral range from 975 nm up to 1120 nm at room temperature. This broad gain bandwidth is also of great interest for short pulse amplification. The excited-state lifetime of ytterbium ions in a glass host is approximately 0.8 ms which is sufficiently long for efficient laser operation.

Basic properties of optical fibres

A standard optical fibre is composed of a core with a high refractive index surrounded by a cladding with a lower refractive index. The light is guided in the core by total internal reflection and the difference in refractive index between core and cladding determines how tightly the optical beam is confined in the core. The core is characterized by a refractive index n_{core} with a typical diameter of 5-10 μm, the cladding refractive index is n_{clad} with a typical diameter of 125 μm. A polymer with an outer diameter of 250 μm is used as a protective jacket. The refractive index difference defines the acceptance angle θ of the core also known as numerical aperture and defined by $NA = \sin(\theta) = \sqrt{n_{core}^2 - n_{clad}^2}$. Therefore the NA is an important parameter to be considered when choosing optics to maximize optical coupling in a waveguide structure. Higher coupling efficiency can be achieved by increasing either NA or the core diameter. However in this case the core may become multimode. Single-mode

propagation is ensured under the following restriction on the core radius a and the core NA [5]:

$$V = \frac{2\pi a NA}{\lambda} < 2.405 \qquad (2.1)$$

where V is the normalized frequency. These waveguide properties are key to understanding the behaviour of RE-doped fibres as described in the next section.

Rare-earth doped optical fibres

A RE-doped fibre maintains the properties of a conventional optical fibre but additionally provides the attractive feature of an active medium by incorporating rare-earth ions with various doping levels in the core. A typical RE doped fibre is presented in Fig. 2.4. In this configuration, pump and signal beams are tightly confined in the core and propagate along the fibre length. The unique combination of long interaction length with high beam overlap between signal and pump results in efficient energy transfer and high gain. In addition, excellent output beam quality is achieved as long as the core is maintained single-mode while the pump can be slightly multimode due to its shorter wavelength.

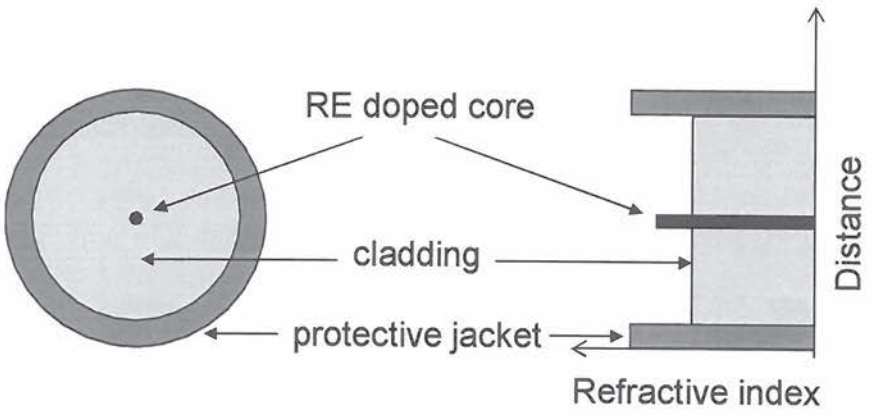

Fig. 2.4. Diagram of the cross-section of a core-pumped rare-earth doped fibre with its typical refractive index profile

A conventional Yb-doped fibre laser or amplifier with a single waveguide (core) within a single cladding is typically pumped by widely available single-mode fibre pigtailed laser diodes emitting at 920 or 977 nm, coupled with a WDM fibre coupler. However the laser output power is restricted to the amount of pump power that can be coupled to the doped core. This is rather modest in conventional core-pumped devices, in which the pump is launched directly into the core. The output power of commercial single-mode laser-diodes, suitable for

core-pumping, is limited to a few hundreds of milliwatts, and though diodes can be combined together, the output power from such fibre lasers is limited to the watt level.

To overcome this problem, J. Kafka at Spectra Physics suggested a breakthrough idea, the so called cladding pumping which can utilise multimode laser diodes [6]. In cladding pumping, the pump beam is launched not directly into the small core, but into the inner cladding of a double-clad fibre while the signal beam propagates in the doped core. The clear advantage of cladding pumping is that high-power single-mode laser beam can be produced from large and powerful multimode diode lasers.

Fig. 2.5 shows a schematic representation of a double-clad fibre. A double-clad fibre is normally a three-layer structure: a central core and two layers of surrounding cladding. The core is the primary waveguide for guiding the signal, surrounded by a lower refractive index inner cladding. The formed waveguide is made of glass. The inner cladding is surrounded by an outer cladding with a lower refractive index polymer or glass to form a new, secondary, or pump, waveguide where the pump beam is guided. The core is typically rare-earth doped, while the inner-cladding is undoped. Since the core is a part of the pump waveguide, the pump light will reach the core and excite the rare-earth ions there. The generated or amplified signal beam is then guided within the core. Depending on the type of applications as well as the output power level, the core of a DCF typically has a diameter of around 10 μm for strictly single-mode operation but larger cores are now widely used.

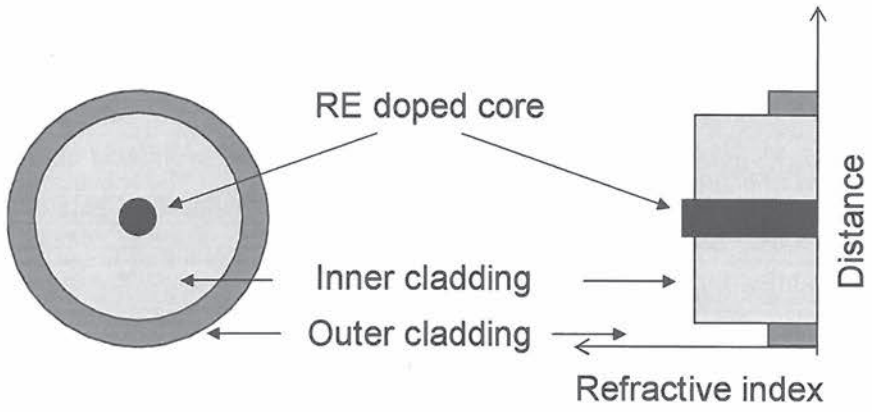

Fig. 2.5. Diagram of the cross-section of a cladding-pumped rare-earth doped fibre with its typical refractive index profile

Double-clad fibres provide an attractive solution for power scaling of high-brightness fibre lasers since the thick inner cladding allows the launch of pump-beams from powerful multimode diode sources while the core structure defines largely the output beam quality.

The inner cladding size and NA are primarily designed according to the type of diode pump sources which can be found commercially in the form of multimode single or multi-emitter including diode bars or stacks. Consequently a double-clad fibre essentially acts as a brightness converter where a low brightness high-power pump beam is gradually converted into a high-power high brightness signal beam through energy transfer in the double waveguide structure. This statement is illustrated in Fig. 2.6.

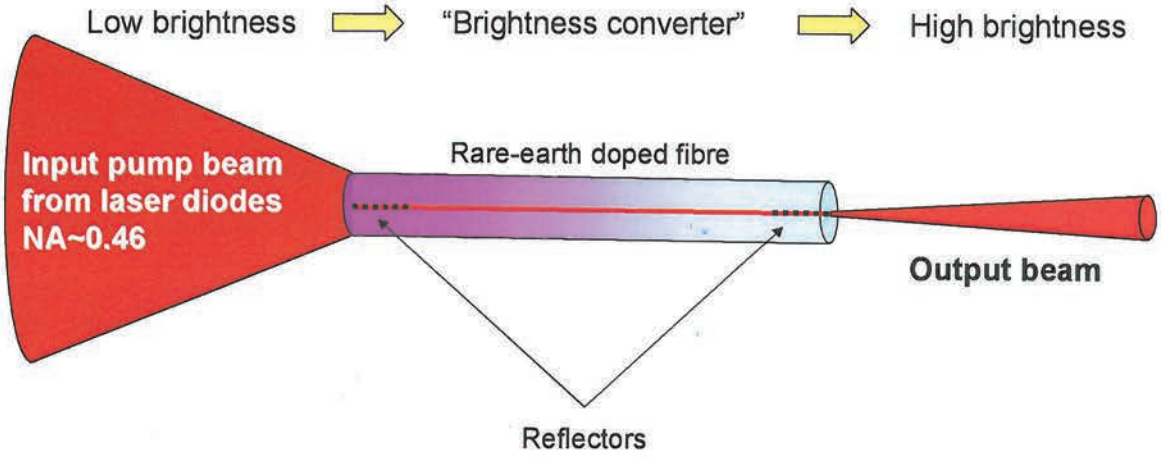

Fig. 2.6. Schematic representation of a cladding pumped fibre laser composed of an active fibre with reflectors. The concept of brightness enhancement is also illustrated by the conversion of a low brightness pump beam into a high brightness output beam.

The maximum power that can be achieved by a fibre-based source depends on the amount of pump power absorbed by the RE-doped core. In a double-clad fibre, the large undoped inner cladding to active core ratio results in lower pump absorption rate compared to single-clad fibre. Higher dopant concentration is therefore required to increase absorption and longer fibres often help to achieve optimal absorption. Consequently the design of an efficient high-power double-clad YDF relies firstly on increased pump coupling efficiency and secondly on the maximization of pump absorption by the doped core.

High pump coupling efficiency can be reached by employing a double-clad fibre with either a high NA or a large inner cladding diameter. The numerical aperture of the inner cladding depends on the refractive index of the material comprising the outer cladding. A solid fluorine doped silica outer cladding allows a relatively low NA of 0.28 compared to a low-index polymer based material with resulting NA of approximately 0.46. A convenient method to reduce the refractive index of the outer cladding consists in introducing air in its composition. This new development resulted in the emergence of jacketed air clad structures with NA exceeding 0.6.

Increasing the cladding dimension allows higher pump coupling efficiency but causes reduced pump absorption unless the core size is scaled accordingly. However a larger core often leads to multimode output beams with poor beam quality. For this reason, LMA fibres have been introduced to increase the active core area while reducing the numerical aperture in order to maintain single-mode operation [7]. Nevertheless conventional MCVD process limits the NA of Yb-doped fibres to 0.06 and alternative microstructured fibres have enabled a reduction of NA to less than 0.05 allowing the use of very large Yb-doped cores with area reaching 2000 μm^2 [8]. Combined with an air-clad structure these novel types of fibres offer an excellent solution for the realisation of devices with high pump coupling efficiency, high pump absorption and consequently high gain in a very short fibre length. This is of particular interest for pulsed applications.

The shape of the inner cladding is another important specification, since with some geometries, a poor overlap between the core and a large number of pump modes can be experienced. This is the case with a circular inner cladding where some pump modes, corresponding to skew rays (e.g. meridional and helical rays), never overlap with a centred doped core, thereby resulting in low pump absorption. This problem can be overcome by bending the DCF, which scrambles the pump mode [9, 10], by having an offset core, or by breaking the circular symmetry of the inner cladding (e.g. D-shape, hexagonal shape) as shown in fig. 2.7.

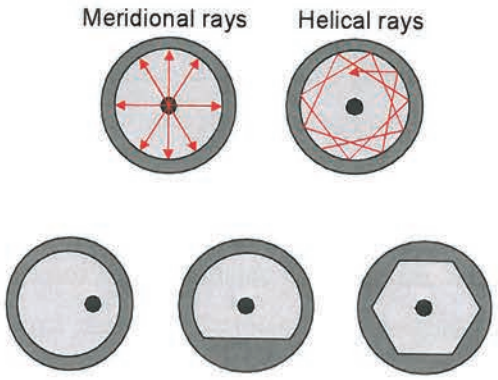

Fig. 2.7. Pump propagation in a circular shape inner cladding with meridional and helical rays leading to poor overlap with the doped core and alternative cladding shapes designed to break the circular symmetry for improved pump absorption.

Cladding pumping has changed the perspective of fibre lasers and amplifiers and did enable scaling of fibre laser output powers from a few watts to several hundreds of watts. Thanks to the development of improved cladding pumped Yb-doped fibres and brighter laser diodes,

fibre lasers are now capable of producing several kilowatts [11-13] with quasi- single-mode output and tens of kilowatts with multimode output [13].

Pumping configurations

Double-clad fibres were designed to take advantage of the high power produced by highly multimoded laser diodes. These diode pump sources are available in various formats with various beam characteristics. They include single emitters with a maximum output power of 10W coupled into a fibre with a core diameter of 105 μm and NA of 0.15, multi-emitters with tens of watts of output power compatible with optical fibres with cores of less than 200 μm in diameter and an NA of 0.22, and diode-stacks capable of producing kilowatts output powers. These three types of sources were used in this study and photos of each pump diode are presented in Fig. 2.8. High-power fibre amplifiers described in the next chapters were pumped using commercial diode stacks manufactured by Laserline and capable of producing up to 550 W around 975 nm.

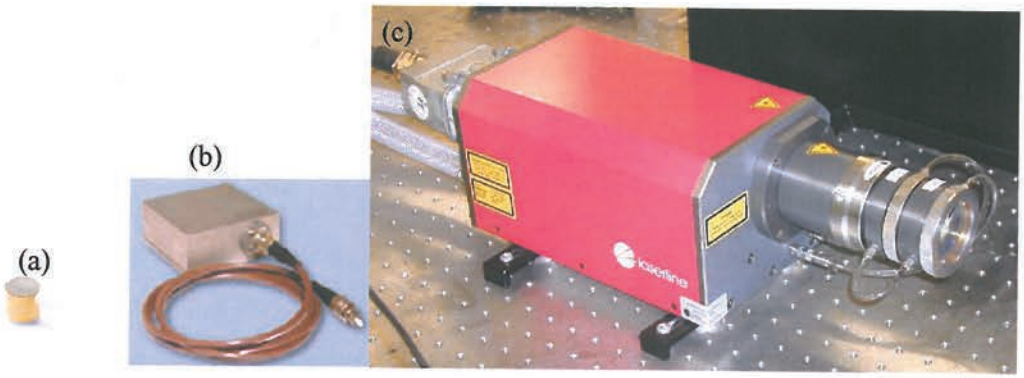

Fig. 2.8. Various types of pump laser diodes: (a) single emitter producing up to 10 W output power (manufactured by JDSU), (b) fibre-coupled multiple emitter (manufactured by Fianium) with up to 40W output power and (c) diode stacks (manufactured by Laserline) producing up to several kilowatts of output power.

To maximise coupling between the multimode pump beam and the double-clad fibre, the brightness of the pump source must be considered. The brightness of a source is defined as the power emitted by a source of area A in a solid angle $2\pi(1-\cos(\theta))$ and is expressed as:

$$B = \frac{P}{2\pi A(1-\cos(\theta))} \approx \frac{P}{\pi A(NA^2)} \qquad (2.2)$$

For optimal coupling, the brightness must be maintained, meaning that the brightness of the optical fibre where the power is launched can not exceed the brightness of the source itself. This is summarized by the following relation:

$$\pi A_s \sin^2(\theta) \leq \pi A_f NA^2 \tag{2.3}$$

where A_s and A_f are the source and fibre areas respectively. Coupling efficiency can be severely degraded if this condition is not respected.

Over recent years, several methods have been proposed to efficiently launch pump beams produced by high-power laser diodes into RE-doped double-clad fibres. Although many configurations have been investigated in laboratories, the techniques described in the following are used in commercial fibre-based devices.

Free-space end-pumping

Free-space end-pumping is the simplest way to pump a DCF and is very convenient for experimental work. This is the main reason why this technique is employed in this work. Its principle is presented in Fig. 2.9. The pump beam is injected directly into the inner cladding through the fibre end facet (e.g., cleaved) using a lens. This pumping scheme offers very good launch efficiency, as long as the focusing lens is adequately chosen to satisfy relation (2.3). This coupling technique allows relatively straightforward power scaling by increasing the inner cladding size to accommodate the very high power produced by low brightness pump diodes such as diode stacks. However with this scheme, the number of injection points is limited since the pump light can be launched only through two ends of the fibre. In addition, the fibre ends will not be accessible for splicing which is often a practical requirement. Furthermore, an all-fibre configuration is often preferred due to its potential for compactness and outstanding robustness. Therefore alternative pump coupling methods were developed to free the fibre ends and eliminate bulk optics.

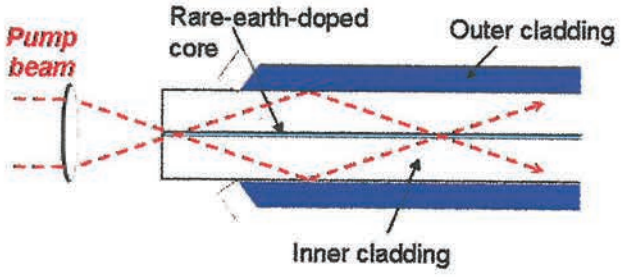

Fig. 2.9. Principle of free-space end-pumping of a RE-doped cladding-pumped fibre

Pumping by tapered fibre bunble

A first technique consists in multiplexing multiple emitters, typically single emitters, using several pump fibres combined to a double-clad fibre. This method relies on a device called TFB which is fabricated in a similar way as a fused fibre coupler by bundling multimode fibres to a double-clad fibre or another multimode fibre and fusing and tapering them together [14, 15]. A schematic representation of a TFB is shown in Fig. 2.10.

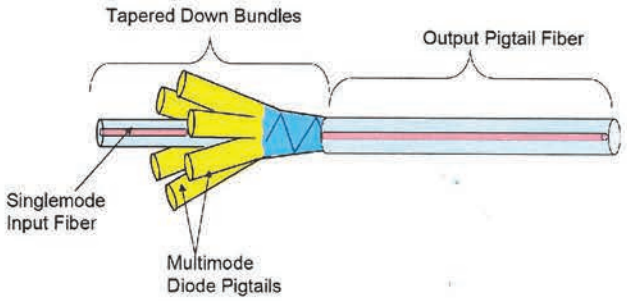

Fig. 2.10. Schematic of a tapered fibre bundle comprising several multimode pump fibres and one signal feed-through.

A TFB can be used as a basic pump combiner. Alternatively some devices offer a signal feed-through which can be spliced to either a seed signal (for amplification) or a FBG (for laser operation). In this case both fibre ends are available for splicing allowing for more advanced amplifier or laser designs. Another attraction of TFBs resides in the high level of integration since all the pump fibres can be spliced and power scaling is provided simply by splicing more diodes to the system. However in this case the maximum number of ports that can be coupled into a single fibre is governed by:

$$N \times (\Phi_S NA_S)^2 \leq (\Phi_{DCF} NA_{DCF})^2 \qquad (2.4)$$

where Φ_S, Φ_{DCF} and NA_S, NA_{DCF} are the respective diameters and numerical apertures for the pump source fibre and the double-clad fibre.

Pumping by side-spliced fibres

Another pumping technique is based on direct splicing of multimode pump fibres on the side of the double-clad fibre [16]. This method is schematically presented in Fig. 2.11. Despite the high control of the parameters (e.g. angle between fibres) required during fabrication, it offers high coupling efficiency.

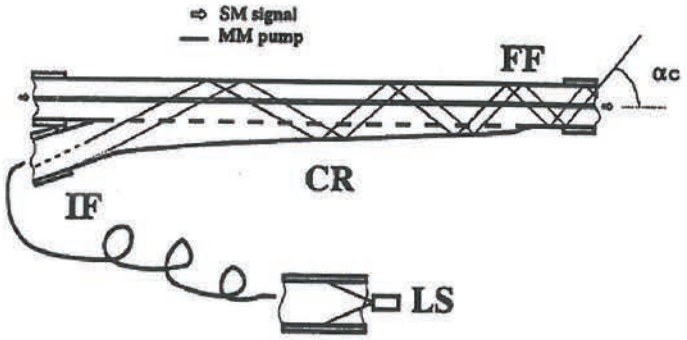

Fig. 2.11. Diagram representing a side-spliced pumping scheme. Light source (LS), RE doped optical fibre (FF) Pump multimode optical fibre (IF), and splicing area (CR). After [16].

V-groove Side-Pumping (VSP)

V-groove Side pumping was introduced and developed by D. J. Ripin and L. Goldberg [17]. This technique consists in coupling the pump power from the side of a DCF via internal reflection on a V-groove etched in the inner cladding as shown in Fig. 2.12. This technique is utilised in commercial products by Keopsys. Similarly to the previous method, the RE doped core is also directly accessible. However the coupler requires complicated fabrication and offers limited span for power scaling due to the high pump intensity involved in the relatively small and sensitive groove.

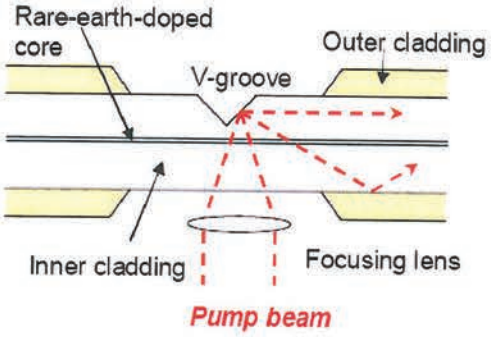

Fig. 2.12. Representation of V-groove side-pumping illustrating the reflection of a pump beam in the double-clad fibre via a V-groove.

GT-Wave pumping technology

GT-Wave has been invented and developed by A. B. Grudinin and P. W. Turner [18] from the ORC as an alternative pumping scheme to facilitate pump coupling in a simple configuration. This technology is schematically shown in Fig. 2.13. It is based on a bundle of typically three uncoated fibres, including a standard RE-doped DCF and two silica pump fibres surrounded by a low index polymer to create the index difference for waveguiding. GT-Wave is a unique pump coupling device where pump beams are gradually distributed between pump and signal

fibres along the device length differing from a TFB where pump beams are coupled into the active fibre at one end of the fibre. This novel waveguide structure offers excellent coupling between the fibre ports in a short distance. This technology is highly suitable for power scaling since the properties of a GT-Wave system after pump coupling does not differ much from a standard double-clad fibre, which is capable of kilowatts power levels. Furthermore, as opposed to the previously described technique pump coupling is achieved along the fibre length which allows for very high power handling. Some pre-amplifiers used in this thesis were based on this technology.

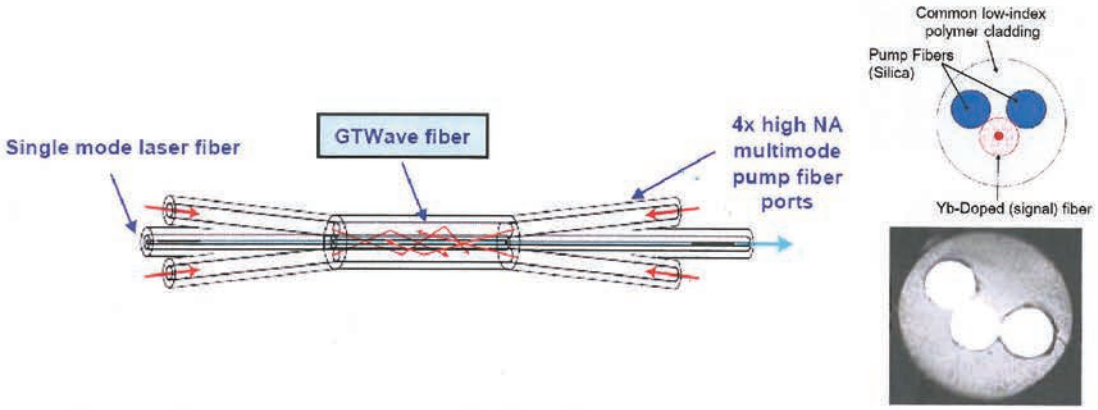

Fig. 2.13. Schematic representation of GT-Wave fibre pumping scheme with diagram and photo of a cross-section of the waveguide. Courtesy of SPI Laser.

2.1.3 Amplifications in Ytterbium doped fibres

The properties of ytterbium ions in a glass host, the waveguide structure in which ions are incorporated and methods to couple pump beams into the RE doped optical waveguide have been introduced. This section reviews the theory related to amplification in an Yb-doped cladding-pumped fibre. Modelling amplification in rare-earth doped fibres has been the topic of many papers and books [19-22] with the growing interest in EDFAs for telecom applications. Here I would like to summarize the basic properties of amplification in Yb-doped fibres based on well known fibre amplifier models. In this thesis, I am principally interested in amplification of signals in the 1040-1080nm wavelength range where the ytterbium system has a nearly four-level behaviour. Since the non radiative transitions are very fast, the four-level structure can be simplified into a two-level system with an upper level labelled 2 and a ground level labelled 1. As previously described, interactions between ions and excited state absorption can be neglected. Furthermore ASE is not considered here.

Population densities

Let N_i be the number of ions in the i^{th} level per unit volume. The total number of ions per cubic metre N_0 is expressed as:

$$N_0 = \rho = N_1 + N_2 \tag{2.5}$$

The rate equations of the population densities for the two-level system are derived as:

$$\begin{aligned} \frac{\partial N_1}{\partial t} &= -R_{12}N_1 + R_{21}N_2 - W_a N_1 + W_e N_2 + N_2/\tau \\ \frac{\partial N_2}{\partial t} &= R_{12}N_1 - R_{21}N_2 + W_a N_1 - W_e N_2 - N_2/\tau \end{aligned} \tag{2.6}$$

where τ is the fluorescence lifetime and the radiation rates are defined as [13]:

$$R_{12} = \frac{\sigma_p^a I_p}{h\nu_p},\ R_{21} = \frac{\sigma_p^e I_p}{h\nu_p},\ W_a = \frac{\sigma_s^a I_s}{h\nu_s},\ W_e = \frac{\sigma_s^e I_s}{h\nu_s}, \tag{2.7}$$

where I_s and I_p are the signal and pump intensities, and σ_p^a, σ_p^e, σ_s^e and σ_s^a are the effective pump absorption, pump emission, signal emission and signal absorption cross-sections, respectively. h is Planck's constant and ν_p and ν_s are the pump and signal optical frequencies. In Eq. 2-7, $R_{12}N_1$ represents the pump absorption, $W_a N_1$ the ground state absorption, $W_e N_2$ the stimulated emission, and N_2/τ the spontaneous emission, respectively.

Considering the steady state regime, (2.6) becomes

$$\begin{cases} N_1 = \rho \dfrac{1 + W_e\tau}{1 + (W_a + W_e)\tau + (R_{12} + R_{21})\tau}, \\ N_2 = \rho \dfrac{R_{12}\tau + W_e\tau}{1 + (W_a + W_e)\tau + (R_{12} + R_{21})\tau} = N_0 - N_1 \end{cases} \tag{2.8}$$

Substituting Eq. 2-7 into Eq. 2-8, we obtain:

$$\begin{cases} N_1 = \rho \dfrac{\dfrac{1}{\tau} + \dfrac{\sigma_s^e I_s}{h\nu_s}}{\dfrac{1}{\tau} + \dfrac{\sigma_s^a I_s}{h\nu_s} + \dfrac{\sigma_s^e I_s}{h\nu_s} + \dfrac{\sigma_p^a I_p}{h\nu_p} + \dfrac{\sigma_p^e I_p}{h\nu_p}}, \\ N_2 = \rho \dfrac{\dfrac{\sigma_p^a I_p}{h\nu_p} + \dfrac{\sigma_s^a I_s}{h\nu_s}}{\dfrac{1}{\tau} + \dfrac{\sigma_s^a I_s}{h\nu_s} + \dfrac{\sigma_s^e I_s}{h\nu_s} + \dfrac{\sigma_p^a I_p}{h\nu_p} + \dfrac{\sigma_p^e I_p}{h\nu_p}} \end{cases} \tag{2.9}$$

In the general case where k beams (including the pump beam) propagate in the doped fibre, the rate equation describing the temporal evolution of the metastable level can be expressed as:

$$\frac{\partial N_2}{\partial t} = \frac{\left(\sigma_p^a N_1 - \sigma_p^e N_2\right)}{h\nu_p} I_p + \sum_{m=1}^{k-1} \frac{\left(\sigma_m^a N_1 - \sigma_m^e N_2\right)}{h\nu_m} I_m - \frac{N_2}{\tau}, \tag{2.10}$$

The population densities in the steady-state regime considering the pump beam and k signal beams are:

$$N_2(r,\theta,z) = \rho(r,\theta,z) \frac{\dfrac{\sigma_p^a \tau}{h\nu_p} I_p(r,\theta,z) + \sum_{m=1}^{k-1} \dfrac{\sigma_m^a \tau}{h\nu_m} I_m(r,\theta,z)}{1 + \dfrac{\tau\left(\sigma_p^a + \sigma_p^e\right)}{h\nu_p} I_p(r,\theta,z) + \sum_{m=1}^{k-1} \dfrac{\tau\left(\sigma_m^a + \sigma_m^e\right)}{h\nu_m} I_m(r,\theta,z)}, \tag{2.11}$$

$$\rho(r,\theta,z) = N_1(r,\theta,z) + N_2(r,\theta,z) \tag{2.12}$$

If we consider that the signal propagates in a multimode doped fibre, the k different beams can represent the different modes supported by the optical waveguide. Since the intensities of the different beams are added, they are assumed to be incoherent.

Mode envelope

The intensities I_m expressed in Eq. 2.11 depend on the waveguiding properties of the active fibre. High-power Yb-doped fibre amplifiers can be multimode and it is often necessary to consider simultaneous amplification of various modes in the doped core where each mode is characterized by a specific intensity distribution. We define a normalized mode envelope $\bar{\phi}_j(r,\theta)$ for the mode j, so that:

$$\bar{\phi}_j(r,\theta)=\frac{\phi_j(r,\theta)}{\int_A \phi_j(r,\theta) r dr d\theta}, \tag{2.13}$$

where ϕ_j is the mode profile of mode j defined in Eq. 2-15.

Therefore the intensity distribution I_j is written as:

$$I_j(r,\theta)=P_j\bar{\phi}_j(r,\theta) \tag{2.14}$$

where P_j is the total power guided by the mode j.

In the weakly guided approximation [5], the mode profiles ϕ_j of a step-index fibre are given by the LP_{nm} power mode envelopes described by:

$$\phi_j(r,\theta)=\phi_{nm}(r,\theta)=\begin{cases} J_n^2\left(U_{mn}\dfrac{r}{a}\right)\cos^2(n\theta) & \text{for } r\le a \\ \dfrac{J_n^2(U_{mn})}{K_n^2(W_{mn})}K_n^2\left(W_{mn}\dfrac{r}{a}\right)\cos^2(n\theta) & \text{for } r>a \end{cases} \tag{2.15}$$

where J_m and K_m are Bessel functions, a is the fibre core radius and U_{mn} and W_{mn} are the eigenvalue parameters defined by the propagation constant β_{mn} of the mode LP_{nm}.

Pump and signal propagation equations

The rate equations previously introduced form a basis for modelling of many aspects including signal and pump power evolution in a double-clad Yb-doped fibre. The evolution of signal and pump power along the fibre propagation is described by the propagation equations as:

$$\begin{aligned} \frac{dP_s(z)}{dz} &= \left[\gamma_s^e(z)-\gamma_s^a(z)-\alpha_s\right]P_s(z), \\ \frac{dP_p(z)}{dz} &= \left[\gamma_p^e(z)-\gamma_p^a(z)-\alpha_p\right]P_p(z) \end{aligned} \tag{2.16}$$

$\gamma^e_{s,p}$, $\gamma^a_{s,p}$ correspond to the signal and pump emission and absorption coefficients expressed as:

$$\gamma^e_{s,p}(z) = \sigma^e_{s,p} \int_0^{2\pi} \int_0^{\infty} N_2(r,\theta,z) \overline{\phi}_{s,p}(r,\theta) r dr d\theta$$
$$\gamma^a_{s,p}(z) = \sigma^a_{s,p} \int_0^{2\pi} \int_0^{\infty} N_1(r,\theta,z) \overline{\phi}_{s,p}(r,\theta) r dr d\theta \quad (2.17)$$

2.1.4 Challenges of high-power fibre amplification

Output beam quality and enhancement techniques

Large multimode core fibre lasers are now widely used because of their potential for power scaling. However beam quality is often severely degraded by higher order modes accompanying the fundamental mode at the fibre output. The beam quality of a laser source determines how tightly the laser beam can be focused and how quickly the beam diverges. It is therefore a critical parameter for most applications. The beam quality is defined in practice by the beam quality factor M^2. The beam quality factor represents a scale of imperfection of the output beam. The minimum value of M^2 is 1 which corresponds to a perfect diffraction limited beam. An increase of M^2 relates to more multimoded output beam with degraded propagation characteristics. A theoretical Gaussian beam is characterized by the following beam waist– divergence product:

$$w_0 \theta_0 = \frac{\lambda}{\pi}. \quad (2.18)$$

A real beam is then defined by:

$$W_0 \Theta_0 = M^2 \frac{\lambda}{\pi}, \quad (2.19)$$

where W_0 and Θ_0 are the waist and divergence of the real beam.

Consequently, the real beam radius evolves longitudinally according to:

$$W(z) = W_0 \sqrt{1 + \left(\frac{zM^2 \lambda}{\pi W_0^2} \right)^2} \quad . \tag{2.20}$$

This expression is useful for beam quality characterisation. The measurement of $W(z)$ at the output of a laser source allows the calculation of the beam quality factor M^2.

A laser beam is considered of high quality or quasi-diffraction limited for $M^2 < 1.3$. The beam quality of a single mode fibre is approximately 1.1. In pulsed fibre lasers and amplifiers a large effective area is often preferred. This results in a degradation of the beam quality. The design of LMA fibres enables operation of fibre amplifiers with large core area and excellent beam quality. The recent development of Yb-doped microstructured fibres has enabled further increase of the core area while maintaining diffraction limited output. However these new fibres are bend sensitive due to the extremely low NA. Therefore in the following, I will describe several methods employed to enhance the beam quality of fibre sources based on conventional fibres.

In a multimode fibre amplifier, single-mode output can be provided by achieving adequate matching between the seed mode and the amplifier mode. This technique works quite well for large mode area fibres but high-power operation often results in amplification of higher order modes. Therefore it becomes critical to find a method to eliminate higher order modes or to avoid their amplification.

The beam quality of multimode fibre lasers and amplifiers can be enhanced using the following principle: higher order modes must undergo higher loss that can be either localised or distributed but this should not lead to significant attenuation of the fundamental mode. Relying on Marcuse's analysis of bend loss in optical fibres [23], Koplow et al. [24, 25] experimentally demonstrated a diffraction limited output from a multimode, large-core fibre amplifier by coiling the fibre, hence inducing high distributed loss to higher order modes while not affecting significantly the fundamental mode. The loss for each mode depends on the fibre bending radius which must be chosen so that bending induces high loss to higher order modes and negligible loss to the fundamental mode. This practical approach can significantly enhance the beam quality with a minimum power penalty but applies only for doped fibres with low NA (NA<0.08).

Utilising the mode filtering properties of a tapered optical fibre, Alvarez-Chavez et al. demonstrated improved beam quality with a fibre laser having a tapered section [26]. In this configuration, the tapered core section makes higher-order modes radiate outside the core

while still supporting the fundamental mode. The resulting power penalty can be satisfactory if the taper is well designed. However this technique requires very delicate fabrication of the tapered section.

Instead of imposing loss to higher order modes, other methods attempt to provide higher gain to the fundamental mode. Although this technique appears a priori promising as it does not involve any loss in the system, its realization is quite challenging as it requires a good understanding of modes propagation and mode competition in fibre amplifiers. Furthermore the modal discrimination is much smaller than it can be for bend loss, for example. Following this approach, some fibre amplifiers were developed with spatial distribution of the active ions to provide optimal gain to the fundamental mode while keeping the gains for any other modes to a significantly lower level [27].

Thermal effects

High-power fibre based devices have excellent thermal properties due to the unique heat dissipation along the fibre length. For this reason, it has long been thought that thermal effects play a limited role in power scaling to high average powers. Nevertheless there has been an increasing interest in thermal effects in YDF with the dramatic rise in power up to several kilowatts from a single YDF. Thermal effects in fibre arise mainly from the quantum defect between the pump and signal photons. Therefore the choice of pump impacts the amount of heat generated along the fibre. This change in temperature may have several effects on the fibre device performance. D. C. Brown and H. J. Hoffman have analyzed these thermal limits for power scaling of fibre lasers. Details of this study can be found in [28] and I provide here a brief outline of the theoretical thermal limits of high-power fibre based sources. A first limit consists in thermally induced material fracture that is commonly observable in bulk solid-state lasers and is even more pronounced in weaker silica based fibres. Although it has not been observed experimentally, a large change in core temperature may result in significant change of refractive index which could affect the waveguiding properties and eventually degrade the laser efficiency. Furthermore, in some cases with very high thermal load, the core temperature may reach extreme values leading to the catastrophic melting of the core itself. An increase of the fibre temperature does not necessarily induce destructive effects. Indeed a change in temperature causes a variation of the populations which implies a change in the actual cross-sections. For instance, a temperature increase induces a shift of the gain spectrum to longer wavelengths with subsequent reduction of the peak gain and in turn leads to a reduced efficiency.

Photodarkening

With increasing power levels produced by fibre sources in CW and pulsed operation, photodarkening has appeared as another limiting factor for further power scaling. Photodarkening can be described by a temporal decay of average output power. The decay rate depends on various parameters. This decay is due to increased absorption of the signal in the Yb-doped doped core and results in a reduction of the device lifetime. The underlying physical process for doped fibre degradation could be attributed to the formation of colour centres or other photoinduced structural transformations in the silica glass host [29] associated to defect sites in the glass. The induced absorption is more pronounced for visible wavelengths and tails out to 1.1 μm. It was observed that the photodarkening rate has a 7^{th} order dependence on the populaton inversion [30]. For this reason, high-energy pulsed system with an average population inversion of 40-50% can degrade 10^4-10^7 faster than standard CW fibre laser operating with 5-10% population inversion. Photodarkening effects can be reduced by employing a counter propagative pumping configuration since it provides a more uniform population inversion than co-propagative pumping. With increasing interest for photodarkening, fibre manufacturers have also started to work on solutions to overcome this issue. This can be done by improving the fabrication process to avoid formation of defects in the glass matrix. Liekki has demonstrated improved performance by fabricating YDF with so-called Direct Nanoparticle Deposition (DND) [31]. Another technique consists in minimising Yb clustering by increasing the aluminium content in the fibre composition [32, 33].

2.2 Pulse propagation in optical fibres

This section describes a brief background to propagation of pulses in optical fibres including nonlinear effects which are observed and utilised in this work. More details related to this theoretical background can be found in [34].

2.2.1 Nonlinear Schrödinger equation

The evolution of an ultrashort pulse in an optical fibre can be determined using the nonlinear Schrödinger equation expressed as:

$$i\frac{\partial \psi}{\partial z} = \frac{\beta_2}{2}\frac{\partial^2 \psi}{\partial t^2} - \gamma|\psi|^2\psi, \qquad (2.21)$$

where ψ is the normalised complex amplitude of the field normalised related to the optical power by $P=\psi^*\psi$. β_2 is the group velocity dispersion per unit length, and γ is the nonlinear coefficient defined by:

$$\gamma=\frac{2\pi n_2}{\lambda A_{eff}}, \tag{2.22}$$

where n_2 is the nonlinear refractive index with a typical value of $3.2\times10^{-20}\,\mathrm{m^2/W}$ for silica. A_{eff} is the effective core area which takes into account the transverse distribution $\phi(x,y)$ of the fibre mode and is defined as:

$$A_{eff}=\frac{\left(\int_{-\infty}^{\infty}\int_{-\infty}^{\infty}|\phi(x,y)|^2\,dxdy\right)^2}{\int_{-\infty}^{\infty}\int_{-\infty}^{\infty}|\phi(x,y)|^4\,dxdy}. \tag{2.23}$$

Two distinct regimes of propagation can be considered: the dispersion dominated regime of propagation and the nonlinearity-dominated regime. Both regimes are determined by two parameters that account for propagation of a Fourier transform limited pulse with a duration T_0 and a peak power P_0 and are defined by:

$$L_D=\frac{T_0^2}{|\beta_2|} \quad \text{and} \quad L_{NL}=\frac{1}{\gamma P_0}. \tag{2.24}$$

L_D and L_{NL} are the dispersion and nonlinear length respectively. A dispersion dominated regime corresponds to the case where $L_D << L_{NL}$, and the nonlinearity-dominated regime is applicable whenever $L_D >> L_{NL}$.

2.2.2 Dispersion-dominated regime

In this case, nonlinearities are neglected, so that $\gamma=0$ in Eq. (2.21), resulting in the following equation:

$$i\frac{\partial \psi}{\partial z}=\frac{\beta_2}{2}\frac{\partial^2 \psi}{\partial t^2}. \tag{2.25}$$

The value of dispersion depends on the material as well as waveguide properties. Dispersion effects can be illustrated by considering the example of an input unchirped Gaussian pulse with amplitude $\psi(0,t)=\exp\left(-\frac{T^2}{2T_0^2}\right)$ and a pulse duration at FWHM of $T_{FWHM}=2\sqrt{\ln 2}T_0$. In this case, the amplitude evolution along the fibre length is expressed as:

$$\psi(z,t)=\frac{T_0}{\sqrt{T_0^2-i\beta_2 z}}\exp\left(-\frac{T^2}{2\left(T_0^2-i\beta_2 z\right)}\right). \tag{2.26}$$

This equation shows that under the effects of dispersion, the pulse maintains its Gaussian shape but its width increases according to the following equation:

$$T_1(z)=T_0\sqrt{1+\left(\frac{z}{L_D}\right)^2}, \tag{2.27}$$

meaning that at a distance L_D, the pulse sees its width broadens by a factor $\sqrt{2}$. This expression also indicates that the pulse broadening is independent of the sign of dispersion.

Furthermore propagation has introduced a time dependent phase defined by:

$$\Phi(z,t)=-\frac{\operatorname{sgn}(\beta_2)\left(z/L_D\right)}{1+\left(z/L_D\right)^2}\frac{t^2}{T_0^2}+\frac{1}{2}\tan^{-1}\left(\frac{z}{L_D}\right), \tag{2.28}$$

This corresponds to a linear chirp given by:

$$\delta\omega(z,t) = -\frac{\partial\phi(z,t)}{\partial t} = \frac{2\,\mathrm{sgn}(\beta_2)\left(z/L_D\right)}{1+\left(z/L_D\right)^2}\frac{t}{T_0^2}, \tag{2.29}$$

Therefore a dispersion-dominated regime causes not only pulse broadening but also an introduction of a perfectly linear frequency chirp whose slope depends on the sign of dispersion. For instance in a normal dispersion fibre ($\beta_2 > 0$), the chirp is negative at the leading edge while the opposite applies for an anomalous dispersion fibre ($\beta_2 < 0$).

Numerical simulations are utilized to illustrate the effect of dispersion on a Gaussian pulse of 4 ps in duration (FWHM) after propagation in an optical fibre. A single-mode fibre with $\beta_2 = 25.10^{-3}$ ps^2.m^{-1} is considered. Fig. 2.14(a) depicts the evolution of the intensity profile along the fibre length with the corresponding frequency chirp. Fig. 2.14(b) shows an unchanged spectrum as the pulse propagates. Fig. 2.14(c) reports the longitudinal evolution of the pulse duration at FWHM.

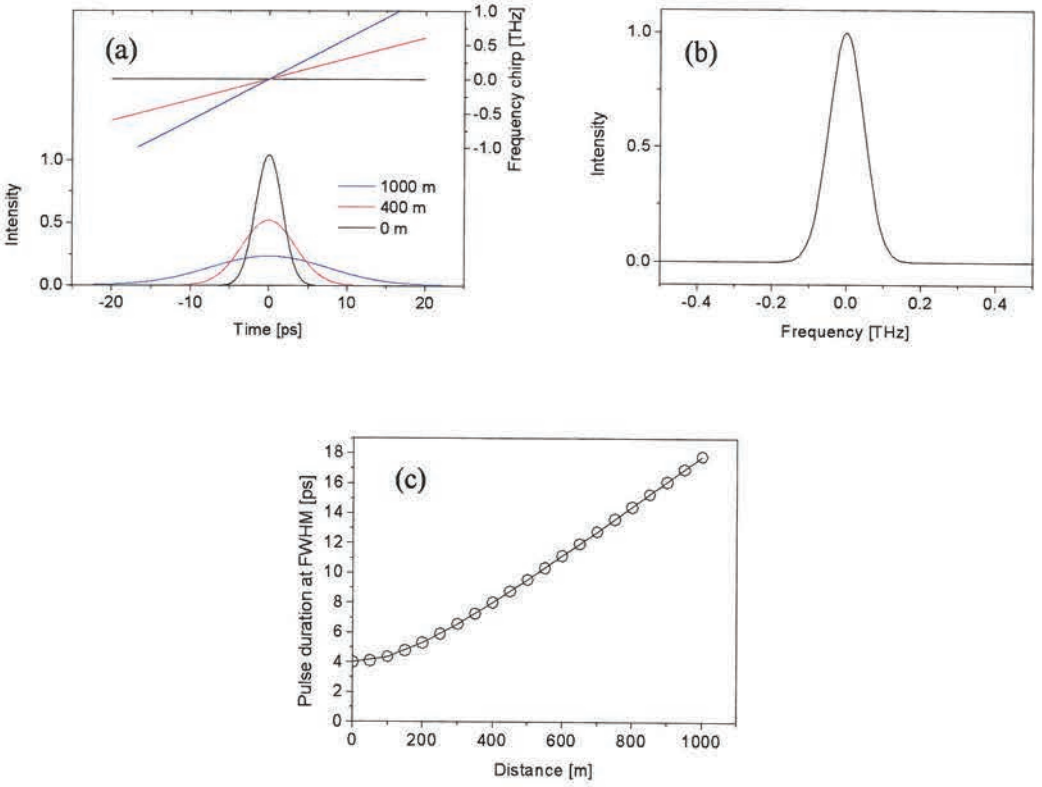

Fig. 2.14. Propagation of a Gaussian pulse with a duration of 4 ps in an optical fibre where dispersion dominates over nonlinear effects. (a) Evolution of intensity profile and chirp at various fibre distances. (b) Evolution of the spectrum showing no changes during propagation. (c) Evolution of pulse duration: numerical results (line) and analytical calculations from eq. (2.27).

2.2.3 Nonlinearity-dominated regime: self-phase modulation

The dispersion term is now neglected ($\beta_2 = 0$), and Eq. (2.21) becomes:

$$i\frac{\partial \psi}{\partial z} = -\gamma|\psi|^2\psi . \tag{2.30}$$

Nonlinear effects presented here are related to the Kerr effect in an optical fibre which represents a change of refractive index induced by high intensities in the silica core. This results in a nonlinear phase change accumulated along a distance L of the fibre and given by:

$$\phi_{NL} = n_2|E|^2 k_0 L, \tag{2.31}$$

where $k_0 = 2\pi/\lambda$ and E represent the amplitude of the field. Therefore this nonlinear effect is called self-phase modulation.
Consequently a solution of Eq. (2.30) is:

$$\psi(z,t) = \psi(0,t)\exp[i\phi_{NL}(z,t)], \tag{2.32}$$

where the nonlinear phase is:

$$\phi_{NL}(z,t) = \gamma|\psi(0,t)|^2 z . \tag{2.33}$$

This induced phase leads to the following frequency chirp:

$$\partial\omega_{NL}(z,t) = -\frac{\partial\phi_{NL}(z,t)}{\partial t} = -\gamma z\frac{\partial|\psi(0,t)|^2}{\partial t} . \tag{2.34}$$

Considering the case of an initial unchirped Gaussian pulse, this frequency chirp becomes:

$$\partial\omega_{NL}(z,t) = \frac{2\gamma z P_0 t}{T_0^2}\exp\left[-(t/T_0)^2\right]. \tag{2.35}$$

Therefore in this case the maximum value of $\partial\omega_{NL}(z,t)$ is expressed by:

$$\partial\omega_{NL}^{\max}(z) = e^{-1/2}\sqrt{2}\frac{\gamma P_0 z}{T_0}. \tag{2.36}$$

This expression shows that as a pulse propagates, the nonlinear chirp increases, resulting in the generation of new photons at these new frequencies. As a result, self-phase modulation causes a spectral broadening. Numerical simulations were carried out to illustrate the effects of SPM on the propagation of a Gaussian unchirped pulse in an optical fibre. The fibre is characterised by $\gamma = 0.006\ \mathrm{W^{-1}.m^{-1}}$ and the Gaussian pulse has a duration of 4 ps with an energy of 400 pJ.

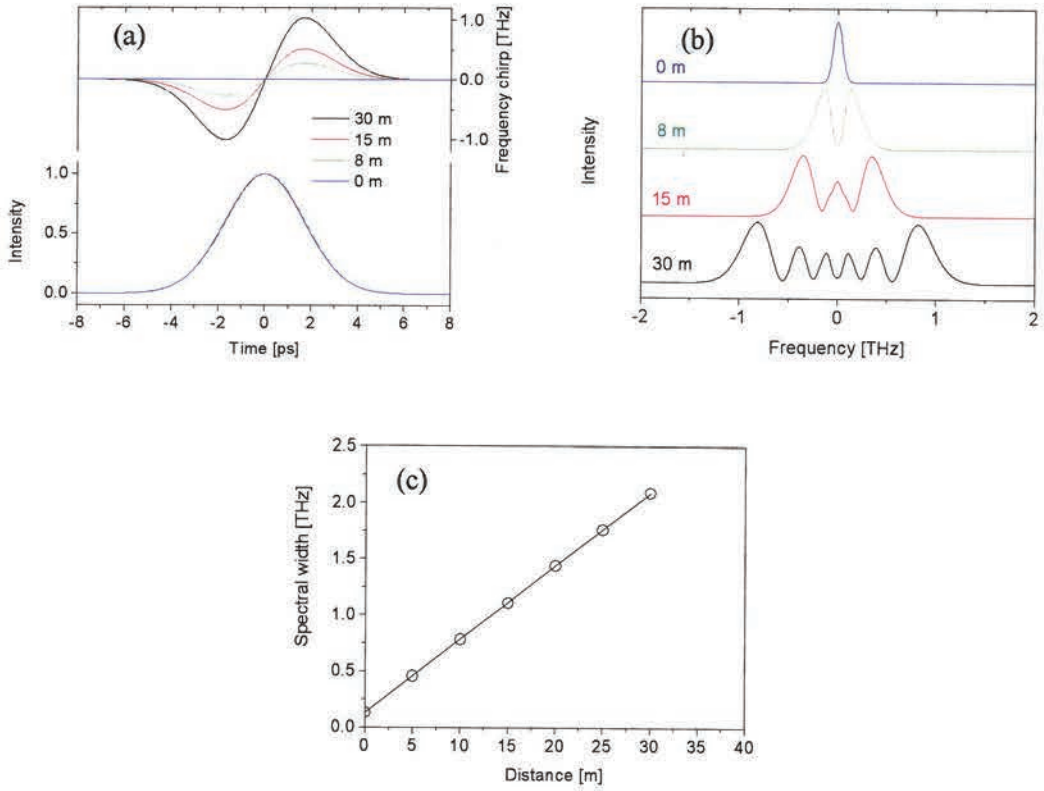

Fig. 2.15. Propagation of a Gaussian pulse with a pulse duration of 4 ps and an energy of 400 pJ in an optical fibre. (a) Evolution of intensity profile and chirp. (b) Evolution of spectrum at various distances. (c) Spectral width evolution based on numerical simulations (line) and based on analytical calculation from eq. (2.36).

Eq. (2.36) is based on the assumption that dispersion effects are negligible compared to nonlinear effects. However with increasing spectral bandwidth, dispersion becomes more significant making the analytical expression not valid. This limit is apparent in Fig. 2.15(c) where analytical and numerical values differ as the spectral width increases.

2.2.4 Cross-phase modulation

Several waves co-propagating in an optical fibre can interact and cause additional nonlinearities. In the case of Stimulated Raman and Brillouin scatterings, harmonic generation and four-wave mixing, these interacting waves create new waves as will be described in the following sections. Coupling between these waves can also happen resulting in a phenomenon called cross-phase modulation. Similarly to SPM, XPM corresponds to a change of refractive index caused by the interaction with other waves. The intensity-dependent nonlinear phase change induced by two co-propagating waves depends on the intensity of each wave and is always accompanied by SPM as expressed in the following:

$$\phi_j^{NL}(z) = \frac{\omega_j}{c}\Delta n_j z = n_2 \frac{\omega_j}{c}\left[\left|\psi_j\right|^2 + 2\left|\psi_{3-j}\right|^2\right]z, \tag{2.37}$$

where $j = 1$ or 2. The first term represents the contribution of SPM. The second term represents the phase modulation induced by the second co-propagating wave or XPM. The factor of 2 applied to the second term shows that for a given intensity, XPM is twice as effective as SPM.

2.2.5 Four-wave mixing

When three waves comprised of two pump waves ψ_1, ψ_2 and a signal wave ψ_3 of respective frequencies ω_1, ω_2 and ω_3 interact in an optical fibre, they generate a fourth wave ψ_4 of frequency $\omega_4 = \omega_1 + \omega_2 - \omega_3$. Four-wave mixing is a phase sensitive process. This process can be maximised along the fibre length if the phase-matching condition imposed by the conservation momentum is met. It is described by:

$$\Delta k = k_1 + k_2 - k_3 - k_4 = \left(\tilde{n}_3\omega_3 + \tilde{n}_4\omega_4 - \tilde{n}_1\omega_1 - \tilde{n}_2\omega_2\right)/c = 0, \tag{2.38}$$

where $\tilde{n}_1$, $\tilde{n}_2$, $\tilde{n}_3$ and $\tilde{n}_4$ are the effective indices of the fibre modes. Considering the nonlinear phase-shift induced by SPM and XPM, the phase mismatch term is given by:

$$\kappa = \Delta k + \gamma(P_1 + P_2), \tag{2.39}$$

with P_1 and P_2, the respective pump peak powers. In the particular case of partially degenerate FWM where $\omega_1 = \omega_2$, two photons of the pump waves are annihilated to create two photons known as Stokes and anti-Stokes with $2\omega_1 = \omega_{aS} + \omega_S$. This case is of great practical interest because this means that a single highly intense pump wave propagating along the fibre can amplify through FWM Stokes and anti-Stokes waves generated from noise. The phase mismatch can be expressed by:

$$\kappa = \Delta k + 2\gamma P_1, \tag{2.40}$$

To realise phase matching, one of these terms should be negative. This can be achieved in practice by employing adequate dispersion profiles, by propagating several modes in a multimode fibre or by the use of modal birefringence.
The corresponding FWM gain is given by:

$$g = \sqrt{\gamma^2 P_1^2 - \left(\frac{\kappa}{2}\right)^2}, \tag{2.41}$$

This expression reveals that FWM gain exists even when the phase matching condition is not fulfilled. The peak gain corresponds to the case of perfect phase matching and is given by $g_{\max} = \gamma P_1$. This gain value is approximately twice as high as the Raman gain. Although this process can be very efficient, in practice phase matching is difficult to maintain over a long propagation distance and in this case stimulated Raman scattering usually dominates.

2.2.6 Stimulated Raman scattering

Raman scattering is inherent to any molecular medium. It relates to the transfer of power from an optical field to another field with a frequency downshift determined by the vibrational modes of the medium. In other words, an incident pump beam can generate a frequency downshifted wave called the Stokes wave. If the pump beam is sufficiently intense, the Stokes wave can grow along the medium and the process is then called stimulated Raman scattering. SRS has proved to be of great interest in optical fibres due to long interaction lengths leading to the development of Raman based fibre amplifiers and lasers. However SRS may also constitute a practical limitation in high-peak fibre based devices.
Considering CW operation and in the case of a passive optical fibre characterised by losses α_p and α_s for the pump and Stokes beams, respectively, the transfer of power from the

pump to the Stokes wave along the fibre length is described by the following coupled equations:

$$\frac{dI_s}{dz} = g_R I_p I_s - \alpha_s I_s, \tag{2.42}$$

$$\frac{dI_p}{dz} = -\frac{\omega_p}{\omega_s} g_R I_p I_s - \alpha_p I_p, \tag{2.43}$$

where I_s and I_p are the Stokes and pump intensities respectively, and g_R is the Raman gain coefficient. Fig. 2.16 shows g_R for fused silica at a pump wavelength of 1 μm as a function of the frequency shift. In this case, Raman gain peaks at a frequency shift of 13.2 THz (440 cm^{-1}).

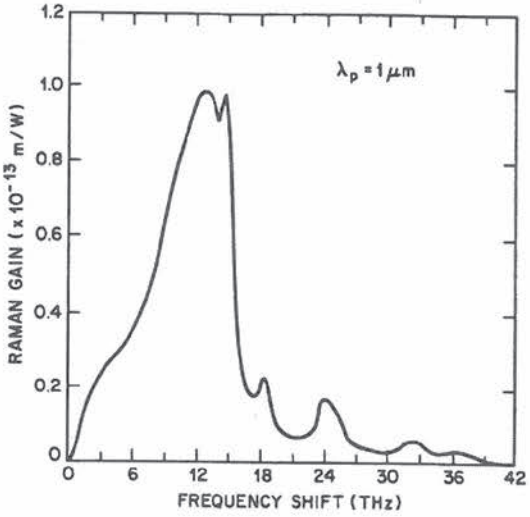

Fig. 2.16. Raman-gain spectrum for fused silica at a pump wavelength λ = 1μm. After [34].

From equations (2.42) and (2.43), an expression for the Raman threshold can be determined. It leads to the definition of a critical pump power that represents the level of input pump power required for the Stokes and pump powers to be equal at the fibre length L and is determined by:

$$\frac{g_R P_0^{cr} L_{eff}}{A_{eff}} \approx 16, \tag{2.44}$$

where L_{eff} represent the effective length given by:

$$L_{eff} = \left[1 - \exp\left(-\alpha_p L\right)\right] / \alpha_p \,. \tag{2.45}$$

The properties of SRS presented in this section relate mainly to the case of a cw signal and provide the basics for understanding the phenomena presented in the following chapters. These considerations can also be employed in pulsed regime if one neglects effects such as pulse walk-off and other nonlinear effects. A thorough theoretical analysis of SRS in pulsed regime can be found in [34].

2.3 Conclusion

In this chapter, various properties of Yb-doped fibres have been introduced to describe the propagation and amplification of a signal in a fibre-based source. The rapid progress of fibre lasers and amplifiers have been enabled by tremendous developments in key technologies such as pump laser diodes, Yb-doped fibres and high-power components described in this chapter. Furthermore it has been outlined that ytterbium ions appear ideal for power scaling of fibre lasers. Nevertheless, there are limiting factors to be considered for further power scaling of such systems with excellent beam quality. One of them includes nonlinear effects arising along the fibre due to high beam intensity. These become even more important in the pulsed regime where peak intensities can reach very high values as will be described in the following chapters of this thesis.

In chapter 3, the interaction of dispersion and SPM in a high-power amplifier leads to the generation of clean femtosecond pulses from picosecond seed pulses.

Chapters 4 and 5 presents experimental observations of spectral broadening induced by SPM caused by amplification of short pulses in high-power amplifiers with various fibre parameters.

In chapter 6, FWM is exploited in a special highly nonlinear fibre to generate red and blue components when pumped by intense green picosecond pulses. This chapter also describes the use of short pulses produced at 1060 nm to generate pulses at 1178 nm via SRS in a fibre amplifier for subsequent frequency doubling at 589 nm. Despite a watt level output, poor conversion efficiency was observed due to significant XPM arising between pump and signal beams. Nonlinear effects are often seen as a limiting factor for efficient amplification of pulsed fibre lasers as described in chapter 4 and 5. Nevertheless they can be an outstanding tool in combination with YDF for the development of advanced fibre sources in a simple configuration as presented in chapter 3 and 6.

References

1. E. Snitzer, "Optical maser action of Nd^{3+} in a barium crown glass," Phys. Rev. Lett. **7**, 444-446 (1961).
2. C. J. Koester and E. Snitzer, "Amplification in a fiber laser," Appl. Opt. **3**,1182-1186 (1964).
3. S. B. Poole, D. N. Payne, and M. E. Fermann, "Fabrication of low loss optical fibres containing rare earth ions," Electron. Lett. **21**, 737-738 (1985).
4. K. I. Ueda, H. Sekiguchi, and H. Kan, "1 kW cw output from fibre embedded lasers", in *proc. Conference on Lasers and Electro-Optics*, Long Beach, USA: postdeadline paper CtuQ5 (2001).
5. D. Gloge, "Weakly guiding fibers," Appl. Opt. **10**, 2252 (1971).
6. J. Kafka, "Laser diode pumped fiber laser with pump cavity," US Patent 4,829,529 (1989).
7. N. G. R. Broderick, H. L. Offerhaus, D. J. Richardson, R. A. Sammut, J. E. Caplen, L. Dong, "Large mode area fibers for high power applications," Opt. Fiber Technol. **5** 185–196 (1999).
8. J. Limpert, O. Schmidt, J. Rothhardt, F. Röser, T. Schreiber, A. Tünnermann, S. Ermeneux, P. Yvernault, and F. Salin, "Extended single-mode photonic crystal fiber lasers," Opt. Express **14**, 2715-2720 (2006)
9. M. Muendel, "Optimal inner cladding shapes for double-clad fiber lasers", *Conference on Lasers and Electro-optics*, Technical Digest, Optical Society of America, Washington, DC, 209 (1996).
10. H. Zellmer, A. Tünnermann, H. Welling, V. Reichel, "Double-clad fiber laser with 30 W output power," *Optical Amplifier and their Applications, in Technical Digest*, Optical Society of America, Washington, DC, 251-252 (1997).
11. Y. Jeong, J. K. Sahu, D. N. Payne, J. Nilsson, "Ytterbium-doped large-core fiber laser with 1.36 kW continuous-wave output power", Opt. Express **12**, 6088-6092 (2004).
12. A. Liem, J. Limpert, H. Zellmer, A. Tünnermann, V. Reichel, K. Mörl, S. Jetschke, S. Unger, H.-R. Müller, J. Kirchhof, T. Sandrock, A. Harschak, "1.3 kW Yb-doped fiber laser with excellent beam quality," *Proc. Conference on Lasers and Electro-Optics 2004*, San Francisco, USA, May 16-21, 2004, postdeadline paper CPDD2.
13. See product specifications in www.ipgphotonics.com

14. D. DiGiovanni and A. Stenz, "Tapered fiber bundles for coupling light into and out of cladding-pumped fiber devices," U.S. Patent 5,864,644 (1999).

15. F. Gonthier, L. Martineau, N. Azami, M. Faucher, F. Séguin, D. Stryckman, A. Villeneuve, "High-power All-Fiber components: The missing link for high power fiber lasers," in Fiber Lasers: Technology, Systems, and Applications. Edited by L. N. Durvasula, Proceedings of the SPIE, Volume 5335, pp. 266-276 (2004).

16. V. P. Gapontsev and I. Samartsev, "Coupling arrangement between a multi-mode light source and an optical fiber through an intermediate optical fiber length," US Patent 5,999,673 (1996).

17. D.J. Ripin and L. Goldberg, "High efficiency side-coupling of light into optical fibres using imbedded v-grooves," Electron. Lett. **31**, 2204-2205 (1995).

18. A. B. Grudinin, D. N. Payne, P. Turner; W. Paul, J. Nilsson, M. N. Zervas, M. Ibsen, and M. Durkin, "Multi-fibre arrangements for high power fibre lasers and amplifiers," US patent 6,826,335 (2004).

19. M. J. F. Digonnet, "Rare-Earth-Doped Fiber Lasers and Amplifiers," Second Edition, Marcel Dekker (2001).

20. M. J. F. Digonnet and C. J. Gaeta "Theoretical analysis of optical fiber laser amplifiers and oscillators," Appl. Opt. **24**, 333-342 (1985).

21. E. Desurvire, *Erbium doped fiber amplifiers*. Wiley, 1994

22. E. Desurvire, C. R. Giles and J. R. Simpson, "Gain Saturation Effects in High-Speed, Multichannel Erbium-Doped Fiber Amplifiers at λ= 1.53 μm," IEEE J. Lightwave Technol. 12, 2095-2104 (1989).

23. D. Marcuse, "Curvature loss formula for optical fibers", J. Opt. Soc. Am. **66**, 216-220 (1976).

24. J. P. Koplow, D. A. V. Kliner and L. Goldberg, "Single-mode operation of a coiled multimode fiber amplifier", Opt. Lett. **7**, 442-444 (2000).

25. F. D. Teodoro, J. P. Koplow and S. W. Moore, "Diffraction-limited, 300-kW peak-power pulses from a coiled multimode fiber amplifier", Opt. Lett. **27**, 518-520 (2002).

26. J. A. Alvarez-Chavez, A. B. Grudinin, J. Nilsson, P. W. Turner and W. A. Clarckson, "Mode selection in high power cladding pumped fiber lasers with tapered section", *Conference on Lasers and Electro-optics*, Baltimore, USA, paper CWE7 (1999).

27. J. M. Souza and O. G. Okhotnikov, "Multimode Er-doped fiber for single-transverse-mode amplification", Appl. Phys. Lett. **74**, 1528-1530 (1999).

28 D. C. Brown and H. J. Hoffman, "Thermal, stress, and thermo-optic effects in high average power double-clad silica fiber lasers," IEEE J. Quantum Electron. **37**, 207-217 (2001).

29 J. J. Koponen, M. J. Söderlund, H. J. Hoffman, and S. K. T. Tammela, "Measuring photodarkening from single-mode ytterbium doped silica fibers," Opt. Express **14**, 11539-11544 (2006)

30 J. J. Koponen, M. J. Söderlund, S. K. T. Tammela, D. Kliner, J. Koplow, "Photodarkening rate in ytterbium doped silica fibers," Photonics West 2006, San Jose, USA. Late breaking news (2006).

31 J. J. Koponen, M. J. Söderlund, S. K. T Tammela, and H. Po," Measuring photodarkening from Yb-doped fibers," CLEO/Europe-EQEC Conference, paper CP2-2-THU (2005).

32 T. Kitabayashi, M. Ikeda, M. Nakai, T. Sakai, K. Himeno and K. Ohashi, "Population Inversion Factor Dependence of Photodarkening of Yb-doped Fibers and its Suppression by Highly Aluminum Doping," OFC2006, Anaheim, USA, paper OThC5 (2006).

33 B. Morasse, S. Chatigny, C. Hovington, É. Gagnon, and J. De Sandro, "Low-photodarkening single cladding ytterbium fiber amplifier," Photonics West 2007, San Jose, USA, paper 6453-17 (2007).

34 G. P. Agrawal, *Nonlinear fiber optics, Second edition*. Academic Press (1995).

Chapter 3 High-power femtosecond sources based on Yb-doped fibre amplification of VECSELs

3.1 Introduction

The previously described remarkable properties of RE-doped fibres and the scientific interest related to amplification of ultrashort pulses have motivated tremendous research effort in the development of high-power femtosecond fibre-based sources. The main axis of research consists in achieving either high peak intensity or high average power. Herein, I will focus mainly on strategies to generate femtosecond pulses at high average power.

Despite all their attractive properties, high-power short pulse fibre sources suffer from the onset of unwanted nonlinear effects which in turn limit the maximum output power and degrade output pulse shape and duration. An initial controlled broadening of the pulse prior to amplification in a fibre amplifier followed by subsequent recompression can be used to alleviate these effects. This technique, called chirped pulse amplification, is typically used to achieve the highest possible pulse energy and peak power whilst maintaining the input pulse duration after recompression of the amplified pulses. The fibre based CPA configuration has enabled the generation of femtosecond pulses with 1 mJ of energy [1] and also average powers of ~100 W [2] from Yb-doped fibre amplifiers.

An alternative technique relies on the direct fibre amplification of ultrashort pulses to high peak power and high average power. In this case, after fibre amplification the short pulses accumulate a large amount of chirp due to self-phase modulation, which is then employed to compress the output pulse using a grating pair. This technique is very simple and highly suitable for generating high peak powers at high average power. Furthermore, it allows efficient and clean pulse compression to durations that are generally much lower than those achievable via the more complex CPA scheme. The compression efficiency depends directly on the linearity of the generated chirp. The optimal condition is satisfied when the pulses are short enough and of adequate energy to undergo the required balanced interplay of dispersion, self-phase modulation, and gain in the fibre amplifier. This leads to parabolic shaped output

pulses with a perfectly linear chirp [3]. The parabolic amplification regime has led to the recent demonstrations of high-power femtosecond fibre lasers involving seed sources producing sub-picosecond pulses with repetition rates at tens of MHz [4, 5, 6]. These seed lasers typically consist of a mode-locked fibre laser [4] or solid state lasers [7].

A passively mode-locked optically-pumped VECSEL capable of generating pulses at GHz repetition rate around 1 μm appears very suitable as a seed source for fibre amplifiers to achieve these types of amplification regimes at high repetition rates. VECSELs produce near-transform-limited ps and sub-ps pulses in near diffraction limited beams with extinction ratios and output powers suitable for high-gain fibre amplification to high powers. They are also inherently wavelength selectable, robust and compact, which are additional features that make them ideally compatible with fibre amplifiers.

In this chapter I introduce some principles for high-power amplification of ultrashort pulses in a fibre amplifier and describe experimental demonstrations of fibre amplification of ps and sub-ps pulses with a repetition rate in the GHz range produced by passively ML-VECSELs. Two fibre MOPA systems seeded by two different VECSELs were designed to investigate amplification to high average power in different nonlinear regimes, where the effects of the nonlinearities produce vastly different results. A first MOPA seeded by relatively long 4.6 ps pulses generated in excess of 200 W of average power with strongly chirped, 6.3 ps long, pulses. This condition, where pulses mainly undergo the effects of SPM, led to a large pedestal when the pulses were compressed to the femtosecond range. This was due in practice to nonlinearities of the chirp at the edge of the pulses. However the amplification of 500 fs long seed pulses produced by a different VECSEL resulted in the generation of parabolic pulses at 53 W average power. These linearly chirped pulses could then be compressed to 110 fs with excellent quality. I compare and discuss these different regimes based on numerical simulations and propose routes towards further power scaling.

3.2 Fibre amplification of ultrashort pulses

The tight beam confinement and long interaction length inherent to fibre devices constitute a challenging problem for achieving high peak powers in fibre lasers due to the onset of optical nonlinearities such as SRS and SPM during pulse propagation. Indeed a basic comparison of mode sizes (~10 μm versus 1-3 mm) and propagation distance (1-10 m versus 1-10 cm) in a fibre and bulk laser respectively shows that despite the low nonlinearities of silica, the sensitivity to nonlinearities in a fibre amplifier is 10^6-10^7 times higher than in bulk solid-state lasers. Therefore fibre based systems were initially considered unsuitable for ultrashort pulse

operation. Nevertheless over the years, technical progress has led to the development of fibre based ultrashort pulse sources with energy and power competing with conventional sources. Some of these techniques, sometimes adopted from standard laser systems such as chirped pulse amplification, can be employed to mitigate nonlinear effects in the rare-earth doped fibre while other methods were designed to make use of nonlinear effects and dispersion for the efficient generation of femtosecond pulses with high-peak power and high average power. This section describes these two techniques with their specifications and introduces some design considerations for high average power femtosecond fibre systems.

3.2.1 Chirped pulse amplification

Introduced in 1985 [8], the technique of CPA has created an explosion in laser peak power by a factor of 10^3 to 10^4. The technique of CPA is based on the reduction of peak power in the amplifying medium to avoid nonlinear effects. Therefore this technique applies very well to fibre amplifiers where nonlinear thresholds are lower. Its principle is illustrated schematically in Fig 3.1.

A low power pulse emitted by an oscillator is first stretched by a factor S by a dispersive device. This introduces a linear chirp that can be compensated by conventional components such as diffraction grating, prism or fibre Bragg grating. The stretching factor S can exceed 1000 [9] allowing a conversion of picosecond pulses into nanosecond regime with a peak power reduced by the same factor. The stretched pulse, less susceptible to nonlinear effects, is then amplified by one or several amplifiers up to a gain G. Finally the amplified pulse is recompressed to restore its initial pulse duration. Recompression can be implemented by prisms, diffraction gratings [10], fibre Bragg gratings [11] or photonic bandgap fibres [12-14]. The system stretcher+amplifer+compressor should introduce a minimum amount of nonlinearities so that the pulse duration can be maintained leading to an increase in peak power proportional to the total gain. However in practice, residual nonlinearities introduced either by the amplifier or during recompression can cause spectral broadening which results in changes in the pulse duration after compression [15]: a pulse shorter than initially is produced if compression compensates exactly all the nonlinearities, and a longer pulse is generated if compression is incomplete or if residual high order dispersion remains [16].

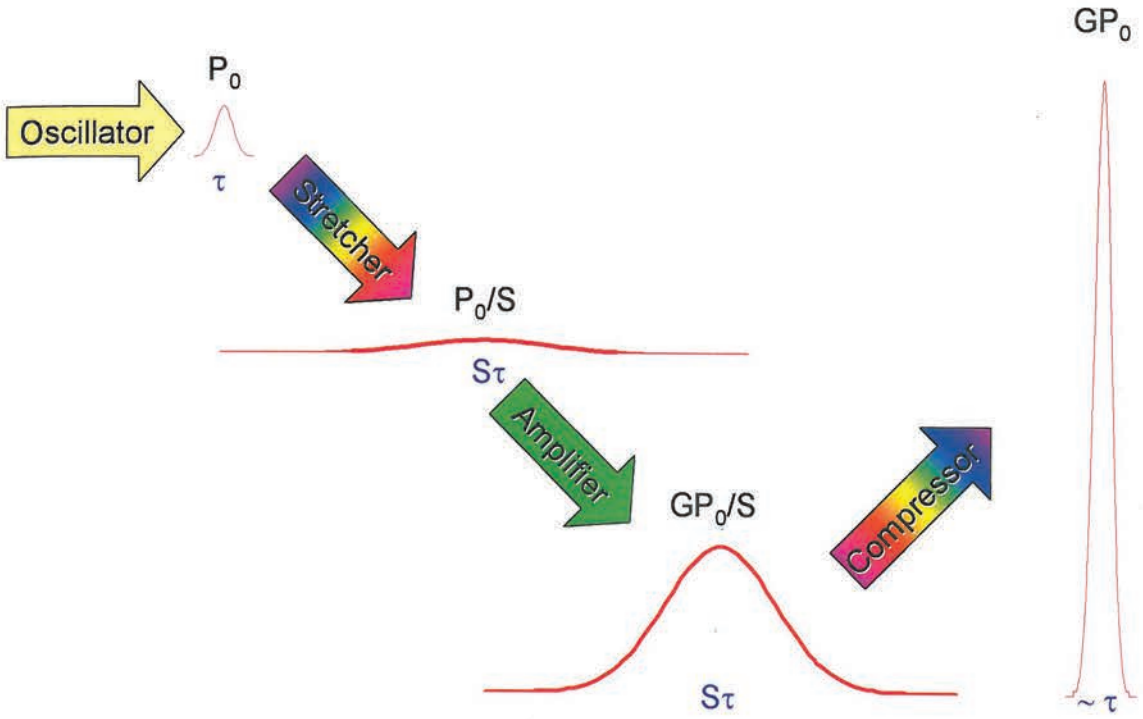

Fig. 3.1. Principle of chirped pulse amplification showing how high peak power can be reached while minimising nonlinear effect in the amplifier.

The use of CPA in fibre based systems has allowed amplification of sub-picosecond pulses by up to 50dB and energies of 100 μJ have been reached [17, 18] for compressed pulses of hundreds of femtoseconds. The peak power can even exceed the MW level [16].

The technique of CPA is very suitable for achieving high energy with compressed femtosecond pulses. However some applications require high average power with moderate energy per pulse and then simpler and more efficient configurations appear more attractive. This alternative method based on nonlinear amplification of short pulses and subsequent grating compression is presented in the next section.

3.2.2 Nonlinear pulse amplification in a normal dispersion fibre amplifier

During amplification, an ultrashort pulse sees not only the gain of the fibre amplifier but also the effects of dispersion and nonlinearities. Therefore the evolution of an ultrashort pulse in a fibre amplifier can be modelled using the nonlinear Schrödinger equation incorporating a gain factor g:

$$i\frac{\partial \psi}{\partial z} = i\frac{g}{2}\psi + \frac{\beta_2}{2}\frac{\partial^2 \psi}{\partial t^2} - \gamma|\psi|^2\psi . \qquad (3.1)$$

To simplify the analysis, the gain coefficient is considered here longitudinally and spectrally constant ($g(z)=g(\omega)=g$). The pulse evolution depends strongly on the dispersion regime. In an anomalous dispersion fibre amplifier, the combination of gain and anomalous dispersion results in a reduction of the pulse duration as it gains power with a shape converging to a soliton which is a solution of the NLSE. However most Yb-doped fibre amplifiers are characterised by a normal dispersion due to the inherent property of the conventional waveguide structure. Consequently, the rest of the study will focus on amplification in fibre amplifier with normal dispersion.

During amplification in a normal dispersion fibre, a short pulse undergoes temporal broadening at a rate which increases with peak power. This amplification is accompanied by a pulse shaping as the propagation distance increases. The pulse shape converges asymptotically to a parabolic pulse and reproduces itself as it propagates. This self-similar behaviour in a nonlinear fibre amplifier with normal dispersion was demonstrated analytically in [19, 20]. This new type of pulse is called a similariton. An example of pulse evolution is presented in Fig 3.2 where a Gaussian input pulse changes to a parabolic shape as it is amplified. These pulses have very attractive characteristics including a linear chirp, that can be well compensated by a bulk grating pair, for instance. Another interesting feature is the fact that under appropriate conditions, all input pulse shapes and durations converge to a parabolic pulse shape. However in conventional YDFA where fibre length does not exceed 10 m, parabolic pulses are not always generated and specific initial conditions for the pulse must be considered. It is therefore necessary to look into the theory of the self-similar regime of amplification.

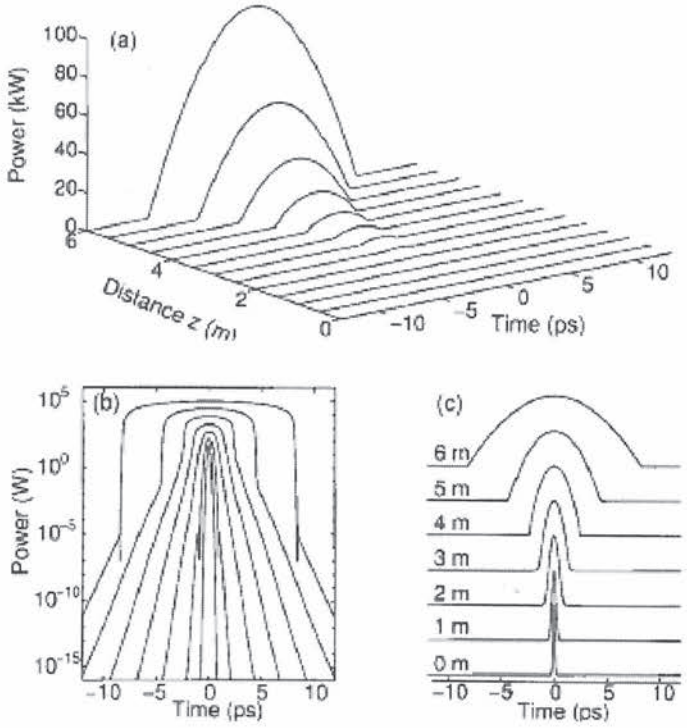

Fig. 3.2. Longitudinal evolution of a Gaussian pulse input pulse to a parabolic pulse shape in a 6-m long fibre amplifier. (a) Three-dimensional representation. (b) Intensity in1-m increment. (c) Normalised intensity in 1-m increment. (After [21])

Calculations that led to analytical expressions for the self-similar regime of amplification are thoroughly described in [21] and I would like to review here only the main properties of the self-similar regime of amplification.

The self-similar asymptotic pulse evolution of the field ψ_p, solution of NLSE is given by:

$$\psi_p(z,t) = A(z,t)\exp\{i\Phi(z,T)\}, \tag{3.2}$$

where

$$\begin{cases} A(z,t) = A_0\sqrt{1-\dfrac{t^2}{T_p^2(z)}}\exp\left(\dfrac{g}{3}z\right), \\ \Phi_p(z,t) = \varphi(z) + C(z)t^2, \end{cases} \tag{3.3}$$

at $|t| \le T_p(z)$.

$A(z,t) = 0$ otherwise

$$\begin{cases} A_0 = \dfrac{1}{2}\left(\dfrac{gU_{in}}{\sqrt{\beta_2\gamma/2}}\right)^{1/3} \\ T_p(z) = \dfrac{6\sqrt{\beta_2\gamma/2}A_0}{g}\exp\left(\dfrac{g}{3}z\right), \\ C(z) = -\dfrac{g}{6\beta_2} \\ \varphi(z) = \varphi_0 + \dfrac{3\gamma A_0^2}{2g}\exp\left(\dfrac{2}{3}gz\right) \end{cases} \tag{3.4}$$

where U_{in} is the input pulse energy and φ_0 is an arbitrary constant. In this case, the quadratic temporal evolution of the phase leads to the following constant chirp Ω_c:

$$\Omega_c(t) = -\frac{\partial\Phi}{\partial t} = \frac{g}{3\beta_2}t, \qquad |t| \le T_p(z), \tag{3.5}$$

A key property of self-similar propagation of pulses in a fibre amplifier is that pulses with various pulse shapes and durations converge to a parabolic pulse shape with the same duration and amplitude. To illustrate this asymptotic behaviour, we consider the amplification of hyperbolic secant pulses with the same energy of U_{in} = 1.5 nJ with different initial pulse durations T_0 between 0.5 and 16 ps in an YDFA with a mode field diameter of 16 μm, a dispersion β_2 = 25.10^{-3} $ps^2.m^{-1}$, a gain g = 2.5 dB/m and a length of 8 m. Third order dispersion is neglected in this analysis. Fig. 3.3 shows the evolution of the temporal width of the pulses along the fibre amplifier. This type of plot already presented in [21, 22] shows that each pulse tends to converge to the asymptotic self-similar solution (thick red line). In addition it appears that shorter initial pulses converge faster to the parabolic pulse duration. Therefore longer pulses would require longer amplification distance to reach self-similar regime of amplification. Otherwise pulses evolve according to an SPM regime of amplification. These observations are very useful for the design of systems where linearly chirped parabolic pulses are required after amplification. However in practice other considerations such as finite gain bandwidth [23], and SRS should also be taken into account to avoid any distortion in the pulse characteristics that prevent pulses to reach the SS regime [24, 25].

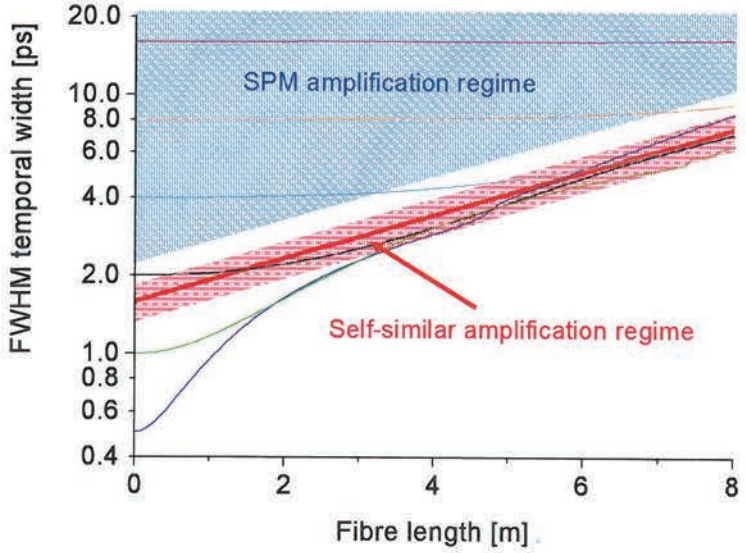

Fig. 3.3. Evolution of the temporal width (FWHM) of pulses with initial durations of 0.5 (blue), 1 (green), 2 (green), 4 (light blue), 8 (orange) and 16 ps (violet) converging to the self-similar regime of amplification sown as a red line. The red zone represents a zone of convergence to a parabolic pulse shape while the blue zone corresponds to the SPM regime of amplification.

Convergence to SS regime of amplification can be further illustrated by plotting the pulse shapes at the output of the YDFA for various input pulse durations. Fig. 3.4(a) shows that as the input pulse duration increases, the pulse shape also differs more from the asymptotic SS solution. This difference is greater away from the central part of the pulse, meaning that the chirp characteristic also differs from the linear characteristics in these parts of the pulse as shown in Fig. 3.4(b). Furthermore, the spectral shape depends on the regime of amplification. The spectrum generated by self-similar regime of amplification is also parabolic in shape. In contrast, the SPM-dominated regime of amplification is characterised by a highly modulated spectrum as shown in Fig. 3.4(c). The spectrum shows smoother features as the pulse converges to the self-similar regime.

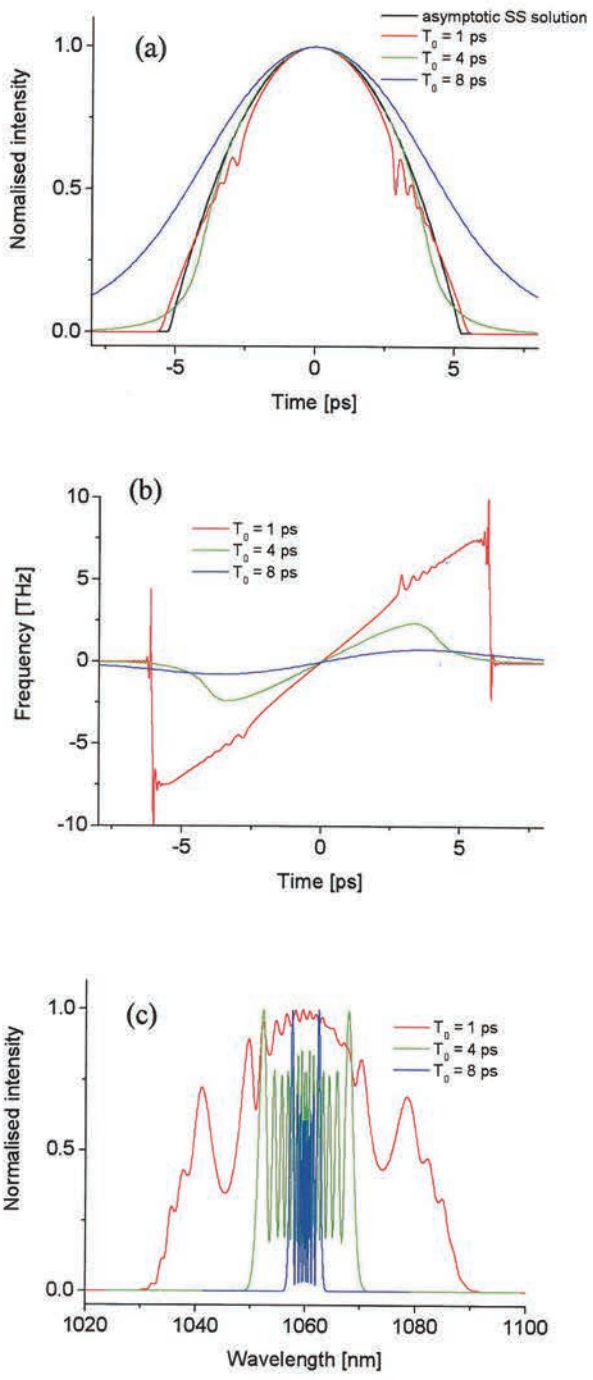

Fig. 3.4. (a) Output pulse shapes, (b) chirp and (c) spectra after amplification of pulses with various initial durations T_0. Parameters used for these numerical simulations were previously introduced (U_{in} = 1.5 nJ, g = 2.5 dB/m in a 8 m long YDFA with a mode field diameter ~ 16 μm, β_2 = 25.10^{-3} ps^2.m^{-1} and a gain g = 2.5 dB/m).

The main practical benefit of the self-similar regime of amplification resides in the generation of pulses with a linear chirp that can easily and efficiently be compensated by a bulk grating

compressor. The next section describes the impact of the nonlinear regimes of amplification on the final linear compression.

3.2.3 Compression of amplified picosecond pulses

Parabolic pulses generated by direct amplification in a YDFA present ideal characteristics for linear compression since the linear chirp can be exactly compensated by bulk gratings commonly employed in high-power applications resulting in very clean ultrashort pulses with very low pedestal. Pulses generated by the SPM regime of amplification are also compressible since the central part of the pulse presents a linear chirp, however the residual uncompensated chirp at the edge of the pulse results in less efficient compression with the appearance of a larger pedestal in the pulse shape. Fig. 3.5 summarises the principle of nonlinear amplification of pulses of different duration: (a) illustrates the SPM regime of amplification and (b) shows the self-similar regime of amplification.

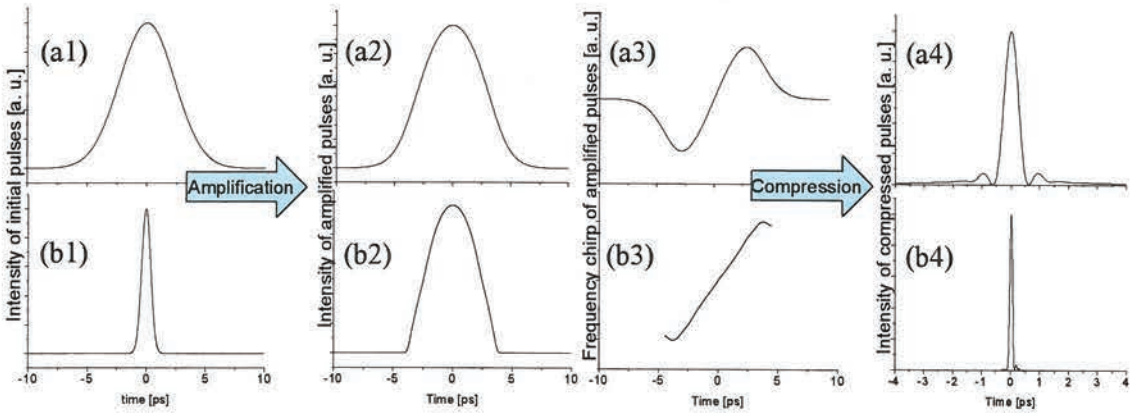

Fig. 3.5. Comparison between amplification of picosecond (a) and sub-picosecond (b) pulses: initial pulse shape (1), pulse shape after amplification (2), chirp (3) and pulse shape after linear compression (4).

The following sections describe experimental demonstrations of these nonlinear regimes of amplifications with high repetition rates and high average power. Numerical simulations based on experimental results provide additional information for further analysis. First, the VECSEL seed source used for this experimental study is described.

3.3 Passively Mode-Locked Vertical-External-Cavity Surface-Emitting Semiconductor Laser

Optically pumped passively mode-locked VECSELs are capable of producing picosecond to subpicosecond pulses in a diffraction-limited output beam. Passive mode-locking is realised in a simple scheme using a SESAM in the cavity making the source compact. Their wavelength agility further enhances their suitability.

Herein, two types of passively ML-VECSELs emitting within the ytterbium gain bandwidth were employed to seed cascaded fibre amplifiers. The aim of this experimental study is the realization of fibre-based sources producing femtosecond pulses at average powers reaching the hundred watts level. These VECSELs were developed by Professor Anne Tropper's group in the Department of Physics and Astronomy at the University of Southampton.
The two lasers used in this study are based on the same laser cavity configuration and differ mainly by their pulse duration and emitting wavelength. A first VECSEL (VECSEL A) produced 4.6 ps pulses at 1055 nm and second source (VECSEL B) generated 500 fs pulse duration at 1042 nm.

The laser cavity is schematically depicted in Fig. 3.6. It is composed of a gain structure which also acts as a folding mirror, a SESAM and a curved output coupler with a transmission of 0.7%. The VECSEL gain structure includes 6 InGaAs/GaAs quantum wells grown above a 27.5-pair AlAs/$Al_{0.84}Ga_{0.16}As$ mirror; the structure design is similar to that described in [26]. The two VECSELs are mode-locked by different SESAM structures. The 4.6 ps long pulses were generated by mode-locking with a SESAM incorporating a single InGaAs/GaAs quantum well grown by low temperature (300°C) molecular beam epitaxy (MBE) on top of a AlAs/GaAs Bragg mirror [27]. Another SESAM containing a single quantum well grown at 735°C by metal organic chemical vapour deposition (MOCVD) on top of a AlAs/GaAs Bragg mirror designed at 1040 nm resulted in the production of 500 fs pulses. The gain sample was pumped by the focused beam of a 1 W fibre coupled laser diode emitting at 830 nm.

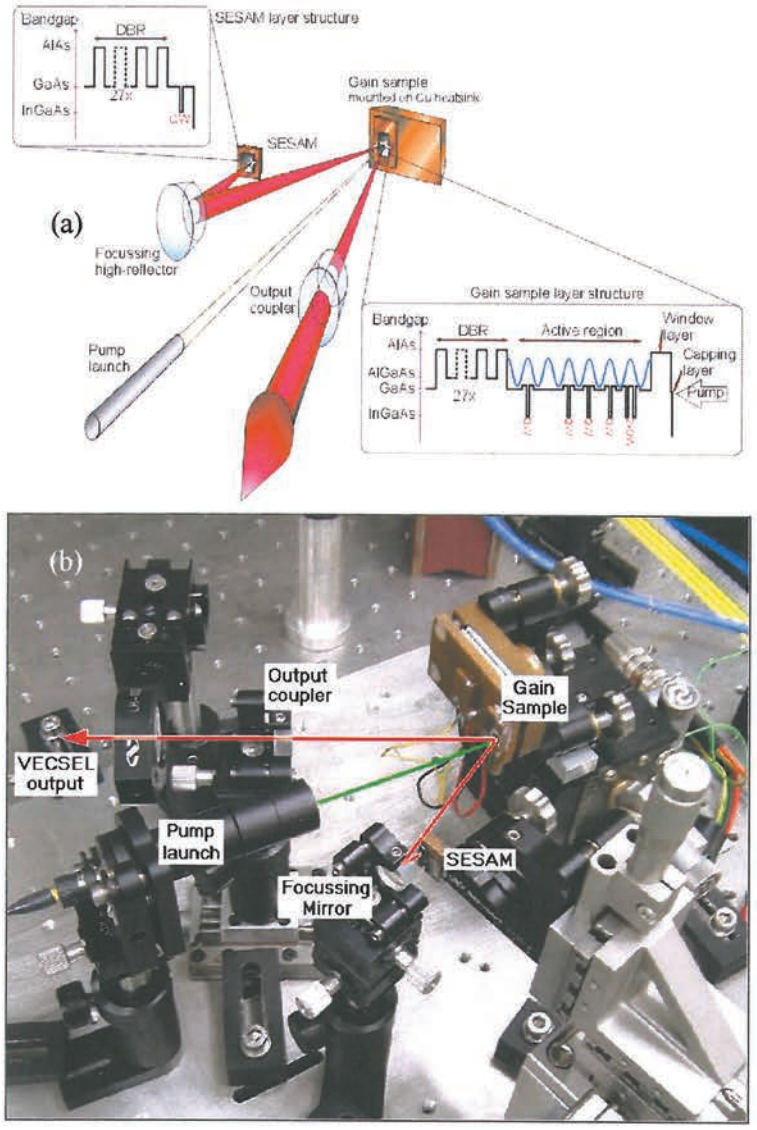

Fig. 3.6. (a) Schematic of a passively mode-locked VECSEL. The signal beam is shown in red. (b) Photo of the laser cavity. The signal and pump beams are outlined in red and green respectively. Courtesy of the VECSEL group, University of Southampton.

The first ML-VECSEL (VECSEL A) produced 4.6 ps pulses at 910 MHz and with 8 mW of average power. Spectrum and autocorrelation trace of this source are shown in Fig. 3.7. The wavelength was near 1055 nm and the linewidth 0.45 nm, corresponding to a time-bandwidth product (TBP) $\Delta\tau\Delta\nu \sim 0.56$.

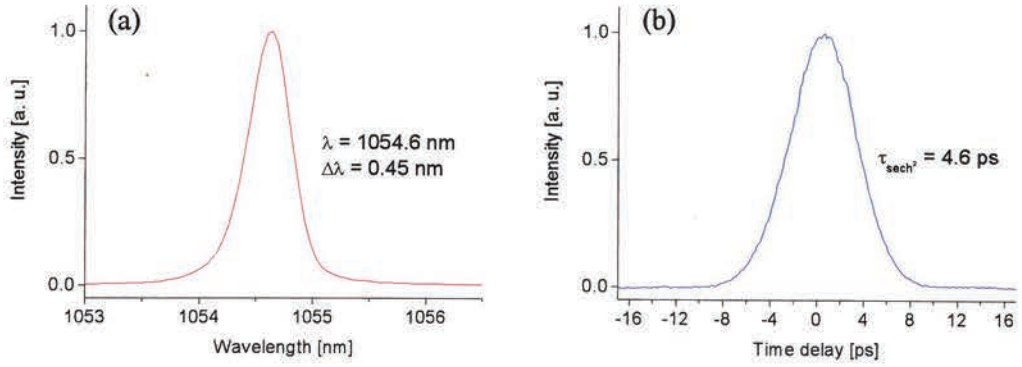

Fig. 3.7. Characteristics of the ML-VECSEL producing sub-picosecond pulses. (a) Output spectrum with a bandwidth of 0.45 nm. (b) Autocorrelation trace of the output pulse with a duration of approximately 4.6 ps.

The second ML-VECSEL (VECSEL B) produces approximately 500 fs pulses at 1.1 GHz with an average power of 25 mW. The laser emits at 1042 nm in a 2 nm linewidth meaning that the hyperbolic secant-shaped pulses were nearly transform-limited. These laser output characteristics are shown in Fig. 3.8. The spectrum shows a slight modulation due to the presence of side pulses 14 ps away from the main pulse. The total power contained in these unwanted pulses was estimated to be less than 1% meaning that their impact after amplification will be negligible.

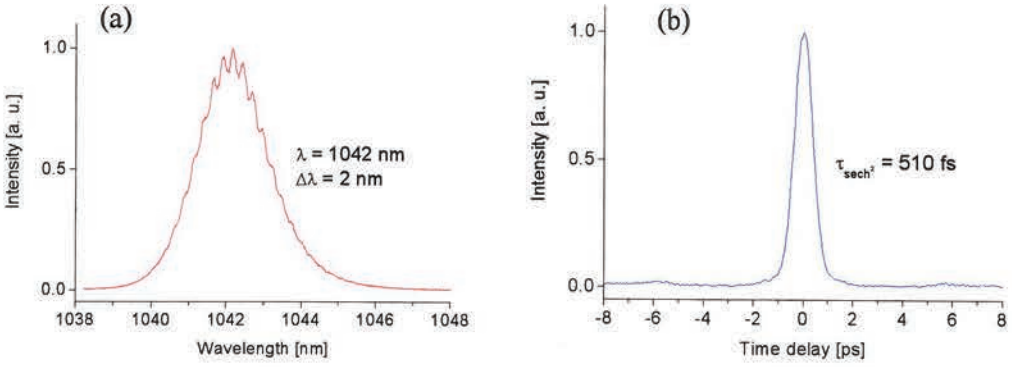

Fig. 3.8. Characteristics of the ML-VECSEL producing subpicosecond pulses. (a) Output spectrum with a bandwidth of 2 nm. (b) Autocorrelation trace of the output pulse with a duration of approximately 500 fs.

Both ML-VECSELs produce diffraction limited beam quality and sufficient average power to saturate an Yb-doped fibre amplifier which can then eventually seed other amplifiers for very high power amplification as described in the following sections.

3.4 High average power femtosecond fibre MOPA design

The VECSELs seed cascaded amplifiers to form a MOPA system as depicted in Fig. 3.9. Since each MOPA was designed according to the seed characteristics, the system is described here in a general manner and further details will be provided latter. The pulses produced by the VECSELs are launched into a fiberised isolator and are then preamplified by one or two YDFAs depending on the seed power level to an average power sufficient to saturate the final high-power fibre amplifier stage. The preamplified beam is brought into free space, collimated and passed through a half-wave plate for partial polarisation control and a free-space single-polarisation isolator. It is then launched into the final-stage power amplifier through a lens chosen for adequate mode matching. The power amplifier consists of a double-clad LMA Yb-doped fibre with a D-shaped 400 μm thick inner cladding. The fibre is pumped through its output end by a diode stack source emitting around 975 nm. Dichroic mirrors placed at both fibre ends separate the signal from the pump beam.

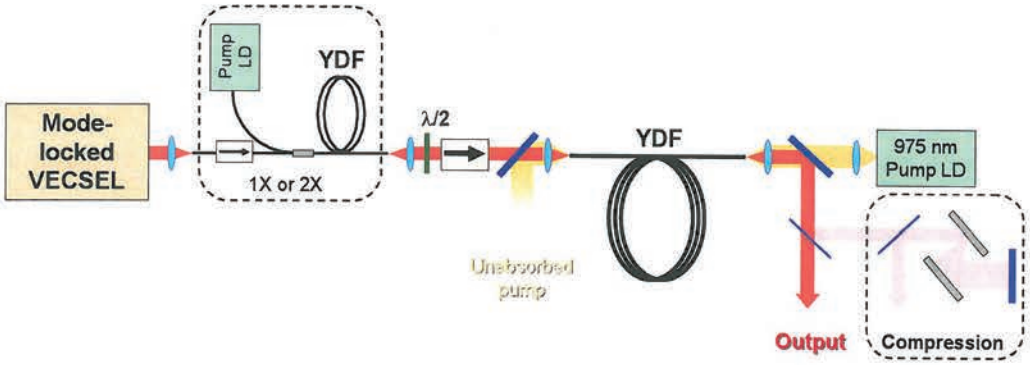

Fig. 3.9. Exprimental arrangement for high-power fibre amplification of passively M-L VECSELs for the generation of high repetition rate picosecond - femtosecond pulses at very high average power. LD: laser diode; $\lambda/2$: half-wave plate.

Average powers, optical spectra and intensity autocorrelation traces are measured at the output of the high-power YDFA. A fraction of the energy is also extracted to investigate the temporal compression characteristics with a reflection bulk grating compressor composed of a pair of 600 lines/mm gratings employed in double-pass configuration with variable spacing. Since a proper chirp analysis technique such as FROG was not available, output compression with bulk grating offers valuable information to investigate the nonlinear regime of amplification.

3.5 Results on amplification of ultrashort pulses from VECSELs

This section presents an experimental demonstration aiming to compare amplification of high repetition rate picosecond pulses with various durations to high average powers and their subsequent compression to generate femtosecond pulses. Computer simulations based on NLSE will also be carried out to analyse the experimental results.

3.5.1 Fibre amplification of 4.6 ps pulses: SPM regime of amplification

Experimental demonstration

We first investigate fibre amplification of pulses with a duration of 4.6 ps and a repetition rate of 910 MHz produced by VECSEL A. The advantage of such relatively long pulses and high repetition rate is that the resulting lower peak power places few constraints on the fibre parameters to achieve short pulses after nonlinear amplification and compression even at high average power. The pulses were amplified to 2 W of average power by cascaded 6- and 8-m long single-mode cladding-pumped YDF preamplifiers. The signal is then launched into the final-stage cladding-pumped YDF, fabricated at the ORC (fibre reference: F453-LF202), with a length of 12 m, a core diameter of 25 μm and a numerical aperture NA < 0.05 providing a large effective area as well as excellent beam quality (M^2 < 1.1, see Chapter 4) when the fundamental mode is selectively excited.

The power amplifier generated more than 255 W of average output power for 350 W of launched pump power. The corresponding slope efficiency was 76% as shown in Fig. 3.10. The output beam was spectrally and temporally characterised up to 200 W of average output power. Instabilities precluded reliable measurements at higher powers.

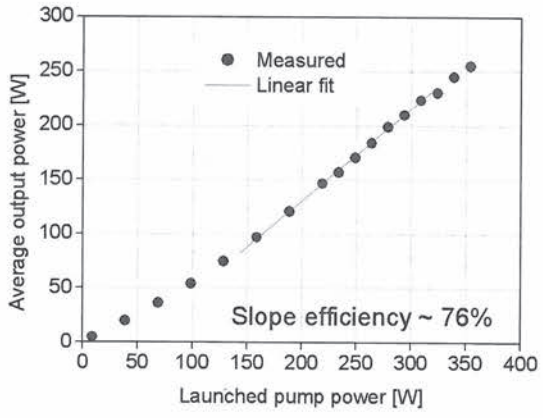

Fig. 3.10. Power conversion characteristics of the final-stage amplifier pumped by a high-power diode stack emitting at 975 nm and seeded by 2 W average power of pre-amplified pulses produced by VECSEL A.

As the power increases the level of ASE rises and severe spectral broadening caused by SPM is also observed with linewidth up to 9 nm as shown in Fig. 3.11. The spectral shape is typical for the regime where SPM dominates over dispersion due to the relatively long pulses. The slight asymmetry of the output spectrum may be attributed to asymmetric seed pulses or to polarisation effects in the non-PM YDFA.

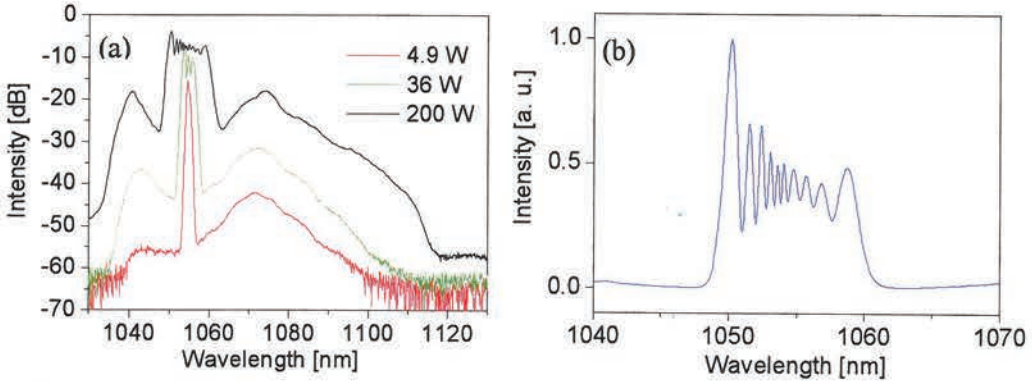

Fig. 3.11. (a) Output spectra measured at various output powers (resolution 0.2 nm) and (b) spectrum at 200 W in linear scale (resolution 0.1 nm).

As the 4.6 ps long pulses propagate in the fibre, they undergo both the effect of SPM and linear dispersion. As a result there is a small increase in pulse duration. Fig. 3.12(a) illustrates this by comparing the autocorrelation trace of the seed and the amplified signal. At 200 W the fibre MOPA produces 6.3 ps pulses, assuming a Gaussian pulse shape. This corresponds to a peak power of 38 kW, which is sufficiently low to keep stimulated Raman scattering at a low level as confirmed by the spectrum in Fig. 3.11(a). The output spectrum with a conventional SPM broadening ensures a reasonably linear chirp in the central part of the pulses. This indicates that pulses can be compressed using bulk gratings for linear compression. At each power level the grating separation was adjusted to optimize pulse compression. With a grating separation of 11 cm, output pulses were compressed down to an autocorrelation time of 430 fs corresponding to 280 fs duration for $sech^2$ pulses. Fig. 3.12(b) shows the autocorrelation trace of the compressed pulse. There is a significant pedestal due to nonlinearities in the chirp along the pulse as expected in the SPM dominated amplification regime with non-parabolic pulses.

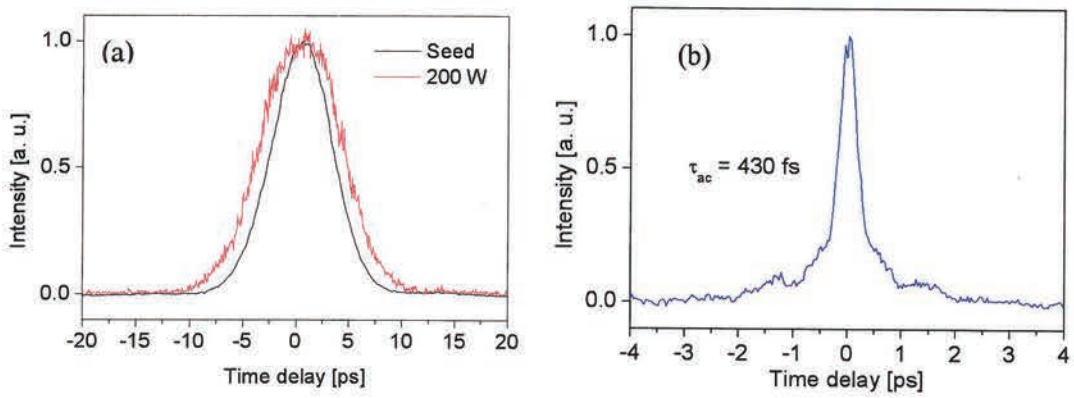

Fig. 3.12. Autocorrelation traces of (a) seed, uncompressed and (b) compressed pulses measured at the output of the fibre MOPA system. The MOPA was seeded by 4.6 ps long pulses which were amplified to 200 W of average output power.

Numerical simulations

Pulse propagation in the final stage of amplification was numerically simulated by solving the nonlinear Schrödinger equation using the split-step Fourier method. The experimental parameters previously introduced for the fibre amplifier and the master oscillator are used for the simulations. The mode field diameter of the fibre was taken to be 22 μm and typical values for dispersion $\beta_2 = 25\text{x}10^{-3}$ $ps^2.m^{-1}$, third order dispersion $\beta_3 \sim 6\text{x}10^{-5}$ $ps^3.m^{-1}$, and nonlinear index $n_2 = 3.2\text{x}10^{-20}$ $m^2.W^{-1}$ are used. The resulting spectrum reported in Fig. 3.13(a) shows typical features of the SPM-dominated regime of amplification as observed in the experimental spectrum. The simulated spectral linewidth is approximately 10 nm. The corresponding pulse duration is 7 ps and the chirp shape confirms the SPM dominated regime of amplification with a linear chirp in the centre of the pulse and significant nonlinear patterns on its edges. The simulated compressed pulse has a pulse duration of about 280 fs for gratings separated by 20 cm in single-pass which agrees well with the experiment and includes a small pedestal which is however lower than the one obtained in the actual system. Therefore, this experimental pedestal can be partly attributed to polarisation mode dispersion in the non-PM YDFA.

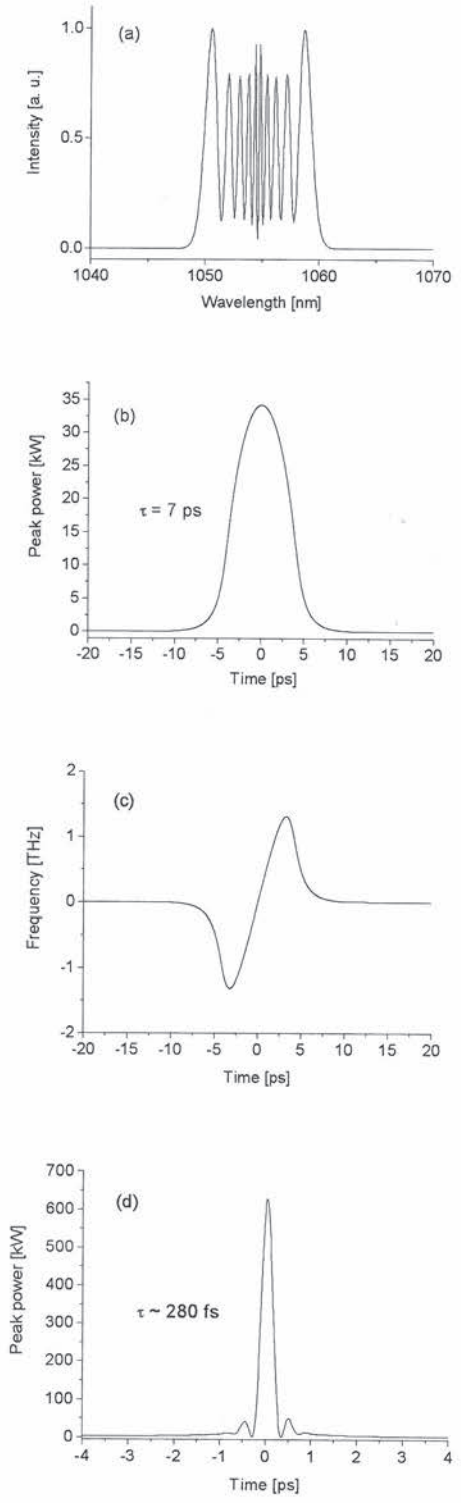

Fig. 3.13. Numerical simulations for the fibre amplifier at 200 W of output power (a) output spectrum, (b) pulse shape, (c) chirp characteristics, and (d) compressed pulse

Discussion

Amplification of 4.6 ps pulses in the fibre MOPA leads to significant SPM induced spectral broadening. Due to the relatively long pulse duration, the system operates in a regime where SPM dominates and linear dispersion becomes negligible. This enables linear compression to femtosecond pulses with a typical pedestal confirmed by numerical simulations. The use of shorter pulses with sufficient energy would allow the generation of parabolic pulses after amplification for the production of cleaner and shorter compressed pulses. The actual compression efficiency was not quantified here as only a fraction of power was extracted for the study. Grating compressors are highly sensitive to polarisation and the fibre MOPA was not designed to operate on a single polarisation. The use of a non-PM YDFA implies that the output polarisation state may vary as a function of power causing severe reduction in the final compression efficiency. Consequently in the next experiment, not only shorter pulses are used but high-power amplification will be done in a PM-YDFA.

3.5.2 Fibre amplification of 0.5 ps pulses: self-similar regime of amplification

Experimental demonstration

For fibre amplification in the SS regime, the fibre MOPA system was designed so that parabolic pulses are generated in the final high-power amplifier. The fibre was chosen to meet the design considerations reported in [21] and numerical simulations allowed verification of the convergence towards parabolic pulses after amplification.

An attractive feature of ML-VECSELs is the ability of producing ultrashort pulses at gigahertz repetition rate enabling the generation of parabolic pulses at high average power after amplification in conventional step index fibres as long as the designs considerations for self-similar amplification are taken into account. To demonstrate this, and to investigate the power scalability in the parabolic pulse regime, we used VECSEL B producing 500 fs pulses at 1.1 GHz as a master oscillator. Since VECSEL B produces higher power than VECSEL A, only one preamplifier is included in the MOPA. This is a 2 m long cladding-pumped YDF with 20 μm core and 128 μm cladding (Coractive HPA-Yb-20-02). The YDF was forward-pumped by a 915 nm laser diode launched through the end of the YDF via a lens. The use of the short fibre with a large core and a relatively small inner cladding ensured minimum pulse distortion by fibre nonlinearities and dispersion. The large core to cladding area ratio also shifted the gain of the YDFA to shorter wavelengths, as is typical for systems with ground-state absorption of the signal [28]. Thus the YDFA was well suited to amplification at 1040 nm. After transmission through the free-space isolator shown in Fig. 3.9, the amplified pulses with an average power of 1.3 W and a duration of about 0.7 ps were launched into the YDF of the final-stage amplifier. This was an 8 m long double-clad PM-YDF fabricated in-house with

a mode-field diameter of 16 μm and a birefringence of 3.5×10^{-4}. This fibre was chosen for its effective area, which is suitable for obtaining appropriate amounts of SPM, with sufficient pump absorption and without significant SRS. The use of a polarisation-maintaining fibre (operating on a single birefringence axis) eliminates any polarisation fluctuations that may affect autocorrelation measurements. A half-wave plate was used to align the seed beam polarisation axis to the slow axis of the PM-YDF. At 1.1 GHz repetition rate the required energy level to reach the parabolic pulse amplification regime in this fibre dictates a watt-level average power which is also sufficient to saturate the final-stage amplifier.

The signal was amplified up to 53 W of average power with 100 W of launched pump power as reported in Fig. 3.14. The power evolution is slightly nonlinear due to the power dependence of the pump wavelength, and hence of the pump absorption. At maximum output power the pump diode emitted near 973 nm where the Yb absorption is increased. Note that the need to keep the YDF short to overcome ground-state absorption of the 1040 nm signal also reduced the pump absorption, to values between 57 and 79%, depending on the pump power. This explains the relatively low amplifier efficiency. The output beam quality was measured to be approximately 1.1 times diffraction limited.

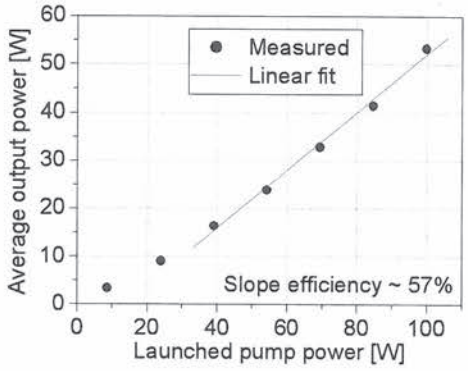

Fig. 3.14. Power conversion characteristics of the final-stage amplifier pumped by a high-power diode stack emitting at 973 nm and seeded by 1.3 W average power of pre-amplified pulses produced by VECSEL B.

Output spectra measured at different average powers are shown in Fig. 3.15(a)-(b). Starting with a seed with spectral width of 2 nm, the spectrum dramatically broadens to a bandwidth exceeding 15 nm at maximum power. The rapidly decreasing wings of the spectra are characteristic of parabolic amplification. As the power increases, the spectrum broadens asymmetrically.

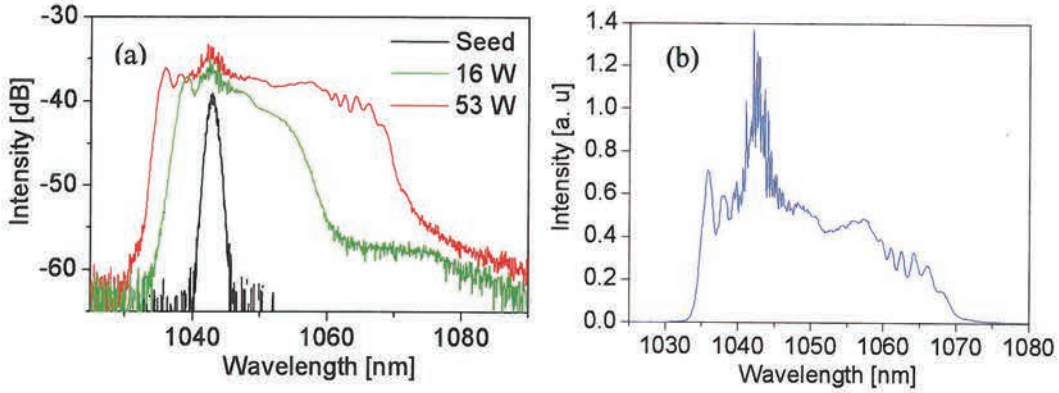

Fig. 3.15. (a) Output spectra measured at different output powers (resolution 0.2 nm) and (b) linear spectrum at maximum power (resolution 0.2 nm).

We also observed temporal broadening of the output pulses, which is typical of self-similar parabolic amplification in normally dispersive fibres. Autocorrelation measurements of the output pulse width at FWHM reveal an increase to between 2.2 ps and about 4.8 ps at minimum and maximum output power respectively (see Fig. 3.16(a)). The 4.8 ps pulses were compressed by the grating compressor down to an autocorrelation width of 170 fs for a grating separation of about 30 mm. This corresponds to a pulse duration of 110 fs FWHM assuming a $sech^2$ pulse shape, assumption commonly employed in similar fibre systems [4, 7] . The duty cycle becomes 10^{-4} and TBP ~ 0.47, close to the transform-limited value. Moreover the autocorrelation trace depicted in Fig. 3.16(b) emphasizes the excellent quality of the compressed pulses with very low pedestal, as opposed to the compression of the longer non-parabolic pulses described in the previous section. This reveals the high linearity of the chirp before compression, a characteristic of parabolic pulses. Moreover the use of a PM amplifier at the final stage provided higher stability in the measurement and would also result in increased compression efficiency.

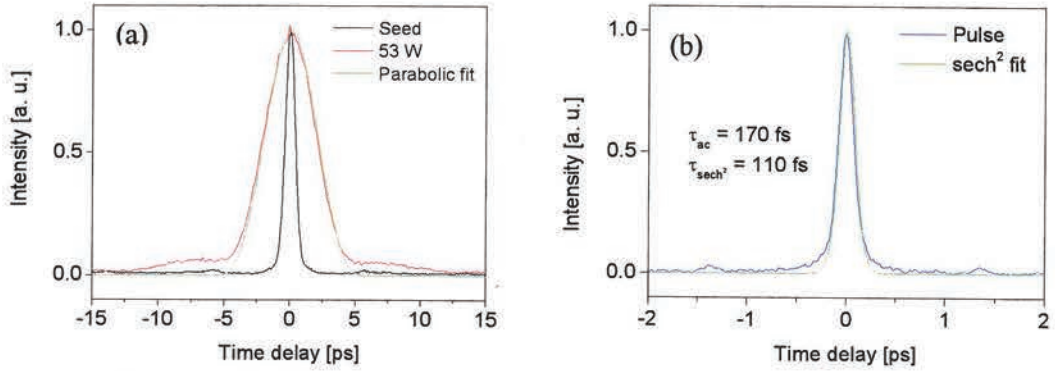

Fig. 3.16. (a) Autocorrelation traces of (a) seed, uncompressed and (b) compressed pulses measured at the output of the fibre MOPA system.

The laser system generated 48 nJ per pulse with picosecond range duration. Further power scaling was prevented by the absence of gain below 1035 nm which resulted in significant spectral and temporal distortions at higher powers.

Numerical simulations

The high-power fibre amplifier was also numerically simulated using the NLSE and incorporating the experimental parameters and the fibre parameters specified earlier. In a first analysis, the gain of the amplifier is considered independent of the emitting wavelength with a constant value g = 1.93 dB/m. The resulting simulated spectrum presents typical features of self-similar parabolic pulse amplification as expected with such seed pulses as shown in Fig. 3.17(a). The corresponding pulse shape and chirp are shown in Fig. 3.17(b)-(c). The typical parabolic pulse shape is revealed and the chirp evolution is linear across the pulse width. Linear temporal compression was also simulated and the resulting pulse shape is reported in Fig. 3.17(d) with a duration of 102 fs. This confirms the excellent quality of compression with very low pedestal. The TOD accounts for the asymmetric features of the pedestal. These simulations are in good agreement with the experimental results. However they do not explain the asymmetric spectrum obtained experimentally. Therefore in a second set of simulations, the gain profile of the amplifier is taken into account. It was approximated by a Lorentzian gain spectrum centered at 1060 nm with a bandwidth of about 40 nm typical for Yb-doped fibre amplifiers. The VECSEL emitting wavelength is now located at the edge of the gain profile leading to an asymmetric spectrum in excellent agreement with the experimental spectrum as shown in Fig. 3.17(e). This causes a distorted pulse shape with a duration of 5.5 ps and consequently slight nonlinearities are observed in the chirp compared to the ideal case as shown in Fig. 3.17(f)-(g). Consequently a larger pedestal is produced after compression and the compressed pulse duration becomes 128 fs. The calculated grating separation in a single-pass configuration is 63 mm which is in good agreement with the experimental value of 30 mm in a double-pass scheme. The gain bandwidth limitation results in a peak power reduction after compression from 450 kW down to 260 kW. Although the experimental autocorrelation trace of the compressed pulse does not reveal a significant pedestal, the resulting pulse duration matches the simulated value.

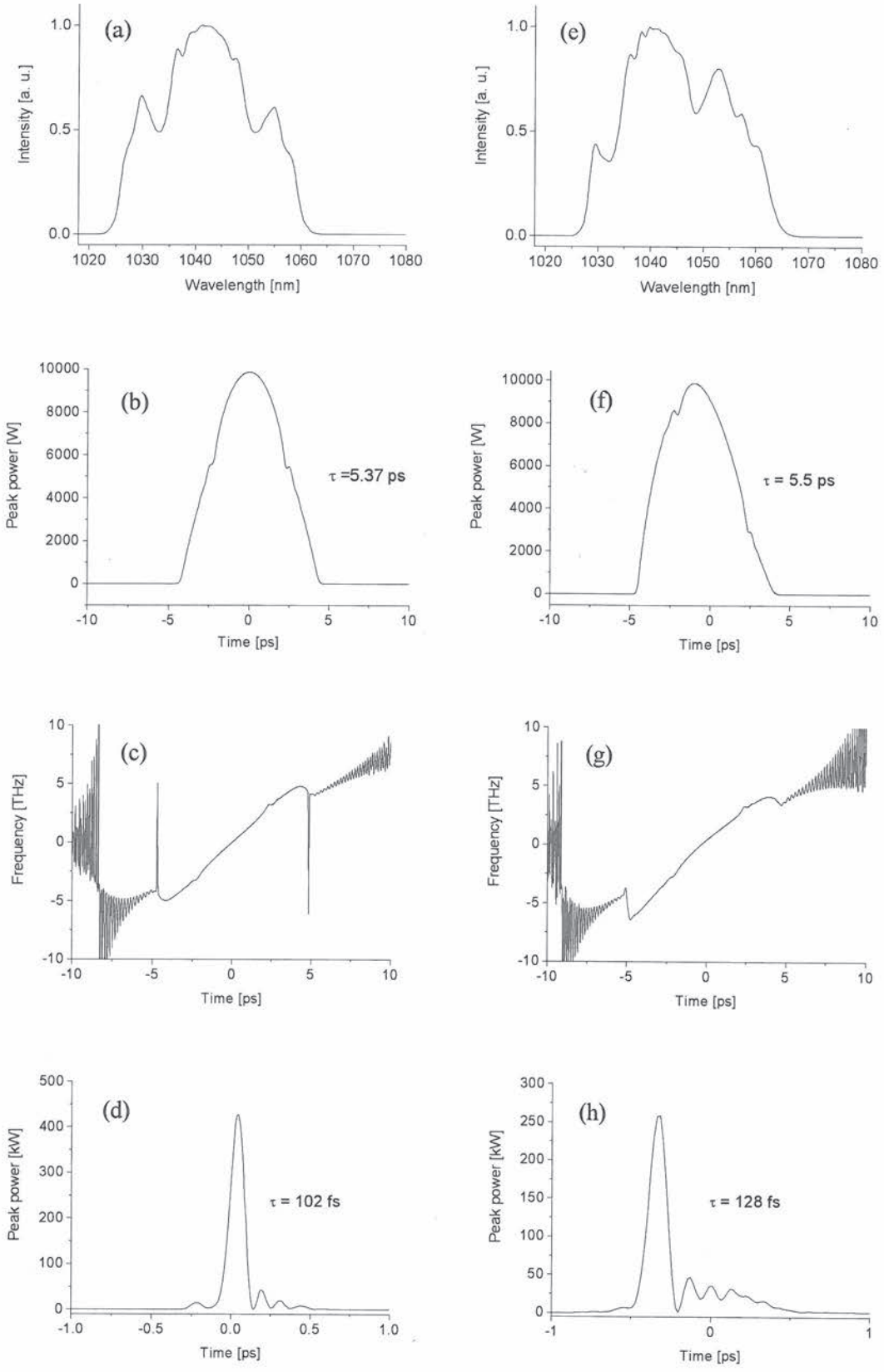

Fig. 3.17. Simulated output characteristics assuming constant gain: (a) spectrum, (b) pulse shape, (c) chirp, and (d) compressed pulse shape. Simulated output characteristics assuming a Lorentzian gain profile: (e) spectrum, (f) pulse shape, (g) chirp, and (h) compressed pulse shape.

These numerical simulations are in good agreement with the experimental results and explain well the output spectral shape as well as the resulting duration of the compressed pulse. It confirms that despite the generation of an asymmetric spectrum, it is possible to produce relatively clean femtosecond pulses at high average power. However the mismatch of the Yb gain profile and the seed emitting wavelength degrade significantly the compression efficiency resulting in lower output peak power.

Discussion

Although the generation of clean femtosecond pulses with average power exceeding 50 W of average power have been successfully demonstrated, higher average power was prevented by the mismatch between the seed laser wavelength and the YDFA gain spectrum. This problem can be overcome by either changing the peak gain wavelength of the YDFA or tuning the emitting wavelength of the VECSEL to longer wavelengths such as 1060nm.

Assuming a constant Yb concentration, the gain profile of an YDFA can be shifted by changing the fibre geometry. For instance a shorter fibre leads to a shift of gain to shorter wavelengths. However this also leads to less efficient operation as well as more constraints on the input pulse parameters to reach the parabolic pulse shape after amplification due to the shorter effective length in the amplifier.

Another approach consists in changing the core to cladding ratio of the fibre amplifier. Keeping the same inner cladding dimension, a larger core size would indeed shift the gain to shorter wavelength but it would also reduce the nonlinear coefficient γ and the fibre length resulting in lower nonlinear effects. On the other hand, reducing the cladding size may dramatically reduce the pump launch efficiency or may restrict the system to the use of low power high-brightness pump diodes limiting significantly the output average power.

Therefore designing a VECSEL emitting at wavelengths more compatible with the Yb gain characteristics appears more suitable. A central wavelength of 1060-1070nm would enable fibre amplification and parabolic pulse generation to powers exceeding 100 W similarly to the results reported with VECSEL A.

3.6 Conclusion

In summary, we have investigated high-power fibre amplification of picosecond and sub-picosecond pulses at gigahertz repetition rates to high average powers. The nonlinear regime of amplification was exploited to produce strongly chirped pulses that can be linearly compressed with bulk gratings. This type of system based on a MOPA configuration and capable of producing high average power is much simpler than CPA-based fibre lasers and

can generate pulses much shorter than the seed pulse duration after compression. Nevertheless efficient pulse compression at high average power requires specific attributes from the Yb-based fibre MOPA. At high repetition rate, the relatively low pulse energy implies that the pulse duration becomes a very important parameter to increase peak power. This chapter has described the pulse evolution in a fibre amplifier as a function of input pulse duration. It was demonstrated that amplified ultrashort pulses undergo pulse shaping induced by a combination of dispersion and SPM and asymptotically converge to a parabolic pulse shape with well defined pulse duration and a linear chirp. For longer pulses with identical energy, longer length of amplification is required to generate a parabolic pulse shape. This was demonstrated experimentally by realising two high-power MOPAs seeded by a two VECSELs with different pulse durations.

A first demonstration employed 4.6 ps pulses amplified to 200 W of average power. There was significant SPM relative to the linear dispersion effects. Thus the pulses did not reach the parabolic regime, and there were nonlinearities in the chirp which severely degraded the pulse compression in a subsequent grating compression. The second experiment involved fibre amplification of shorter sub-picosecond pulses in which adequate balance of normal dispersion and SPM generated parabolic shaped pulses with linear chirp leading to excellent pulse compression at an average power of 53 W.

This latest experiment represents the first demonstration of high-power parabolic pulse generation with GHz repetition rate in the 1 micron wavelength range. Clean pulse compression was experimentally demonstrated, however numerical simulations reveal sub-patterns suggesting that parabolic pulse generation was not necessarily of the best quality. Further power scaling was limited by a mismatch in the gain spectrum of the YDFA and the VECSEL emitting wavelength causing this degradation in the simulated compressed pulses. The eventual design of a new VECSEL seed source with an emitting wavelength ideally located in the Yb gain spectrum would enable the generation of femtosecond pulses of excellent quality with average powers exceeding hundred watt level. This new type of source would be suitable for many applications including THz generation [29].

This novel combination of VECSEL and high-power Yb-doped fibre amplifiers opens up a new route towards the development of high brightness, high average power, gigahertz, femtosecond pulsed sources emitting in the 1-1.1 micron wavelength range.

References

1. K.-H. Liao, K.-C. Hou, G. Chang, V. Smirnov, L. Glebov, R. Changkakoti, P. Mamidiputi, and A. Galvanauskas, "Diffraction-limited 65-μm core Yb-doped LMA fiber high energy CPA systems," CLEO/QELS 2006, Postdeadline paper CPDB4, (2006).

2. F. Röser, J. Rothhard, B. Ortac, A. Liem, O. Schmidt, T. Schreiber, J. Limpert, and A. Tünnermann, "131 W 220 fs fiber laser system," Opt. Lett. **30**, 2754-2756 (2005).

3. M. E. Fermann, V. I. Kruglov, B. C. Thomson, J. M. Dudley, and J. D. Harvey, "Self-similar propagation and amplification of parabolic pulses in optical fibers," Phys. Rev. Lett. **84**, 6010 (2000).

4. A. Malinowski, A. Piper, J. H. V. Price, K. Furusawa, Y. Jeong, J. Nilsson, and D. J. Richardson, "Ultrashort-pulse Yb^{3+}-fiber-based laser and amplifier system producing >25-W average power," Opt. Lett. **29**, 2073-2075 (2004)

5. J. Limpert, A. Liem, T. Gabler, H. Zellmer, A. Tünnermann, S. Unger, S. Jetschke, and H. -R. Müller, "High-average-power picosecond Yb-doped fiber amplifier ," Opt. Lett. **26**, 1849-1851 (2001)

6. T. Schreiber, C. K. Nielsen, B. Ortac, J. Limpert, and A. Tünnermann, "Microjoule-level all-polarization-maintaining femtosecond fiber source," Opt. Lett. **31**, 574-576 (2006).

7. J. Limpert, T. Schreiber, T. Clausnitzer, K. Zöllner, H. Fuchs, E. Kley, H. Zellmer, and A. Tünnermann, "High-power femtosecond Yb-doped fiber amplifier," Opt. Express **10**, 628-638 (2002).

8. D. Strickland and G. Mourou, "Compression of amplified chirped optical pulses," Opt. Commun. **56**, 219-221 (1985).

9. M. Pessot, P. Maine, and G. Mourou, "1000 Times expansion/compression of optical pulses for chirped pulse amplification," Opt. Commun. **62**, 419-421 (1987).

10. A. Galvanauskas, M. E. Fermann, and D. Harter, "High-power amplification of femtosecond optical pulses in a diode-pumped fiber system," Opt. Lett. **19**, 1201-1203 (1994).

11. A. Galvanauskas, P.A. Krug, and D. Harter, "Nanosecond-to-picosecond pulse compression with fiber gratings in a compact fiber-based chirped-pulse-amplification system," Opt. Lett. **21**, 1049-1051 (1996).

12. C. J. S. De Matos, J. R. Taylor, T. P. Hansen, K. P. Hansen, and J. Broeng, "All-fiber chirped pulse amplification using highly-dispersive air-core photonic bandgap fiber," Opt. Express **11**, 2832-2837 (2003).

13. C. J. S. De Matos and J. R. Taylor, "Chirped pulse Raman amplification with compression in air-core photonic bandgap fiber," Opt. Express **13**, 2828-2834 (2005).

14. J. Limpert, T. Schreiber, S. Nolte, H. Zellmer, and A. Tünnermann, "All fiber chirped-pulse amplification system based on compression in air-guiding photonic bandgap fiber," Opt. Express **11**, 3332-3337 (2003).

15. D. Anderson, M. Lisak, and P. Anderson, "Nonlinearly enhanced chirp pulse compression in single-mode fibers," Opt. Lett. **10**, 134-136 (1985).

16. J. Limpert, T. Clusnitzer, A. Liem, T. Schreiber, H. J. Fuchs, H. Sellmer, E. B. Kley, and A. Tünnermann, "High average-power femtosecond fiber chirped-pulse amplification system," Opt. Lett. **20**, 1984-1986 (2003).

17. A. Galvanauskas, "Mode-scalable fiber-based chirped pulse amplification systems," IEEE J. Select. Top. Quantum Electron. **7**, 504-517 (2001).

18. A. Galvanauskas, G. C. Cho, A. Hariharan, M. E. Fermann, and D. Harter, "Generation of high-energy femtosecond pulses in multimode-core Yb-fiber chirped-pulse amplification systems," Opt. Lett. **26**, 935-937 (2001).

19. M. E. Fermann, V. I. Kruglov, B. C. Thomsen, J. M. Dudley and J. D. Harvey, "Self-Similar Propagation and Amplification of Parabolic Pulses in Optical Fibers", Phys. Rev. Lett. **84**, 6010-6013 (2000).

20. V. I. Kruglov, A. C. Peacock, J. D. Harvey, and J. M. Dudley, "Self-similar propagation of parabolic pulses in normal-dispersion fiber amplifiers ," J. Opt. Soc. Am. B **19**, 461-469 (2002).

21. C. Finot, F. Parmigiani, P. Petropoulos, and D. Richardson, "Parabolic pulse evolution in normally dispersive fiber amplifiers preceding the similariton formation regime," Opt. Express **14**, 3161-3170 (2006).

22. D. B. Soh, J. Nilsson, and A. B. Grudinin, "Efficient femtosecond pulse generation using a parabolic amplifier combined with a pulse compressor. II. Finite gain-bandwidth effect," J. Opt. Soc. Am. B **23**, 10-19 (2006).

23. G. Chang, A. Galvanauskas, H. G. Winful, and T. B. Norris, "Dependence of parabolic pulse amplification on stimulated Raman scattering and gain bandwidth," Opt. Lett. **29**, 2647-2649 (2004)

24. D. B. Soh, J. Nilsson, and A. B. Grudinin, "Efficient femtosecond pulse generation using a parabolic amplifier combined with a pulse compressor. I. Stimulated Raman-scattering effects," J. Opt. Soc. Am. B **23**, 1-9 (2006).

25. A. Garnache, S. Hoogland, A.C. Tropper, I. Sagnes, G. Gaint-Girons and J.S. Roberts, "Sub-500-fs soliton-like pulse in a passively mode-locked broadband surface-emitting laser with 100 mW average power," Appl. Phys. Lett. **80**, 3892-3894 (2002)

26. S. Hoogland, S. Dhanjal, A. C. Tropper, J. S. Roberts, R. Haring, R. Paschotta, F. Morier-Genoud, U. Keller, "Passively mode-locked diode-pumped surface-emitting semiconductor laser," IEEE Photonics Technol. Lett. **12**, 1135-1137 (2000).

27. J. Nilsson, W. A. Clarkson, R. Selvas, J. K. Sahu, P. W. Turner, S.-U. Alam, and A. B. Grudinin, "High-power wavelength-tunable cladding-pumped rare-earth-doped silica fiber lasers", Opt. Fiber Technol. **10**, 5-30 (2004).

28. G. Matthäus, T. Schreiber, J. Limpert, S. Nolte, G. Torosyan, R. Beigang, S. Riehemann, G. Notni, and A. Tünnermann, "Surface-emitted THz generation using a compact ultrashort pulse fiber amplifier at 1060 nm," Opt. Commun **261** (2006) 114-117 (2006)

Chapter 4 High average power picosecond fibre sources

4.1 Introduction

Laser sources capable of generating picosecond pulses at high average power are very attractive for many applications including micromachining, laser display and harmonic generation in nonlinear media. For this reason, in recent years there has been an increasing interest in the development of high average power ultrashort pulse sources by the use of various technologies and configurations. Conventional solid-state mode-locked oscillators can directly produce high average powers. Such lasers are based on passive mode-locking of a laser cavity composed of a combination of either thin-disk gain or rod structure with a SESAM [1, 2]. Further power scaling can also be achieved by employing a MOPA configuration. However thermal effects arising in the bulk crystals are the main limiting factor for further increase of average power [3]. Therefore MOPA configuration based on Yb-doped fibre amplification appears to be an alternative technology for power scaling ultrashort pulse sources. Such sources have been demonstrated by fibre amplification of bulk mode-locked Nd:YVO_4 lasers [4] and mode-locked fibre lasers [5]. However, although the relatively low repetition rate of the order of tens of MHz allowed the generation of high energy, the average output power was limited to tens of watts because of the onset of nonlinear effects such as SPM and SRS despite the use of LMA fibres. A method to mitigate nonlinear effects while achieving high power resides in increasing the repetition rate of the master oscillator. In this section, I will describe the development of high-power fibre sources based on the amplification of a laser diode gain-switched at a repetition rate reaching up to 1 GHz. This Chapter reports on the investigation of power scaling of such sources and nonlinear effects associated with various fibre amplifiers aiming for the realisation of efficient harmonic generation.

4.2 Gain-switched laser diode at 1.06 μm

Optical Time Division Multiplexing (OTDM) was proposed as a technique to increase the capacity of communications systems. This technology enables bit rates up to Terabit per second, requiring the generation of picosecond and sub-picosecond pulses in a flexible format. Gain-switching of semiconductor lasers has proved to be a very attractive method to produce picosecond pulses for communication systems [6] due to its simplicity, versatility, low-cost and compatibility with high-speed telecommunications components. Consequently there has been extensive work on the development of gain-switched laser diodes emitting in the telecommunications wavelength bands [7-9]. These types of laser diodes have also been employed as seed sources for high-power Er:Yb doped fibre based sources to produce high average power in the eye-safe window [10].

Consequently the recent progress in high-power fibre laser and amplifier technology and the need for simple generation of nanosecond pulses from a fibre pigtailed device has led to the development of high-speed laser diodes emitting in the 1 μm wavelength. These diodes can be directly modulated and offer a simple alternative to expensive master oscillators to generate nanosecond pulses in a flexible format. Their potential for gain-switching is also of great interest to produce picosecond pulses in a well controlled way.

4.2.1 Gain-switching of laser diode

The gain-switching of semiconductor laser diodes [11-13] was first introduced by Ito et al. [13] as a simple technique to generate picosecond pulses with a repetition rate dictated by the driving electronics. Gain-switching relies on the fast modulation of the gain in the semiconductor laser. As opposed to direct modulation of a laser diode where optical pulses generated by a laser diode tend to follow the driving electrical pulse shape, gain-switching generates optical pulses much shorter than the electrical pulse durations. The key attractions of gain-switching are its simplicity and its capability to adjust the repetition rate continuously in a wide range without modifying the laser cavity.

The principle of gain switching is based on the excitation of relaxation oscillation in the laser diode. When driven with electrical pulses biased below threshold, the laser generates a series of relaxation oscillation spikes. The idea is to terminate the electrical pulses before the onset of the second optical peak so that a single pulse much shorter than the electrical pulse is produced.

Fig. 4.1 illustrates the principle of gain-switching. Initially the current pulse is biased below the threshold current i_{th} where the photon density remains very low. Then the rapid injection of electrons raises the carrier density to a level above lasing threshold resulting in the rapid increase of the photon density via stimulated emission. This results in the quick depletion of the

electron density which stops the photon emission. If the current is maintained constant at this point, the photon density will oscillate, generating a succession of spikes until it eventually reaches a steady state. Once again, terminating the injection of electron after the first depletion of the carrier density enables the generation of a single spike. Although such peaks are extremely short (few tens of picoseconds), the reduction in pulse duration is limited by the difficulty in sustaining a large initial inversion before optical emission.

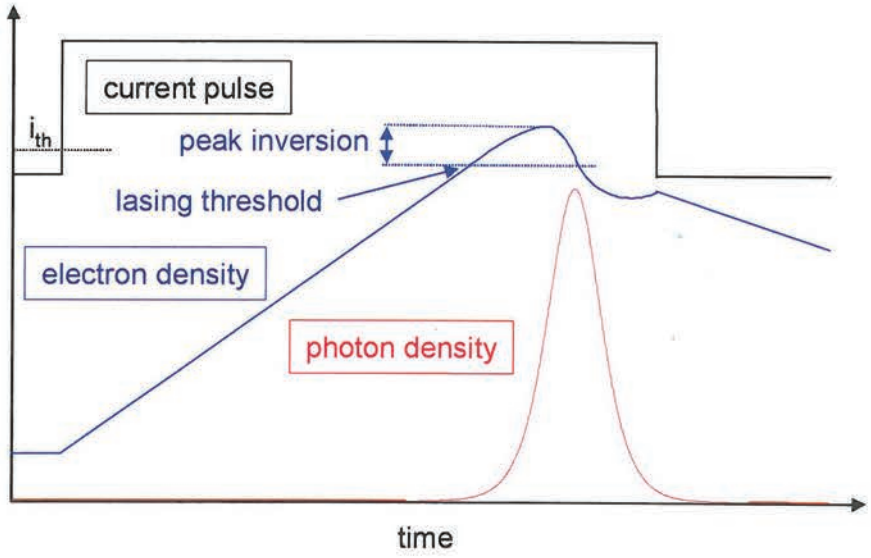

Fig. 4.1. Schematic illustrating gain-switching of a semiconductor laser.

4.2.2 Gain-switched laser diode at 1060 nm

A system based on a gain-switched laser diode emitting at 1060 nm was developed by Andy Piper with the aim to employ it as a novel master oscillator for a fibre MOPA system [14]. The system is presented schematically in Fig. 4.2. It is composed of an InGaAsP Fabry-Pérot semiconductor laser mounted on a PCB circuit board that incorporates an impedance of 47 Ω. This ensures impedance matching between the forward resistance of the laser diode of 3 Ω and the 50 Ω of a standard radio-frequency (RF) cable.

The laser diode was gain-switched by driving it with a 1 GHz, 35.6 V peak to peak amplitude sinusoidal electrical signal generated by a signal generator (HP 8647A) and amplified with an RF amplifier. The signal generator provided an RF output power of 0 dBm which was split with a 6 dB splitter to feed and saturate the RF amplifier and allow triggering of a high-speed oscilloscope. The laser was biased below threshold by applying a DC voltage via a bias-T and a DC block which provided isolation from low frequencies components (<10 kHz) between the DC bias source and the RF modulation signal. It is worth noting that in this configuration the output repetition rate does not depend on the cavity length of the laser diode and can be

continuously adjusted with the signal generator offering increased versatility compared to other picosecond pulsed seed sources.

At room temperature, the FP laser diode is characterized by a lasing wavelength of approximately 1048 nm, a threshold current of 20 mA and a modulation bandwidth exceeding 1.3 GHz. The temperature of the diode is increased to shift the peak gain of the cavity wavelength towards 1060 nm. The laser diode operates on few longitudinal modes with a mode spacing of 0.2 nm. Single longitudinal mode locking is provided by injection seeding with a CW narrow linewidth (<100 kHz) laser consisting of a DFB fibre laser emitting at 1059.94 nm coupled through a 90/10 fibre coupler. The seed polarisation is adjusted with a polarisation controller to maximize optical coupling and to optimize injection. The diode temperature was also tuned for optimal coupling between the longitudinal modes of the FP diode and the fixed seed wavelength. As a result, injection seeding not only ensures single longitudinal mode operation but provides increased SMSR and reduced timing jitter. A single longitudinal mode can also be selected internally by gain-switching a DFB laser diode making the system simpler and more compact [15].

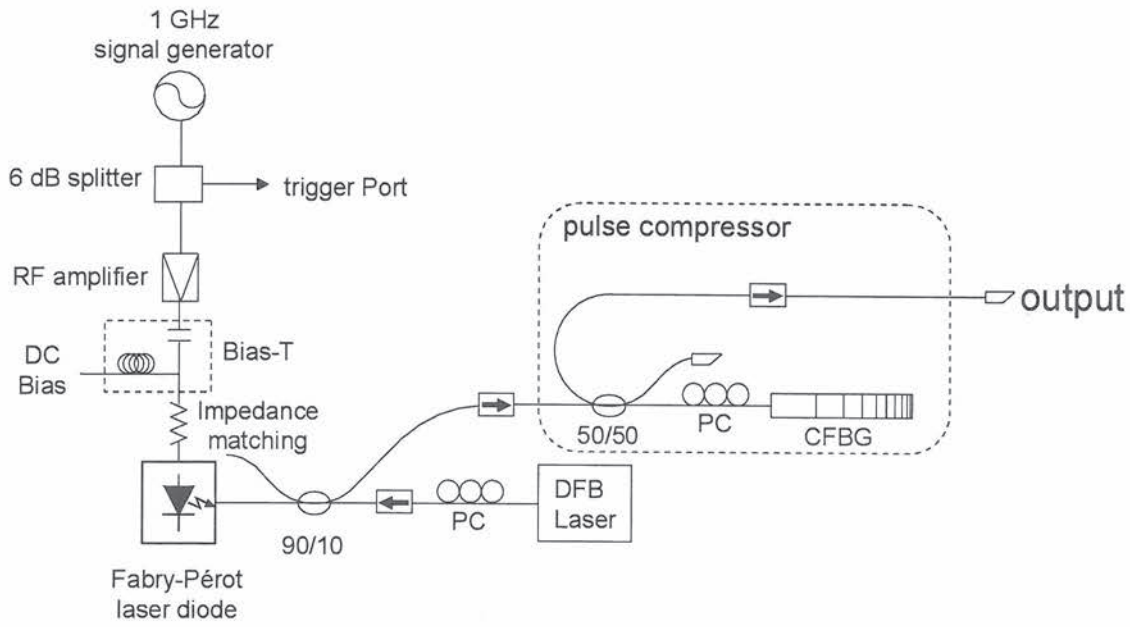

Fig. 4.2. Experimental set-up of the picosecond pulsed seed source based on a gain-switched laser diode at 1060 nm.

The output pulse shape produced by the laser diode gain-switched at 1 GHz is shown in Fig. 4.3(e). CW seed power and bias current were optimized to 0.1 mW and 8.1 mA respectively to increase the SMSR to more than 30 dB and minimize timing jitter. This resulted in the

generation of pulses of about 60 ps FWHM duration with a linewidth of 0.16 nm and a corresponding timing jitter of 2.2 ps. The average power produced by the pulsed diode in this configuration was 7 mW.

The 60 ps chirped pulses are compressible through 15 km of standard single mode fibre (SMF-28, multimode at 1 μm); however, this leads to significant loss (roughly 12.7 dB) for the signal because of the high absorption of SMF-28 at 1060 nm as well as the necessity for mode-filtering at the fibre output. The corresponding total dispersion value was 671 ps/nm. Based on this measurement, a chirped fibre Bragg grating was designed and fabricated at the ORC for optimal pulse compression with reduced loss. I have incorporated and characterised the CFBG based pulse compressor to the gain-switched laser diode system. The CFBG is characterized by a peak reflectivity of 78% at 1059.9 nm and a 3 dB bandwidth of 0.48 nm. Since fiberised circulators at 1060 nm were not available at the time of the experiment, the CFBG was used in reflection after transmission through a 3 dB coupler causing 7 dB of overall loss. The compressed pulse autocorrelation trace is presented in Fig. 4.3 (f). The resulting pulse duration was ~16 ps with excellent spectral characteristics as the CFBG provided also narrowband filtering as shown in Fig. 4.3 (a-d). The FWHM spectral width was 0.16 nm ($\Delta\tau.\Delta\nu \sim 0.7$) corresponding to a time-bandwidth product $\Delta\tau.\Delta\nu \sim 0.68$ which is nearly twice the TBP of a Fourier transform limited $Sech^2$ pulse. An interesting feature of the gain-switched diode is that the amount of chirp and the consequent level of compression vary as a function of seed power.

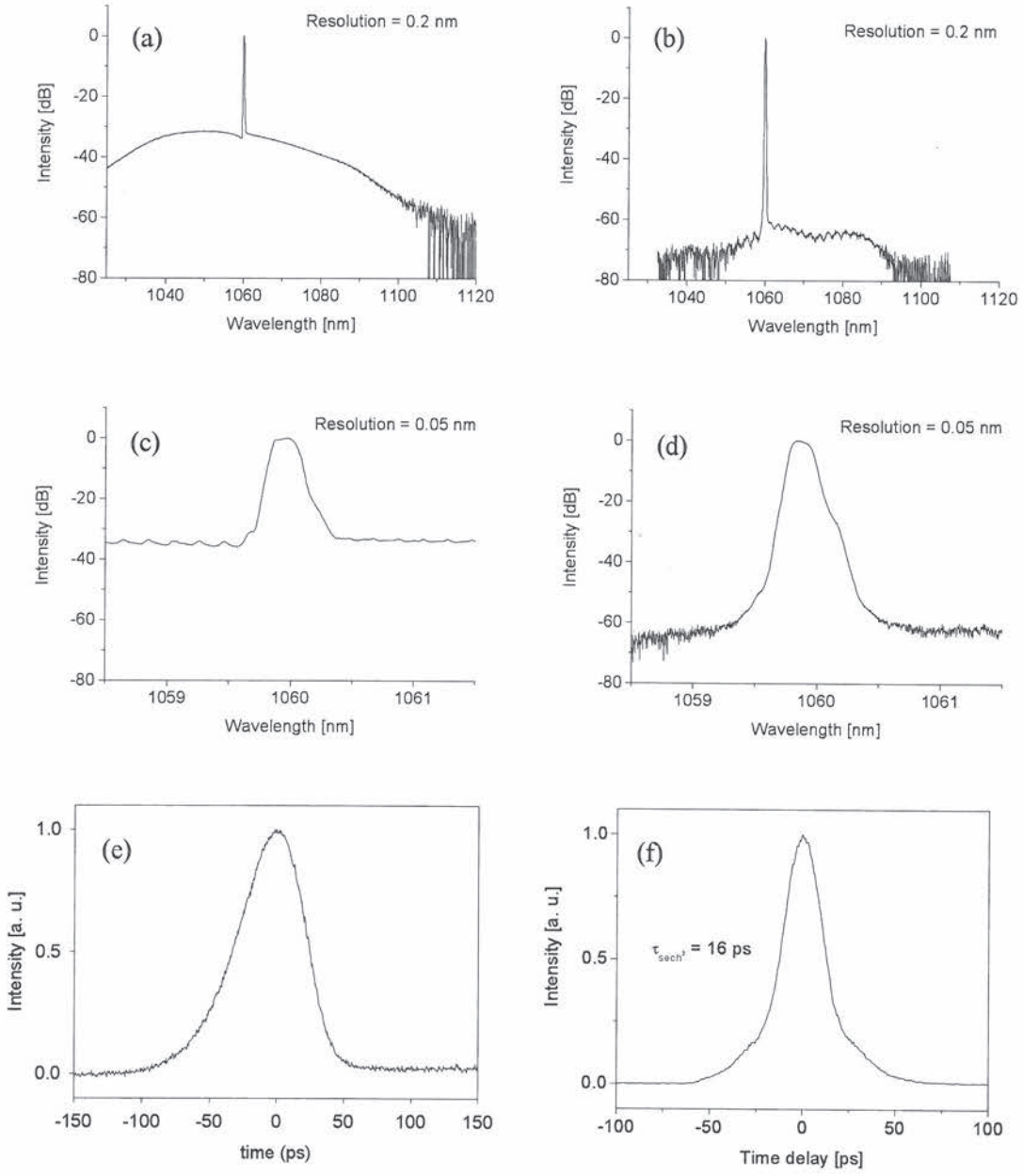

Fig. 4.3. Broad spectra of uncompressed (a) and compressed (b) output pulsed signal. Closer view of the same spectra for uncompressed (c) and compressed (d) system. (e) Pulse shape measured with a 20 GHz digital communication analyzer before compression. (f) Autocorrelation trace of a compressed pulse with a pulse duration of 16 ps.

4.3 High average power picosecond fibre MOPA design

The gain-switched laser diode system presented earlier appears very attractive for fibre amplification to high average power. The continuously variable repetition rate would allow fine

control of the output pulse even at high-power after amplification. In addition the pulsed laser wavelength suits very well most Yb-doped fibre amplifiers. Here I report experimental demonstrations of fibre amplification of the gain-switched laser diode to average powers exceeding 100 W with a maximum record power of 320 W. Although the repetition rate can be electrically tuned in a wide range, this section concentrates on results obtained with 1 GHz modulation.

Starting with the pulsed laser diode, a chain of amplifiers was built to reach high average power with an effort to limit nonlinear degradation, and particularly self-phase modulation. The fibre-based MOPA configuration is presented in Fig. 4.4. The compressed pulses are first amplified by a 4 m long core-pumped Yb-doped fibre preamplifier and then by a cladding-pumped YDFA GTWave® with a fibre length of 6 m and core diameter of 10 μm, pumped by two 915 nm diodes. The double-clad fibre is then spliced to an 8 m, 12.3 μm core (NA<0.05), double-clad Yb-doped fibre pumped by a 975 nm diode that amplifies the signal up to 3 W of average power. Isolators are placed between amplifier stages to prevent unwanted feedback. After transmission through a high power free-space isolator (OFR IO-5-1064-HP) with 1.5 dB of insertion loss, the signal is launched into the final high-power fibre amplifier stage. The cladding-pumped fibre power amplifier is pumped in a counter-propagating scheme by a diode stack capable of producing up to 550 W of power at 975 nm. Dichroic mirrors are placed at each side of the doped fibre to separate signal and pump beams. This pumping configuration allows maximum efficiency while reducing nonlinear effects in the doped fibre.

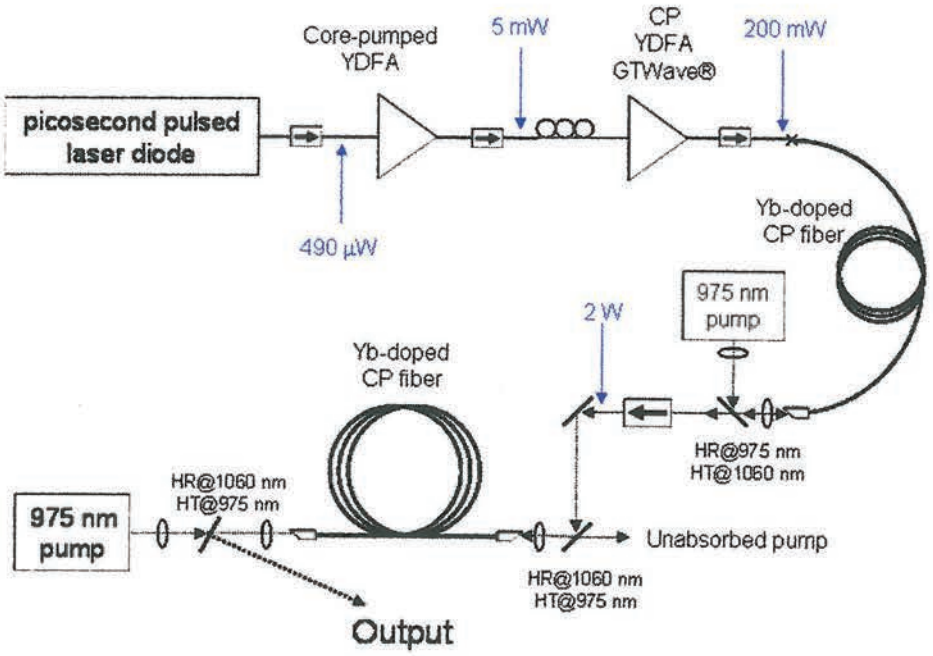

Fig. 4.4. Experimental arrangement for the high average power fibre MOPA system. Average powers measured at various stages are reported in blue.

Various Yb-doped fibres were incorporated in the high-power amplification stage leading to different output characteristics. These fibre characteristics were all designed to offer high launch efficiency from the pump beam with a large inner cladding and sufficient absorption for efficient operation with a large highly doped core.

4.3.1 Output characteristics before high-power amplification

The purpose of the amplification stages before the high-power final stage amplifier is to increase the signal power to a level sufficient to saturate the final amplifier stage. However, it is important to do this while minimizing any nonlinear distortion and reducing noise such as spontaneous emission arising from successive amplification.

Fig. 4.5. shows the evolution of the signal spectrum through cascaded amplification, as the signal is amplified. While the core-pumped amplifier is well designed for amplification at 1060 nm, amplification in the second amplifier based on GTWave® technology has a peak gain near 1080 nm due to a relatively long length and small core to cladding ratio which causes a rise of ASE at this wavelength. As expected, ASE is accumulated through successive amplification. However spectral and temporal measurements reveal insignificant distortions up to 3 W preamplification thanks to the use of a LMA Yb-doped fibre.

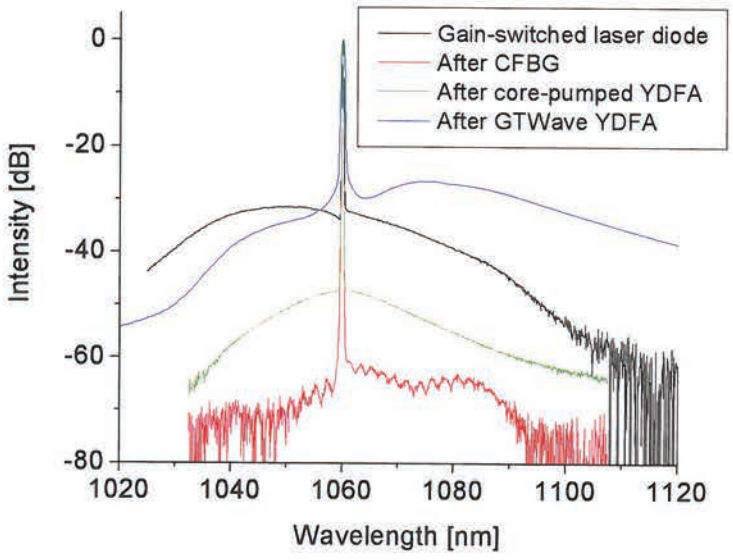

Fig. 4.5. Normalised spectra at various stages of amplification. All spectra acquired with a resolution = 0.2 nm except spectrum after GTWave YDFA with resolution = 0.5 nm.

4.3.2 Picosecond fibre laser with diffraction limited output beam

The choice of Yb-doped fibre dictates the output characteristics. A large effective area is required to mitigate nonlinear effects and a low numerical aperture is also important to reduce the number of modes amplified in the fibre. The interest of this section is in the generation of high average power with picosecond pulses in a diffraction limited output beam. The active fibre selected for this experiment has already been described in chapter 3 and used for amplification of pulses produced by a VECSEL. It is a D-shaped double-clad 360/400 μm cladding with an Yb-doped core of 25 μm in diameter and with an NA < 0.05 (fibre reference: F453-LF202). With a normalised frequency V of ~3, single-mode operation of the amplifier is achieved by exciting properly the fundamental mode of the doped fibre with adequate signal launch lens configuration; coiling was not used for mode filtering. The fibre length was 8 m and the total pump absorption was about 4.5 dB. This relatively low absorption is due to a low Yb concentration required to reduce the NA of the fibre.

In this experiment the gain-switched laser diode produced 18 ps pulses. The laser output characteristics are shown in Fig. 4.6. A maximum average output power of 125 W was achieved with slope efficiency of 79% with respect to absorbed pump power at the final amplifier stage (Fig. 4.6(a)). The nonlinear evolution of the output power with respect to launched pump power observed in Fig. 4.6(b) was caused by the pump wavelength drift towards the peak absorption of the ytterbium at 976 nm. The relatively short fibre amplifier became more efficient as pump power increased with a maximum conversion efficiency of 57%.

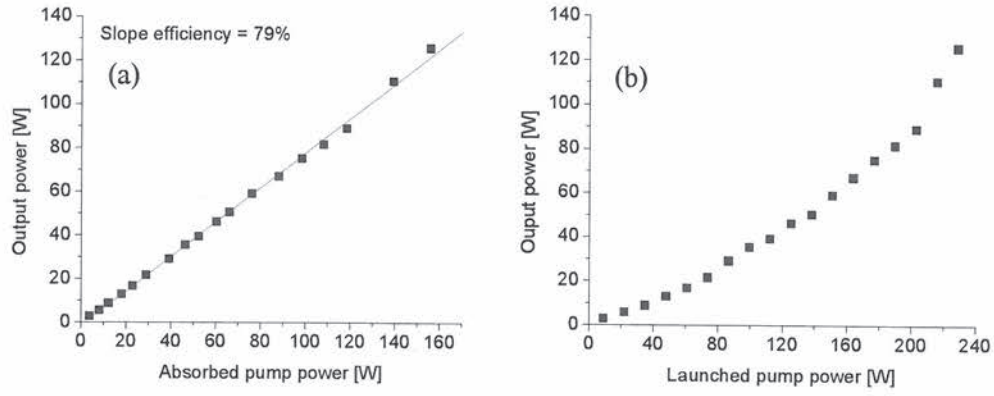

Fig. 4.6. Output power characteristics for the high-power fibre amplifier incorporating a large core fibre amplifier with respect to (a) absorbed pump power, and (b) launched pump power

The output beam quality factor or M^2 was measured with a scanning slit profiler beamscan from Photon Inc. and calculated to be approximately 1.1 as reported in Fig. 4.7. This

excellent output beam quality confirms the adequate single-mode excitation into the high-power fibre amplifier without the need for coiling.

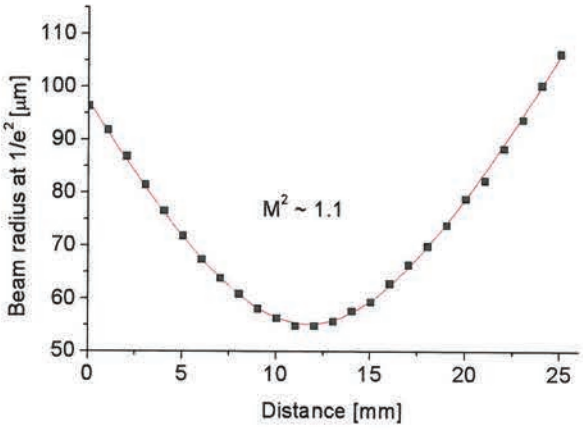

Fig. 4.7. Beam quality measurement at the laser output showing quasi-diffraction limited output beam with $M^2 \sim 1.1$.

The output spectra measured at 13 W and 125 W average power are shown in Fig. 4.8. They reveal clean amplification with a signal to ASE extinction ratio exceeding 22 dB. The ASE rises preferentially at shorter wavelengths near 1040 nm due to the short absorption length of the fibre amplifier. As expected, stimulated Raman scattering was not observed.

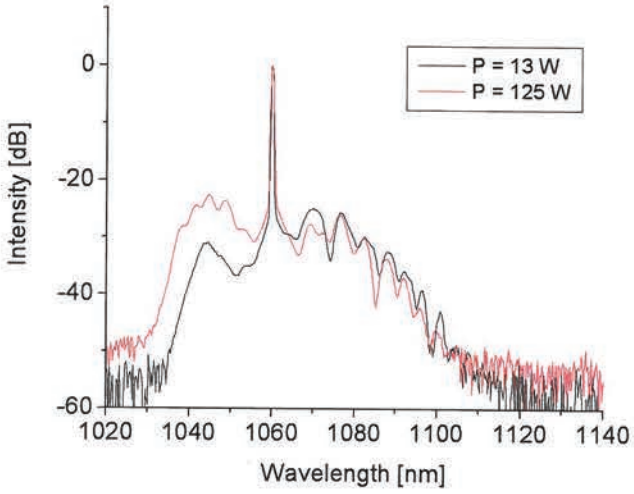

Fig. 4.8. Output spectra measured at 13 and 125 W (resolution = 0.5 nm).

Autocorrelation traces measured at various levels of amplification and reported in Fig. 4.9(a) show very little pulse distortion after propagation through the cascaded fibre amplifiers and after high-power amplification. However, spectral broadening is observed as power increases

due to self-phase modulation as presented in Fig. 4.9(b). The final spectral linewidth reached about 0.4 nm at maximum power.

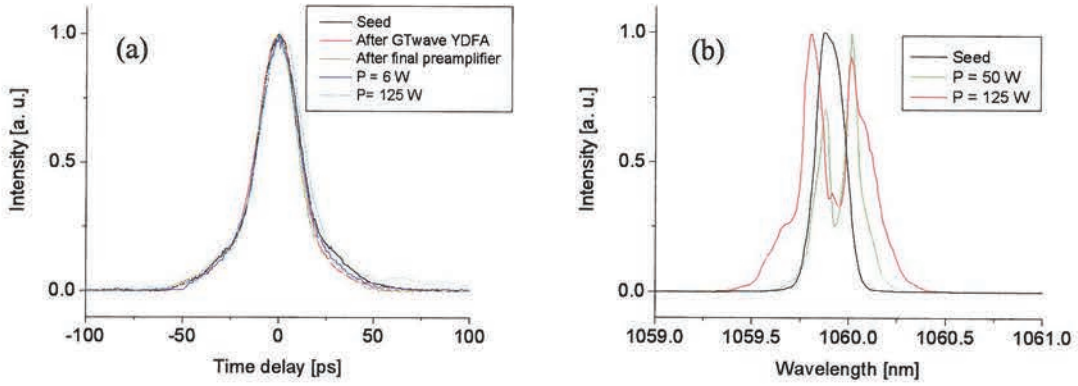

Fig. 4.9. (a) Autocorrelation traces measured at various power levels. (b) Linear spectra at various power depicting SPM-induced spectral broadening (resolution = 0.05 nm).

SPM-induced spectral broadening was modelled by solving numerically the NLSE (Eq. 3.1) incorporating a fibre with an effective area of 380 μm^2, a nonlinear index coefficient $n_2 \approx 3.2 \times 10^{-20}$ m^2/W and assuming seed pulses with Fourier transform $sech^2$ pulse shape undergoing amplification under constant gain. The calculated linewidth evolution as a function of average output power shows a good agreement with the measured spectral width as shown in Fig. 4.10. Few discrepancies can be observed at low and high output powers. At low power, the assumption of an unchirped seed pulse significantly underestimates the spectral bandwidth, while at high-power, fluctuations in polarisation may reduce the value of the nonlinear coefficient. Since autocorrelation measurements are polarisation dependent, this point was confirmed where unstable autocorrelation traces were observed as pump power was increased. This may also partially explain the difference between the measured and calculated spectral shape plotted in inset in Fig. 4.10.

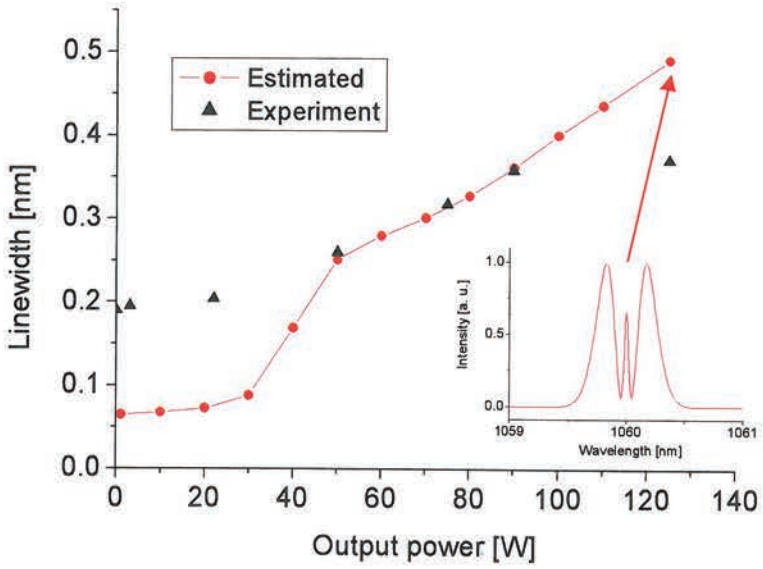

Fig. 4.10. Spectral linewidth evolution as a function of output power.

A novel picosecond fibre laser based on amplification of a gain-switched laser diode was realized to produce 125 W at 1 GHz with 18 ps pulse duration. The developed fibre MOPA system offers a diffraction limited output beam quality provided by a low NA Yb-doped and proper single-mode excitation of the final fibre amplification stage. The output linewidth reaches 0.5 nm for 7 kW of peak power. Further increase of average power was limited by the relatively low launched and absorbed pump power and would have resulted in increased spectral broadening.

Therefore the following section explores further power scaling of the laser system by employing a high-power Yb-doped fibre amplifier with larger cladding and core diameters for increased launched pump power and absorbed pump power respectively. The larger core also ensures reduced nonlinear spectral broadening.

4.3.3 Power scaling of the picosecond fibre MOPA with a large core Yb-doped fibre

Many applications such as nonlinear frequency conversion require high average power and high peak power while maintaining reasonably narrow linewidth, for instance below 1 nm. The spectral broadening of an initially unchirped pulse approximated by a Gaussian pulse shape is given by Eq 2.36 and when power evolution is taken into account [16] becomes:

$$\partial\omega_{NL}^{\max}(z) = e^{-1/2}\sqrt{2}\frac{\gamma P_0 L_{eff}}{T_0}, \tag{4.1}$$

where L_{eff} is the effective length defined by:

$$L_{eff} = \frac{\exp(-gL)-1}{g}, \tag{4.2}$$

with g corresponding to the fibre amplifier gain, and L the fibre length. Therefore a strategy to minimize spectral broadening while increasing peak power consists in scaling up the Yb-doped core size. Here I have chosen to employ a fibre already designed and made at the ORC to achieve 1 kilowatt from a continuous-wave fibre laser [17]. This fibre (F349-LF134) had been originally designed with a larger D-shaped inner cladding to maximize pump launch efficiency with diode stack laser diodes. Hence a larger core was required to increase pump absorption and maintain the fibre length sufficiently short to reduce loss and minimise stimulated Raman scattering. Here the large core provides another advantage: it reduces nonlinear distortion such as self-phase modulation. The fibre had an Yb-doped core of 43 μm in diameter with a numerical aperture of 0.09. The D-shaped inner cladding had a 650/600 μm diameter for the longer/shorter axis and was coated with a low index polymer coating providing a nominal NA of 0.48. The pump absorption rate in the inner cladding was ~3 dB/m at the pump wavelength. The fibre length used in the final stage of amplification was 8 m.

The power amplifier was seeded with 2 W and the gain-switched laser diode generated pulses with 20 ps duration. When pumped with 430 W of power at 975 nm the fibre produced about 320 W of average power with a corresponding slope efficiency of 78% with respect to launched pump power (79% w. r. t. absorbed pump power) as shown in Fig. 4.11. As opposed to the MOPA presented in Sec. 4.3.2, the characteristics with respect to launched pump power is quasi linear since the laser diode stack temperature was kept constant. Furthermore with higher absorption, changes in absorption have smaller effect.

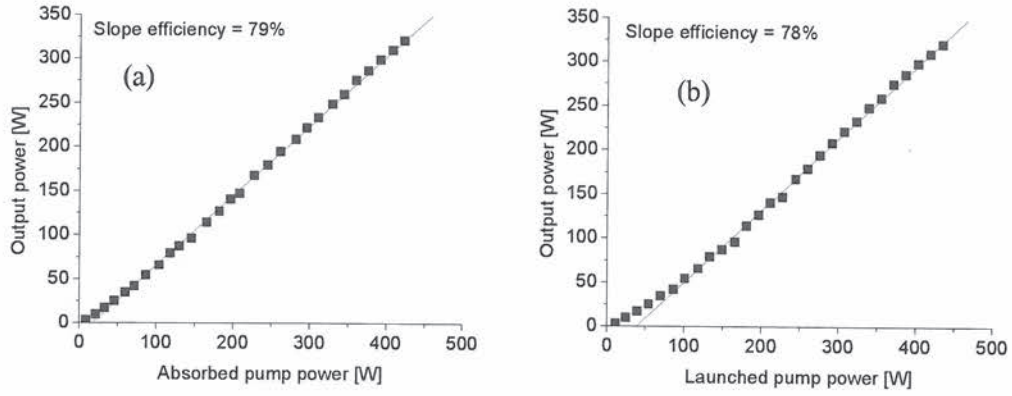

Fig. 4.11. Output power characteristics for the high-power fibre amplifier with a large core fibre amplifier with respect to (a) absorbed pump power, and (b) launched pump power

Despite providing many benefits, the large core is also characterised by a high V-parameter of 11.4 making single-mode operation extremely challenging. In laser configuration, where no mode selection technique was applied, the fibre offered a beam quality factor M^2~3.4 [17]. An improved performance can be expected from the fibre amplifier seeded by the fundamental mode. Despite the best efforts to enhance the beam quality of the system, the beam quality factor was measured to be 1.6 at average powers below 40 W and increased to 2.4 at higher powers as shown in Fig. 4.12. This result means that higher order modes are still propagating in the fibre amplifier.

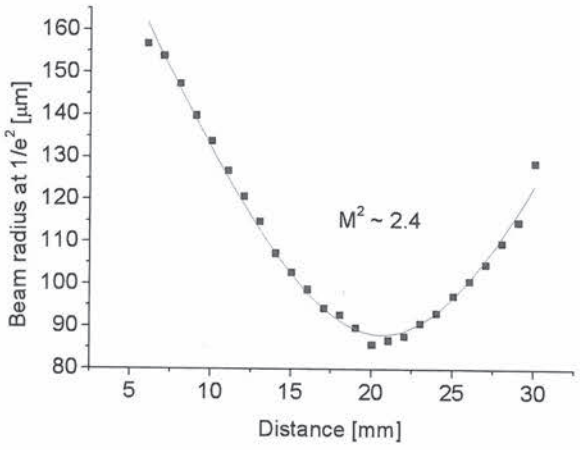

Fig. 4.12. Beam quality measurement at the output of the large core high-power fibre amplifier.

The optical spectra at low power and maximum power measured over a broad wavelength range are shown in Fig. 4.13. At 321 W of average output power the 1060 nm signal peak was 20 dB above the peak of the background ASE. Although the level of ASE increased significantly at the maximum power, it was estimated from the spectrum that the signal power represented 82% of the total average output power leading to an estimated peak power of 13 kW. Mid-stage spectral filtering would significantly improve the spectral quality. The stimulated Raman scattering threshold was estimated to be 76 kW peak power and, as expected, SRS was not observed even at the maximum power.

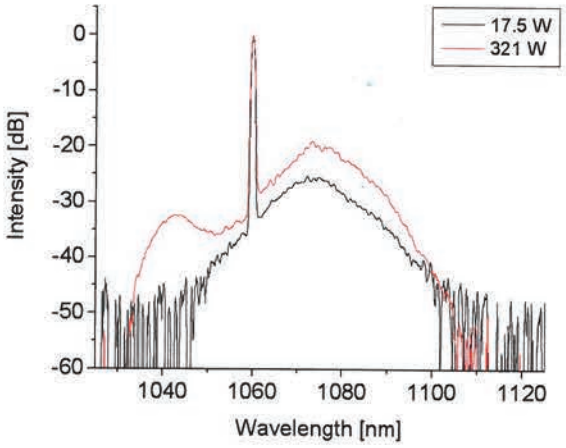

Fig. 4.13. Output spectra at 17.5 W and 321 W output powers (resolution = 0.5 nm).

Autocorrelation traces measured at various power levels up to 221 W reveal no degradation in either the 20 ps pulse duration or the pulse shape as illustrated in Fig. 4.14(a). While the degree of polarisation was not carefully monitored, measurement of autocorrelation relying on wave-plate alignment indicated variations of the state of polarisation at different output powers due to thermally induced birefringence fluctuations, making the measurement difficult. Therefore at power levels higher than 221 W, pulse shapes were only monitored with a 20 GHz communication analyser with a polarisation insensitive detector. However, we could not see any significant degradation of the pulse shape even at the maximum level of amplification (although the resolution of this observation was limited to the bandwidth of the detector).

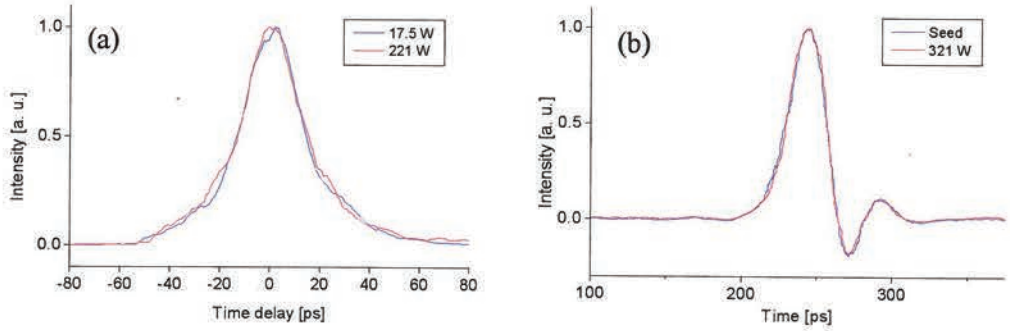

Fig. 4.14. (a) Autocorrelation traces at 17.5 W and 221 W output powers. (b) Pulse shapes measured with a 20 GHz DCA up to maximum output power.

A detailed view of the spectra and their evolution as a function of output power are presented in Fig 4.15(b). As a result of self-phase modulation, the 0.12 nm linewidth of the seed source, preserved at the input of the power amplifier, was broadened to 0.49 nm at 321 W of average power. This is still a relatively low value thanks to the large core area of the ytterbium-doped fibre and is fully compatible with frequency doubling, for example.

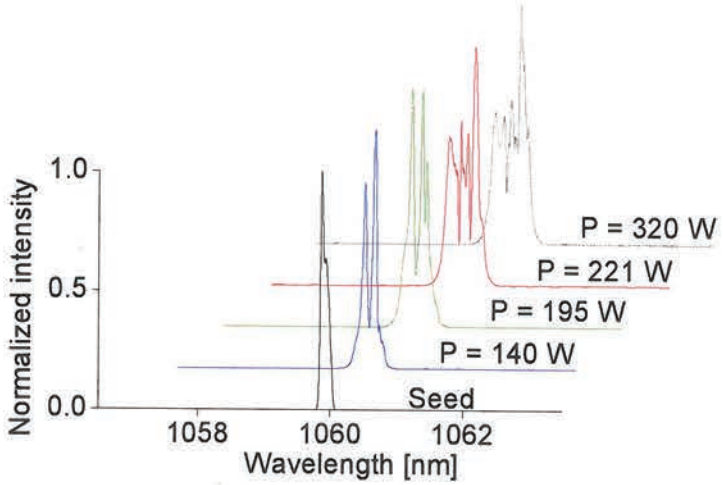

Fig. 4.15. Output spectra versus output power showing the spectral broadening evolution from $\Delta\lambda$ =0.12 nm of the laser diode seed to 0.5 nm at maximum output power.

Although the fibre amplifier supports several modes, calculations based on NLSE are still in good agreement with the measurements as illustrated in Fig. 4.16.

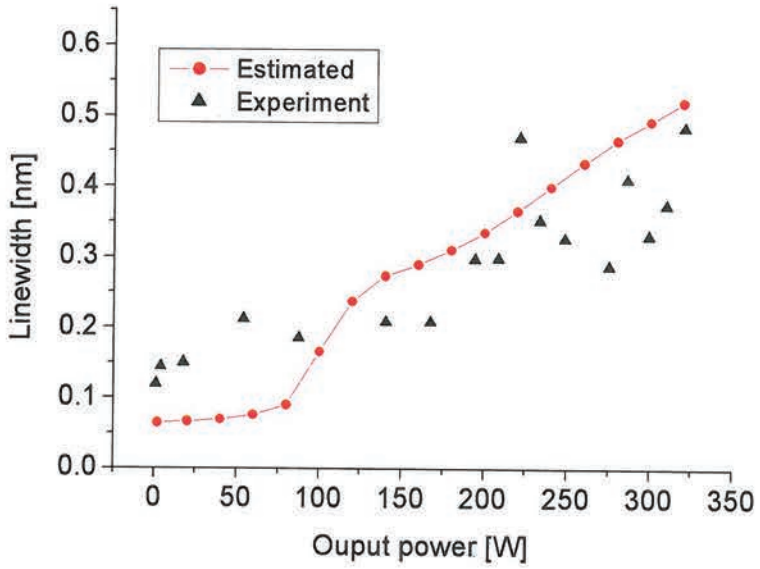

Fig. 4.16. Spectral linewidth evolution as a function of output power. The estimated laser linewidth was based on calculation of FWHM linewidths after numerical simulations.

4.4 Conclusion

This chapter described various experimental demonstrations illustrating strategies to power scale picosecond fibre lasers. These sources are suitable for frequency doubling as long as SPM is maintained below a critical level. Although a fibre amplifier with a large core mitigates this effect, the resulting beam quality can be degraded which may affect the application such as efficiency and stability of harmonic generation. In addition many applications are polarisation dependent and the fibre MOPA developed here were not designed for optimized polarisation control. This aspect will be considered in chapter 5.

Furthermore the electrically controlled master oscillator offers a continuously tunable repetition rate which enables the generation of various output peak powers at a fixed average power allowing some control on nonlinear effects. This benefit will be discussed in the following Chapter.

References

1. E. Innerhofer, T. Sdmeyer, F. Brunner, R. Hring, A. Aschwanden, R. Paschotta, C. Hnninger, M. Kumkar, and U. Keller, "60-W average power in 810-fs pulses from a thin-disk YbYAG laser ," Opt. Lett. **28**, 367-369 (2003)

2. L. McDonagh, R. Wallenstein, R. Knappe, and A. Nebel, "High-efficiency 60 W TEM_{00} Nd:YVO_4 oscillator pumped at 888 nm," Opt. Lett. **31**, 3297-3299 (2006)

3. C. Pfistner, R. Weber, H. P. Weber, S. Merazzi, and R. Gruber, "Thermal beam distortions in end-pumped Nd : YAG, Nd : GSGG and Nd : YLF rods," IEEE J. Quantum Electron. **30**, 1605-1615 (1994).

4. P.L. Mason, A. Wonfor, D.D. Marcenac, D.G. Moodie, M.C. Brierley, R.V. Penty, I.H. White and S. Bouchoule, "The effects of pedestal suppression on gain-switched laser sources for 40Gbitls OTDM transmission," LEOS TuS2, 289-290 (1997).

5. H. F. Liu, Y. Ogawa, and S. Oshiba, "Generation of an Extremely Short Single-Mode Pulse (Approximately-2ps) by Compression of a Gain-Switched Pulse from a 1.3 μm Distributed-Feedback Laser Diode," Appl. Phys. Lett. **59**, 1284-1286 (1991).

6. Y. Matsui et al., "Generation of wavelength tunable gain-switched pulses from FP MQW lasers with external injection seeding," IEEE Photon. Technol. Lett. **9**, 1087-1089 (1997).

7. J. Limpert, A. Liem, T. Gabler, H. Zellmer, A. Tünnermann, S. Unger, S. Jetschke, and H. -R. Müller, "High-average-power picosecond Yb-doped fiber amplifier," Opt. Lett. **26**, 1849-1851 (2001)

8. T. Schreiber, C. K. Nielsen, B. Ortac, J. Limpert, and A. Tünnermann, "Microjoule-level all-polarization-maintaining femtosecond fiber source," Opt. Lett. **31**, 574-576 (2006)

9. L. P. Barry et al., "Characterization of 1.55 μm pulses from a self seeded gain-switched Fabry-Perot laser diode using frequency-resolved optical gating," IEEE Photon. Technol. Lett. **10**, 935-937 (1998).

10. B.C.Thomsen, Y.Jeong, C.Codemard, M.A.F.Roelens, P.Dupriez, J.K.Sahu, J.Nilsson, D.J.Richardson, "60W 10GHz 4.5ps pulse source at 1.5microns", CLEO/IQEC 2004 San Francisco 16-21 May 2004 CMAA

11. H. Ito, H. Yokoyama, S. Murata, H. Inaba, "Picosecond optical pulse generation from an RF modulated AlGaAs Diode Laser ," Electron. Lett. **15**, 738-740 (1979).

12. P. L. Liu, C. Lin, I. P. Kaminow, and J. J. Hsieh, "Picosecond Pulse Generation from InGaAsP Lasers at 1.25 and 1.3 μm by Electrical Pulse Pumping," IEEE J. Quantum Electron. **17,** 671-674 (1981).

13. K. Y. Lau, "Gain Switching of Semiconductor Injection-Lasers," Appl. Phys. Lett. **52**, 257-259 (1988).

14. A. Piper, A.Malinowski, B.C Thomsen, D.J.Richardson, L. M. B. Hickey, and M. N. Zervas, "11.1 W average power, 20 ps pulses at 1 GHz repetition rate from a fiber-amplified gain-switched 1.06 μm Fabry-Perot laser diode," *CLEO/QELS 2005* Baltimore 23-26 May 2005 CTuCC3.

15. P. Gunning, R. Kashyap, A. S. Siddiqui, K. Smith, " Picosecond pulse generation of <5 ps from gain-switched DFB semiconductor laser diode using linearly step-chirped fibre grating," Electron. Lett. 13, 1066-1067 (1995).

16. G. P. Agrawal, *Nonlinear fiber optics, Second edition.* Academic Press (1995).

17. Y. Jeong, J.K. Sahu, D. N. Payne, and J. Nilsson," Ytterbium-doped large-core fibre laser with 1 kW of continuous-wave output power", Electron. Lett. **40**, 470-472 (2004).

Chapter 5 Efficient frequency-doubling of a picosecond fibre source

5.1 Introduction

The development of high average power sources producing ultrashort pulses in the visible spectrum has widespread applications including laser projection display and micromachining. Second-harmonic generation via single-pass external frequency doubling through a nonlinear crystal is the most convenient and efficient method to shift the optical power to shorter wavelengths. While this technique has been employed for many years in commercial bulk solid-sate lasers, the development of frequency doubled fibre sources is still in its early stages due to limitations inherent to optical fibres. Indeed high peak power is usually necessary to achieve efficient frequency conversion through a conventional nonlinear crystal. Nevertheless this same peak power can degrade the performance of the fibre systems due to nonlinear effects.

Despite these limitations and due to advances in fibre technology, 60 W of average power has been demonstrated in the green based on the frequency doubling of an Yb-based fibre source pulsed at 10 MHz with 5 ns pulse duration [1]. In this nanosecond regime, the onset of SRS in the fibre amplifier constitutes the main limitation. In addition to SRS, fibre amplification of shorter picosecond pulses is also affected by SPM which, as will be presented in this chapter, represents a major challenge for achieving efficient frequency-doubling of an ultrafast fibre based-source.

Chapter 4 has already described the development of a high-power picosecond fibre sources with high brightness and reduced SPM-induced spectral broadening. The experimental study presented in this chapter will be based on an improved design of this fibre MOPA source. In this chapter I will first introduce key design requirements to efficiently frequency double a picosecond fibre source. Then I will apply these considerations to the demonstration of high-power SHG at 530 nm.

5.2 Second-harmonic generation

Second-harmonic generation, also called frequency-doubling, is a very convenient and efficient technique to extend the laser radiation to shorter wavelengths and in particular to the visible part of the optical spectrum. A principal challenge of this technique is to convert most optical power of the fundamental frequency to its second harmonic utilizing a nonlinear crystal.

The second harmonic can be generated by various optical schemes designed to maximize frequency conversion of beams with different pulsed or cw characteristics. They include intracavity [2, 3], external resonant [4] and single-pass external frequency doubling. Here the analysis focuses on single-pass external nonlinear frequency doubling where a pulsed fundamental beam is focused into the nonlinear crystal and generates the second harmonic along the crystal length.

5.2.1 Phase matching

Second-harmonic generation is a nonlinear optical process which converts a laser beam into a new laser beam with twice the optical frequency of the input beam. This phenomenon is enhanced, when the phase velocity of the fundamental beam matches the phase velocity of the second harmonic beam: this is called phase matching. The adequate crystal used for high-power SHG is based on type I phase matching (later described) and in the following study, I will assume only this type of phase-matching.

Nonlinear frequency conversion increases with the crystal length only when phase velocities are adequately matched. Otherwise conversion efficiency will change periodically as a function of the crystal length over a distance known as the coherence length.

A second order nonlinear process involves the interaction of three optical waves with frequencies ω_1, ω_2, and ω_3 so that $\omega_3 = \omega_1 + \omega_2$. Second-harmonic generation is a special case where two frequencies are identical: $\omega_1 = \omega_2$. Phase matching means that the wavevectors must satisfy the condition $\Delta k = k_3 - k_1 - k_2 = 0$ or $\Delta k = k_{2\omega} - 2k_{\omega} = 0$ in the case of SHG. This also implies matching of refractive indices $n_{2\omega} = n_{\omega}$. This phase matching condition can not be met in dispersive isotropic media where the refractive index depends directly on the optical frequency. Anisotropic crystals characterised by different axis having different refractive indices and dispersion coefficients enable phase matching under specific conditions. This is the

technique employed in this section. An alternative approach is quasi-phase matching, where the nonlinear refractive index is artificially modulated along the medium to periodically compensate for the phase error between the fundamental and second harmonic beam.

Consider the case of phase matching with anisotropic materials. In uniaxial crystals, two refractive indices can be differentiated depending on the beam polarisation. An ordinary wave with a polarisation direction perpendicular to the optical axis sees a refractive index n_o, while an extraordinary beam polarised in the plane of the Poynting vector (i.e. the ray direction) and the optic axis experiences a refractive index n_e which is dependent upon the angle between its polarisation and the optic axis.

Second harmonic can be generated according to two types denoted I and II. In type I SHG two photons having an ordinary polarisation will combine to produce one photon with extraordinary polarisation and twice the frequency. In type II SHG, one photon with ordinary polarisation and one photon with extraordinary polarisation will combine to produce one photon with extraordinary polarisation and twice the frequency.

5.2.2 Efficiency of SHG with focused Gaussian beams

It is important to be able to predict the SHG efficiency. The theory of second-harmonic generation with focused Gaussian beams has been developed by G. D. Boyd and D. A. Kleinman [5]. The authors have derived an equation to express the conversion efficiency as a function of key experimental parameters which, under undepleted pump approximation is given by:

$$\eta_{nd} = \frac{P_{2\omega}}{P_{\omega}} = KP_{\omega} l k_{\omega} h(\sigma, B, \xi). \tag{5.1}$$

Here,

$$K = \frac{2\omega^2 d_{eff}^2}{\varepsilon_0 n_{\omega}^2 n_{2\omega} c^3 \pi}, \tag{5.2}$$

and P_{ω} and $P_{2\omega}$ are the peak powers of the pump and the frequency doubled beams and the function $h(\sigma, B, \xi)$ known as the Boyd-Kleinman factor accounts for the focusing in the crystal

and has been derived in [5]. The approximation (5.3) has an error of less than 1% when $B<50$ and is given by [6]:

$$h(B) \approx \frac{B+0.568}{1.421B^2+0.791B+0.537}, \tag{5.3}$$

where $B=\rho\sqrt{\frac{\pi \cdot l \cdot n_\omega}{2\lambda}}$ is the non-dimensional walk-off parameter with ρ being the walk-off angle. In fact, the Boyd-Kleinman factor h is not too sensitive to the crystal length implying a better tolerance in the estimate of conversion efficiency.

In the weak pump depletion approximation, the conversion efficiency can be expressed by [7]:

$$\eta = \frac{\eta_{nd}}{1+\eta_{nd}}, \tag{5.4}$$

where η is now the efficiency including pump depletion. In practice, if the system operates in the pump depletion regime, calculation of conversion efficiency based on (5.1) under the non-depleted pump beam approximation leads to unrealistic values exceeding 100%. In contrast, Eq. (5.4) gives a conversion efficiency between 0 and 100%. For very small values of η_{nd}, η tends to η_{nd}, meaning that SHG can be considered to be in the non-depletion region where $\eta=\eta_{nd}$.

5.3 Frequency doubling with a picosecond fibre source

Efficient second-harmonic generation in preferred nonlinear crystals such as LBO requires several kilowatts of peak power, preferably in a diffraction-limited, linearly polarized, beam. At these peak powers, fibre nonlinear effects such as self-phase modulation and stimulated Raman scattering may affect the laser output characteristics (e.g. linewidth) and subsequently the second-harmonic generation efficiency. Thus, a challenge is to design a fibre system that can reach the peak powers required for efficient SHG while maintaining nonlinear degradation in the fibre below critical levels imposed by the crystal. In this section, I will review some of the requirements and parameters to be considered for efficient nonlinear frequency conversion.

5.3.1 Choice of crystal

The first recent demonstrations of high-power SHG in the green with a fibre laser employed nonlinear crystals such as Potassium titanyl phosphate ($KTiOPO_4$; KTP) or PPKTP because their high nonlinear coefficients implied that low peak power was required to achieve high conversion efficiency. The maximum green power reported with a fibre laser frequency doubled with PPKTP was 6 W [8]. However this demonstration revealed an efficiency roll off attributed to local heating effects at high average powers. Furthermore there are numerous reports of creation of colour centers or gray-tracks in KTP [9-12].

Therefore, an LBO crystal was chosen for the experimental demonstration of high-power SHG. The optimal crystal used in the experiment was anti-reflection coated on both faces and type-I non-critically phase-matched (NCPM, $\theta = 90°$, $\phi = 0°$) at 154°C to match the 1060 nm fundamental wavelength and I will assume this type of crystal in the following sections. The choice of such a crystal was governed by its unique highly versatile nonlinear optical properties such as small walk-off angle, moderate temperature sensitivity and high damage threshold. The demonstration of 60 W average power in the green from a frequency-doubled nanosecond fibre MOPA source presented in reference [1] has already proved LBO's suitability for high-power frequency doubling. However the relatively low peak power in ref. [1] dictated the need to use a sophisticated configuration with two cascaded 25-mm long crystals in order to reach high SHG efficiency. In contrast, the design of picosecond green laser relies only on a simple single-pass external frequency doubling with a single crystal with a more practical length.

5.3.2 Peak power requirement

As described in Sec. 5.2, under the assumption of phase-matching, SHG efficiency is proportional to peak power and interaction length. A long LBO crystal may a priori appear as the best choice to increase conversion efficiency; however a longer crystal implies a narrower spectral acceptance bandwidth. In a first approach and for simplicity, an analysis of SHG conversion efficiency will be considered by neglecting bandwidth considerations.

SNLO, a public domain software developed at Sandia National Laboratory [13] is employed to calculate the single-pass conversion efficiency for various incident peak powers and crystal lengths. The software models propagation of the fundamental beam and its second harmonic in a single-pass taking into account parameters such as beam profiles, pump depletion, walk-off and more.

Fig. 5.1 shows conversion efficiency calculated for various crystals operating in confocal configuration where the crystal length is chosen to match the Rayleigh range of the focused beam. These results provide a range of suitable parameters in order to achieve a satisfactory

level of conversion efficiency. For instance, with a 15-mm long LBO crystal, at least 12 kW of peak power at 1060 nm is required to achieve a conversion efficiency in the green exceeding 50%.

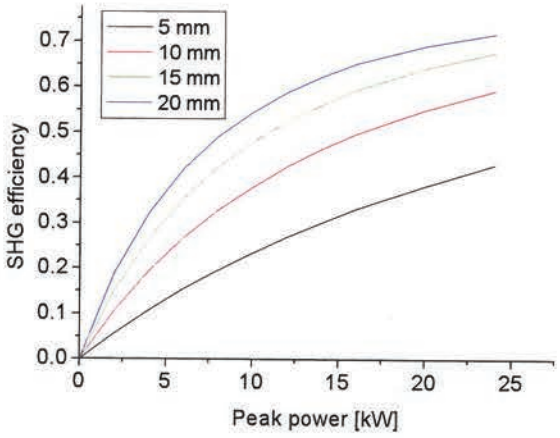

Fig. 5.1. Single-pass external frequency doubling conversion efficiency versus peak power and crystal length.

5.3.3 Stimulated Raman scattering

Stimulated Raman scattering constitutes one of the limitations for power scaling picosecond fibre laser systems. Optimal frequency conversion is achieved when the signal peak power is high enough for efficient conversion in the green while still below a critical value where SRS becomes significant. The evolution of signal and SRS peak power was calculated as a function of the amplifier gain or the targeted signal peak power. This was done assuming amplification in an Yb doped fibre amplifier with a mode field diameter of 16 μm and a fibre length of 8 m and considering both Raman and Yb gain at the Stokes wavelength as described by the following coupled differential equations:

$$\begin{aligned} \frac{dP_R}{dz} &= g_R \frac{P_R P_S}{A_{eff}} - \alpha_R P_R + g_R^{Yb} P_R \\ \frac{dP_S}{dz} &= -\frac{\nu_S}{\nu_R} g_R \frac{P_R P_S}{A_{eff}} - \alpha_S P_S + g_S^{Yb} P_S \end{aligned}, \tag{5.5}$$

where P_R is the Raman Stokes peak power and P_S is the signal peak power. α_R and α_S correspond to the loss coefficient at the Stokes and signal wavelengths respectively, while g_S^{Yb}

and g_R^{Yb} represent the gain produced by the ytterbium ions at the signal and Raman wavelength respectively. These equations are solved numerically using the initial conditions $P_R(0)$ provided in [14] and given by:

$$P_R(0) = h\nu_R B_{eff}, \tag{5.6}$$

where

$$B_{eff} = \Delta\nu \sqrt{\frac{\pi}{4\frac{P_0}{A_{eff}} L_{eff} g_R}}, \tag{5.7}$$

is the effective bandwidth of a Lorentzian gain profile with a FWHM bandwidth $\Delta\nu$ typically equal to 10 THz and the peak gain coefficient of SRS is $g_R \sim 10^{-13}$ m/W. P_0 is the signal peak power at the input and L_{eff} represents the effective propagation distance given by Eq. (4.2).

The results presented in Fig. 5.2 show an increase of SRS power above 20 kW, meaning that the signal peak power must be maintained below 20 kW to avoid any degradation in SHG conversion efficiency.

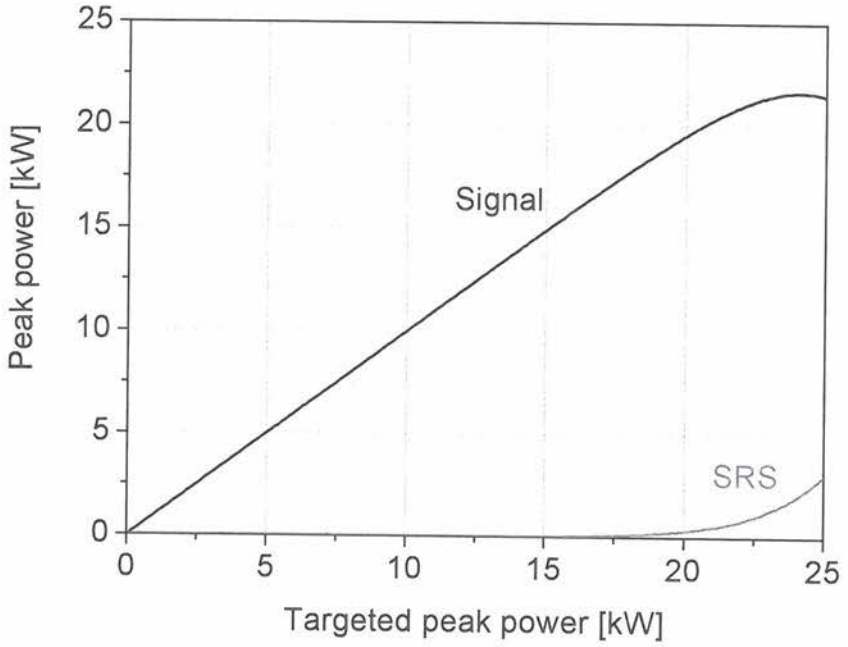

Fig. 5.2. Calculated peak power for signal and stimulated Raman scattering as a function of targeted signal peak power.

5.3.4 Spectral broadening and crystal acceptance bandwidth

SPM-induced spectral broadening

High peak power is conventionally preferred to maximize frequency doubling efficiency. However picosecond pulsed fibre lasers suffer from SPM which broadens the laser linewidth as the peak power increases. Spectral broadening was calculated by solving numerically the NLSE and assuming constant gain in an Yb-doped fibre amplifier with a mode-field diameter of 16 μm, a length of 8 m seeded with Fourier transform-limited 80 ps pulses with 1.3 W average power at 120 MHz. These longer 80 ps pulses compared to the 20 ps long pulses reported in Chapter 4 are preferred to reduce the laser linewidth before and after fibre amplification. They can be obtained by changing the driving current of the gain-switched laser diode and after compression through the CFBG. The calculated spectrum after amplification up to 175 W average power corresponding to 18 kW peak power reveals a final spectral linewidth of approximately 0.6 nm as shown in Fig 5.3.

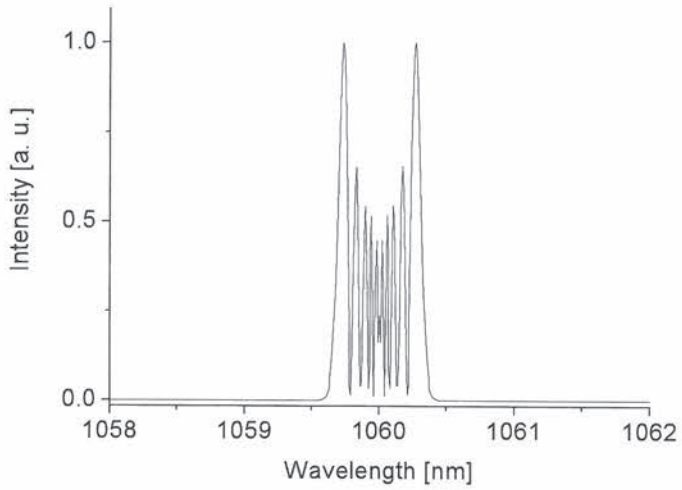

Fig. 5.3. Calculated spectrum for a 80 ps fibre MOPA producing 18kW peak power.

Crystal acceptance bandwidth

A peak power of 18 kW is a priori sufficient to achieve 50% conversion efficiency in the green in combination with a LBO crystal of more than 10 mm in length. Fig. 5.1 shows that increasing

crystal length would improve conversion efficiency. However this reduces the spectral acceptance bandwidth of the crystal. The spectral acceptance bandwidth was calculated by considering phase matching incorporating Sellmeier equations for the refractive indices of the LBO crystal, type I NCPM, with temperature dependence and based on the following expression:

$$\eta(T,\lambda) \propto \operatorname{sinc}^2\left(\frac{\Delta k(T,\lambda)L}{2}\right). \tag{5.8}$$

The spectral acceptance bandwidth is estimated to be approximately 1nm·cm and the calculated bandwidth for a 15 mm long LBO crystal is shown in Fig. 5.4 with an acceptance bandwidth at FWHM of 0.7 nm. Therefore an LBO crystal with a length of 15 mm should be able to accommodate 0.6 nm linewidth and appears suitable for efficient SHG with the previously modelled 18 kW, 80 ps fibre laser.

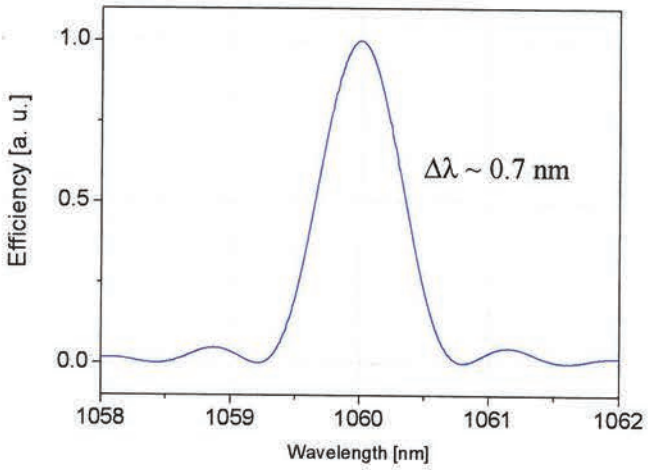

Fig. 5.4. Calculated spectral acceptance bandwidth of a 15 mm long LBO crystal

Taking into account fibre and crystal parameters such as spectral broadening, SRS and crystal acceptance bandwidth, the operating regime for efficient SHG can be summarized in Fig. 5.5. This figure confirms that with the choice of a 15mm long LBO crystal, the main limitation is the onset of SRS in the fibre amplifier with these fibre and pulse parameters. The laser linewidth after amplification up to 20 kW is still maintained below the crystal acceptance bandwidth. The crystal acceptance bandwidth is defined at full-width half-maximum meaning that for the laser linewidth should in fact be slightly narrower than the calculated crystal bandwidth to ensure optimal frequency conversion which explains the offset between crystal bandwidth and laser linewidth at the SRS limit in Fig. 5.5.

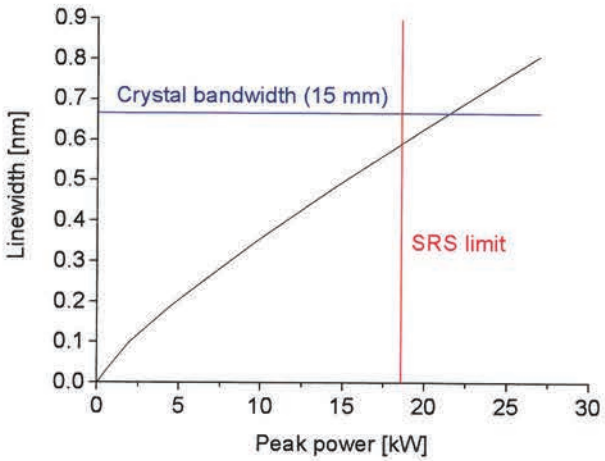

Fig. 5.5. Calculated SPM induced linewidth broadening versus peak power.

One would like the output to be scalable to high average powers, and also the system to be versatile and maintain a high efficiency across a wide range of operating regimes, e.g., with different pulse durations and repetition rates. New pulsed high-power sources based on diode-seeded Yb-doped fibre MOPAs are far superior to conventional sources from these perspectives. Importantly, their repetition rate is continuously variable over a wide range, which allows the average power to be scaled to high powers, or reduced to low powers, while maintaining a fixed peak power that maximizes the SHG efficiency

5.4 Experiments on high-power frequency doubling with a picosecond fibre source

Design requirements for efficient frequency-doubling of an ultrafast fibre source have been described in sections 5.2 and 5.3. This section presents an experimental demonstration of high-power SHG achieved with a fibre MOPA designed according to these requirements.

The green laser configuration is based on the external frequency doubling of a picosecond Yb-doped fibre source. Fig. 5.7 shows the experimental set-up composed of a picosecond fibre MOPA system similar to the one described in Chapter 4 followed by single-pass second-harmonic generation through a nonlinear crystal (LBO). These two main components will be described in detail in the next sections.

5.4.1 High-power picosecond fibre laser at 1060 nm for efficient frequency doubling

The analysis in Sec. 5.3 showed that the fibre MOPAs described in chapter 4 should be optimised in the following respects: excellent beam quality, high polarisation extinction ratio, peak and average power exceeding 10 kW and 100 W respectively in an output linewidth lower than 1 nm. Therefore both seed source and MOPA were modified to satisfy these requirements. These changes are presented in this section.

The seed source was modified to operate within a wide range of repetition rate by driving it with a pulse generator with a bandwidth of 3 GHz (Agilent 8133A) and is presented in Fig. 5.6. A pulse pattern was preferred to a sinusoidal pattern to minimize continuous wave background between pulses even at low repetition rates.

A broadband RF amplifier (LA 32-04-03) was used with this pulse generator. It provided lower driving current to the laser diode than in the system reported in chapter 4 which results in longer pulses with a different chirp characteristic. The diode can produce 140 ps pulses with more than 30 dB cw background to pulsed signal ratio based on integrated average power.

Since the average power produced by the diode is proportional to the duty cycle, at low repetition rate pulses were amplified with a core-pumped YDFA before reaching the CFBG. A newly developed circulator operating at 1064 nm was also employed instead of a 3 dB coupler used in chapter 4 to reduce the loss of the compressor to 5 dB. As a result the seed source produced pulses of 80 ps duration with an average power of more than 0.6 mW within 32 MHz-1 GHz range.

The pulse shape is shown in the inset of Fig. 5.6. The pulsed diode linewidth was measured to be 0.07 nm with an optical spectrum analyzer with a resolution of 0.01 nm. This corresponds to a time-bandwidth product ($\Delta\nu\Delta t$) of about 1.5 after the first preamplifier and compressor. Varying only the repetition rate, the pulse duration remained constant for repetition rates ranging from 32 MHz to 1 GHz. In this configuration pulse compression was not as efficient as previously demonstrated; however the CFBG provided additional filtering of both ASE and longitudinal modes of the laser diode.

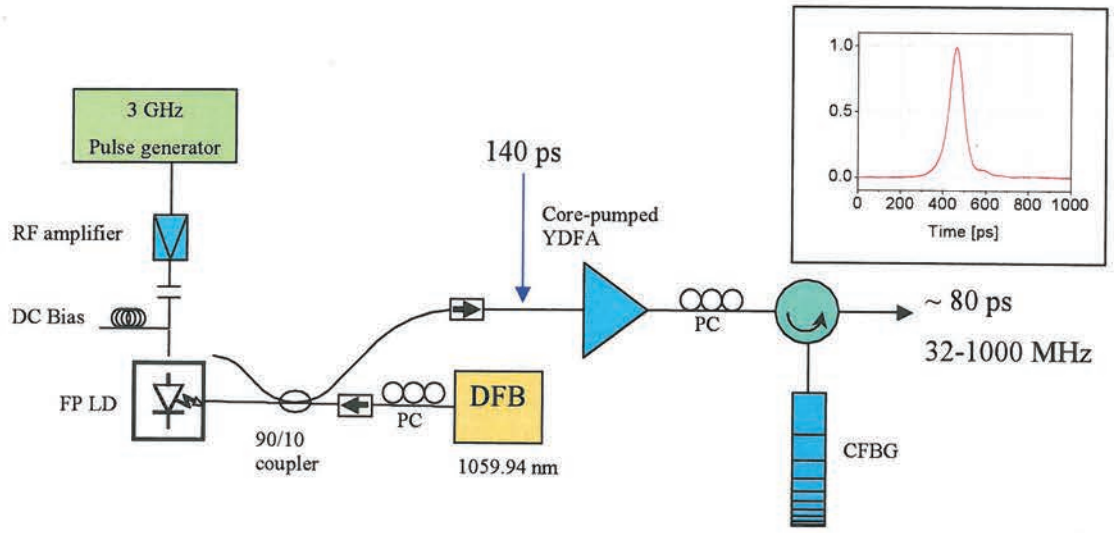

Fig. 5.6. Schematic set-up of the modified seed laser providing wide range of repletion rate. Inset: output pulse shape.

The high-power frequency doubled fibre MOPA laser system is depicted in Fig. 5.7. The signal from the diode was successively amplified to 10 mW by the first Yb-doped fibre amplifier and then to 250 mW in a second, single-mode, cladding-pumped, fibre amplifier.

In low repetition rate operation the seed generates low average powers resulting in a rise of ASE along the amplifier chain. Therefore the ASE accumulated in the amplifiers was filtered out by a circulator and a fibre Bragg grating of 2 nm bandwidth centered at 1060 nm.

The insertion loss at the signal wavelength was 6 dB. The filtered signal was then amplified in the same final preamplifier as the one described in chapter 4. The output beam was collimated and passed through a high-power single-polarisation free-space isolator (OFR IO-5-1064-HP). A half-wave plate positioned before the isolator allowed for partial polarisation control and was adjusted for maximum transmission through the isolator. An average power of 1.3 W in a linearly polarized signal was launched via a second half-wave plate and a lens into the final-stage power amplifier. This comprised an Yb-doped PM double-clad LMA fibre with a 19 μm diameter core with an NA of 0.08 embedded in a 400 μm diameter, 0.48 NA, D-shaped inner cladding. The polarisation angle of the input beam was adjusted with the second waveplate to coincide with the slow birefringence axis of the fibre, to maximize the polarisation extinction ratio at the output of the power amplifier. Although the large core increases nonlinear thresholds, it can also lead to multimode output due to the relatively large V-number of 4.5. Therefore careful mode matching between the final preamplifier and the power amplifier was necessary to achieve single mode excitation and thus good output beam quality.

The power amplifier was pumped by a diode stack source emitting at 975 nm launched through the signal output end of the fibre. The fibre was 8 m long and absorbed 87% of the launched

pump power. The pump and signal beam paths were separated by highly selective dichroic mirrors at both ends of the LMA fibre.

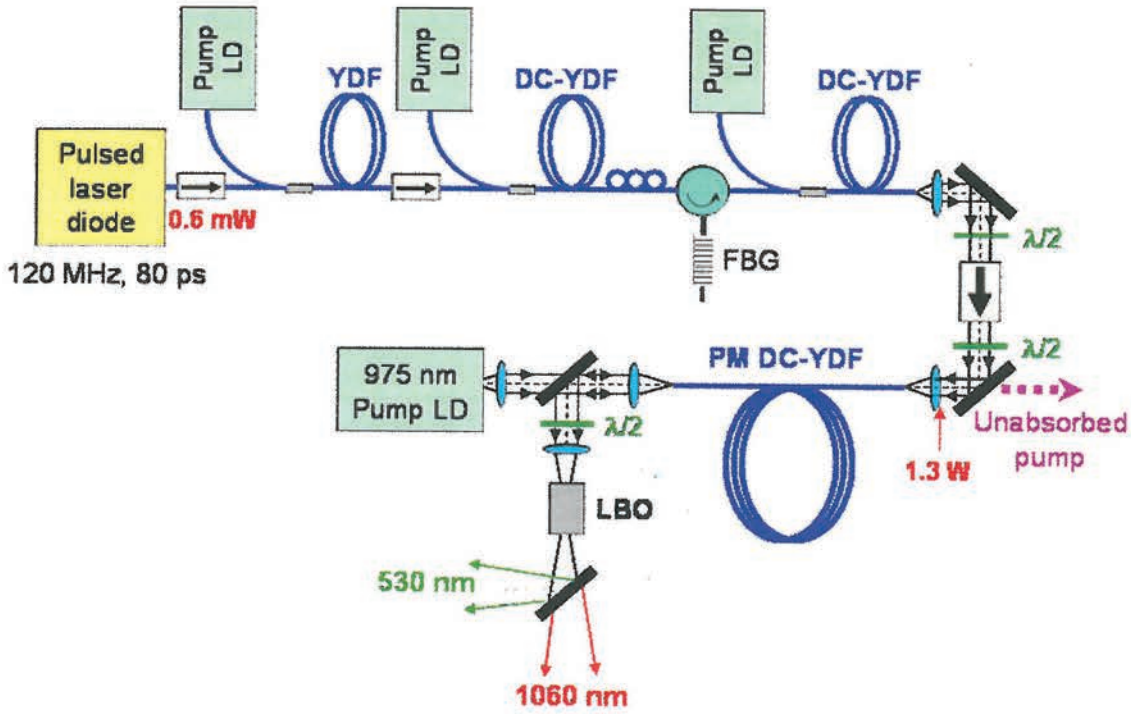

Fig. 5.7. Schematic set-up of the high-power green laser.

The fibre MOPA system produced in excess of 175 W of total average output power with a maximum launched pump power of 267 W and with the seed providing 80 ps pulses at a repetition rate of 120 MHz, corresponding to a slope efficiency of 68% for the high-power amplifier as shown in Fig. 5.8. The onset of SRS precluded higher peak powers although at higher repetition rates it was possible to reach higher average powers with increased pump power.

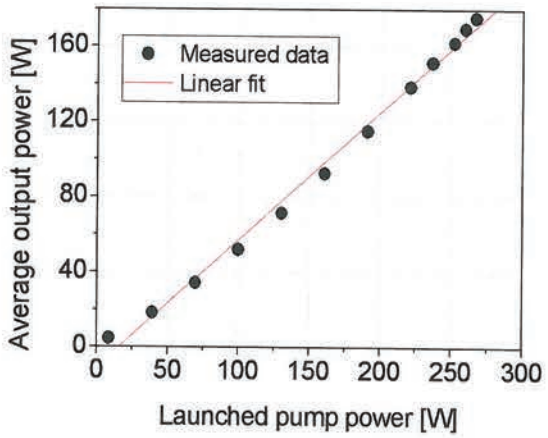

Fig. 5.8. Output power vs. last-stage pump power for the fibre MOPA source at 1060 nm

The polarisation extinction ratio, measured at various output powers, was in excess of 93% and the beam quality factor (M^2) was measured to be better than 1.1 as reported in Fig. 5.9.

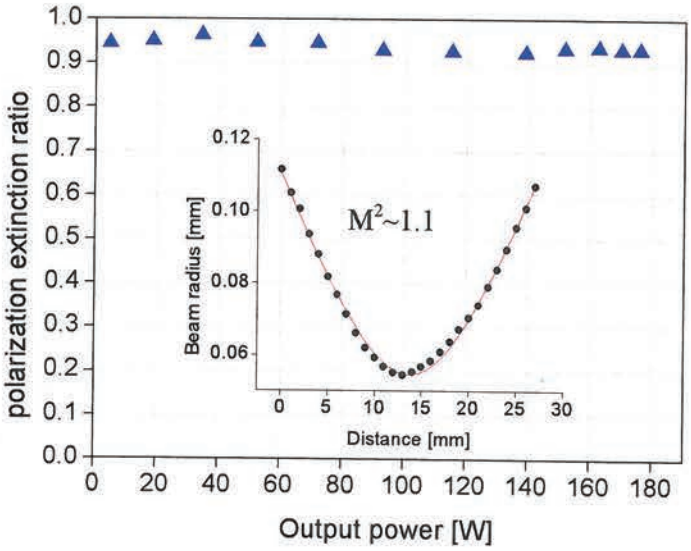

Fig. 5.9. Output power vs. last-stage pump power for the fibre MOPA source at 1060 nm

The output spectrum at the maximum power (~ 175 W) shows negligible SRS power around 1110 nm (see Fig. 5.10(a)). Furthermore the signal level was maintained 30 dB above the ASE level at 0.2 nm optical resolution (Fig. 5.10(a)). Spectral broadening induced by SPM resulted in a laser linewidth of 0.5 nm (full width at half maximum) as shown in Fig. 5.10(b) which is in agreement with the predicted linewidth. The signal was estimated to contain more than 96% of the total average power within a 1 nm bandwidth.

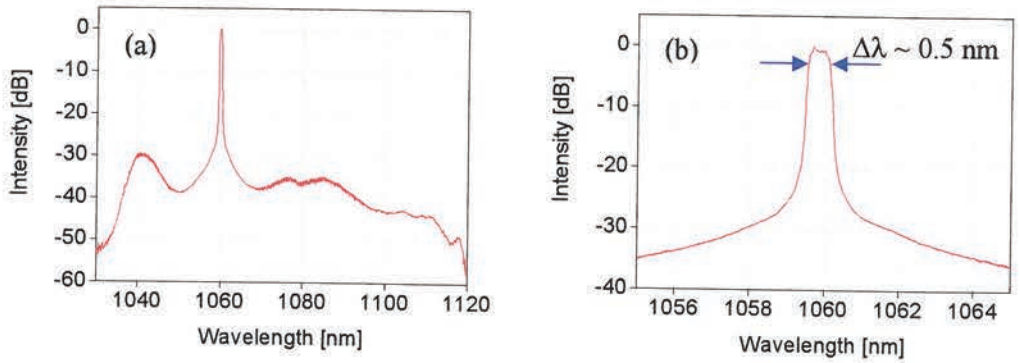

Fig. 5.10. (a) Optical spectrum of the output of the MOPA at maximum power (resolution = 0.2 nm). (b) Closer view of the output spectrum showing a laser linewidth of approximately 0.5 nm (resolution = 0.05 nm)

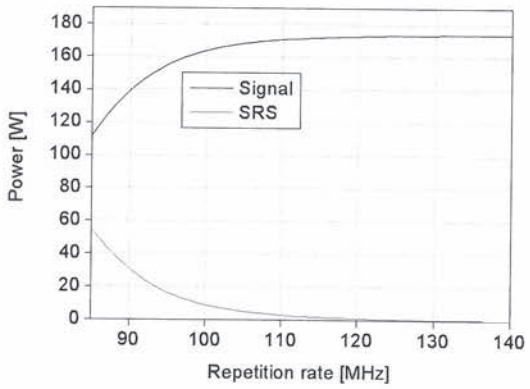

Fig. 5.11. Calculated Signal and SRS average power versus repetition rate for a constant output average power and pulse duration of 175 W and 80 ps respectively.

In typical operating regimes, the green conversion efficiency is expected to increase with the peak power of the fundamental beam. The peak power can be directly adjusted by changing the repetition rate of the seed laser. The maximum peak power achievable by our fibre MOPA source is dictated by the onset of SRS.

The Raman threshold (or critical power) is normally defined as the point at which the Stokes output peak power equals the signal output peak power [15]. However in practice the tolerance to SRS is much lower than this value. We adopt a more conservative working definition of the SRS threshold and define it as the power at which the Raman-scattered power represents only 1% of the output power. At this point the power losses as well as the spectral and temporal distortions caused by SRS are still insignificant. The Raman threshold of the high-power amplifier was calculated numerically to be 18.6 kW. Assuming constant average power and pulse duration of 170 W and 80 ps respectively and by plotting signal and Raman average power as a function of repetition rate, it was possible to determine the minimum repetition rate to employ before the onset of SRS as shown in Fig. 5.11. This was confirmed experimentally by changing the repetition rate between 80 and 130 MHz at a constant average power of 175 W while monitoring the output spectra. Following this experiment, the repetition rate was fixed at 120 MHz corresponding to a peak power of 17.7 kW at maximum output power.

5.4.2 Frequency-doubling and experimental results

The output beam from the fibre MOPA was launched through a lens arrangement into a 15 mm-long temperature-controlled LBO crystal for frequency-doubling. A half-wave plate was used to adjust the polarisation angle of the fundamental beam incident on the crystal.

There is scope for increasing the SHG conversion efficiency by employing a longer LBO crystal albeit at the cost of a reduced spectral acceptance bandwidth. The collimated fundamental beam was focused into the crystal to a beam waist (radius) of 40 μm using a single antireflection-coated lens. The maximum peak intensity of 350 MW/cm^2 was below the crystal damage threshold of 1 GW/cm^2 specified by the manufacturer. A dichroic mirror at the output of the crystal separated the green and fundamental beams.

The green power was measured and the power conversion characteristics are shown in Fig. 5.12. A maximum power of 80 W at 530 nm was achieved for a fundamental power of 175 W corresponding to an SHG efficiency of 46%. The repetition rate was varied and the 120 MHz was confirmed to result in the maximum power in the green. At the higher fundamental average powers achievable with increased repetition rate we observed green power instabilities despite a stable average power of the fundamental beam. This may be attributed to thermally induced fluctuations in either the fibre MOPA, or the LBO crystal. Fig. 5.12 also shows that at fixed repetition rate, the conversion efficiency gradually increases to 48% at 55 W green power, but decreases at higher power despite the stable polarisation extinction ratio and fundamental average power in this power range. This could be attributed to slight misalignment of the fibre amplifier output or to output beam quality degradation at high pump powers.

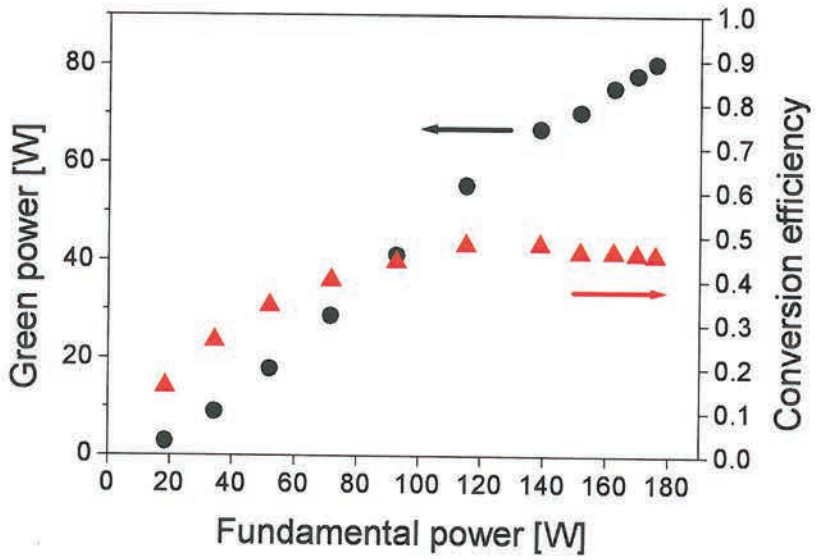

Fig. 5.12. Green power and conversion efficiency versus fundamental power achieved with pulses of 80 ps in duration at an optimised repetition rate of 120 MHz.

The output spectrum at maximum power presented in Fig. 5.13 shows clean frequency doubling with a resulting linewidth of 0.3 nm.

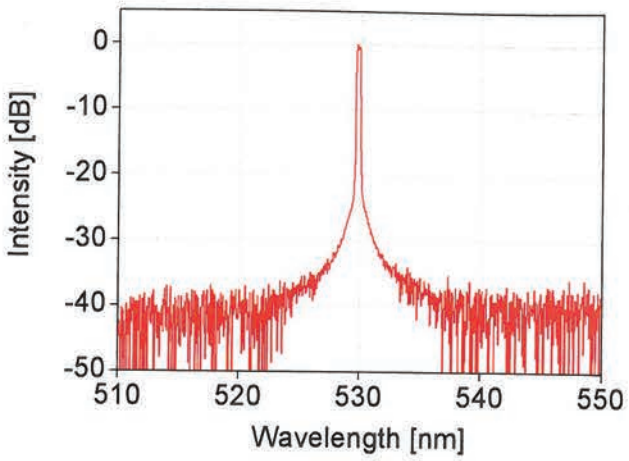

Fig. 5.13. Spectrum of the frequency-doubled fibre source measured at maximum output power of 80 W (resolution = 0.1 nm).

The output beam of the green laser was nearly diffraction limited with a measured beam quality factor M^2 of 1.15.

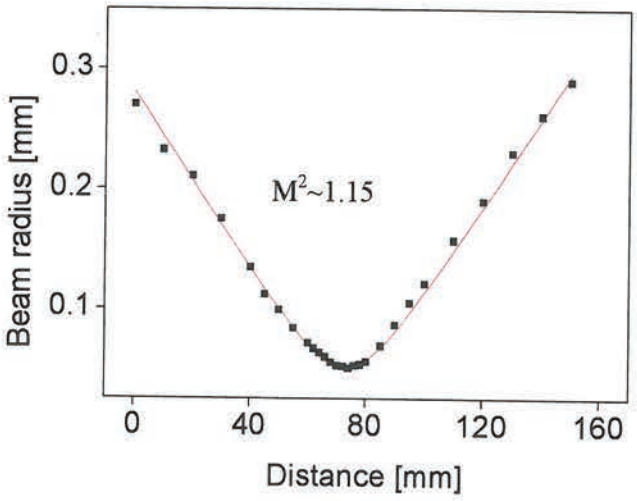

Fig. 5.14. Beam quality quality measurement obtained at the output of the green picosecond fibre laser. The beam quality factor $M^2 \sim 1.15$ corresponds to a nearly diffraction-limited beam.

5.5 Future direction: spectral compression in a high-power fibre amplifier

The previous sections have shown that ultrashort pulse fibre lasers can be suitable for efficient SHG at high average power. However SPM induced spectral broadening appears to be a key

limiting factor to reach higher peak power of the green laser. Nevertheless, under appropriate conditions for the seed pulse, SPM can result in significant reduction of the spectral linewidth. This is achieved by inducing a negative chirp to the input pulse to be amplified so that SPM induced in the fibre amplifier compensates this chirp resulting in the best case in the generation of a transform limited pulses with reduced spectral bandwidth [16]. Here I would like to review briefly the benefits and limitations of this method for efficient frequency conversion in a nonlinear crystal.

For this analysis, I use numerical simulations based on NLSE incorporating parameters reported in [17]. The seed source emits 310 fs $sech^2$ pulses at 1030 nm with a repetition rate of 47 MHz and an average power of 1.5 W. A grating pair produces a negative chirp that stretches the pulses to 10 ps. An Yb-doped fibre amplifier with a mode field diameter of 35 μm and a length of 1.5 m is used for high-power amplification and spectral compression. The experiment shows that amplification up to 97 W leads to a spectral compression from 3.7 nm to 0.5 nm. The numerical simulations validate this measurement as shown in Fig. 5.15. However simulations also show the appearance of a significant pedestal. Integrations on the spectral intensity reveal that up to 30% of power can be included in the pedestal. C. Finot et al. have proposed in [18] that spectral compression of parabolic pulses can significantly enhance the quality of spectral compression. Therefore the same numerical simulations were realised assuming pulses with a parabolic intensity profile and the results are presented in Fig. 5.15. The nonlinear spectral compression of parabolic pulses is of very high quality with very little pedestal compared to $sech^2$ pulses. The logarithmic representation of the spectra reveals an increase in extinction of the pedestal from 10 dB for $sech^2$ pulses up to 20 dB for parabolic pulses. The amount of power contained in the pedestal is estimated to be approximately 2 % of the total power.

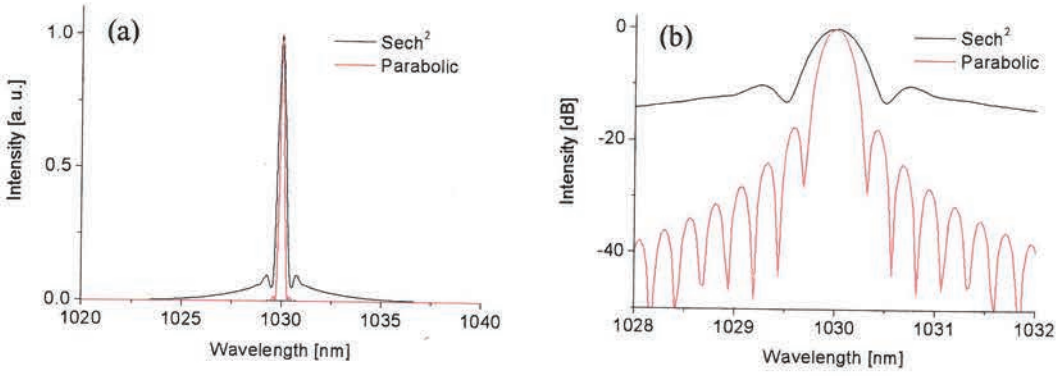

Fig. 5.15. Simulated optical spectra after SPM induced spectral compression of negatively chirped $sech^2$ and parabolic pulses. (a) Linear spectra; (b) Logarithmic spectra.

There have been few reports on frequency doubling after spectral compression of $sech^2$ pulses [17, 19] but there is no clear evidence of the benefit of spectral compression for efficient frequency doubling. Although spectral compression of parabolic pulses looks very promising, there has not been any experimental demonstrations of such a method. This is most likely due to the lack of availability of parabolic pulse sources. Nevertheless it is possible to generate parabolic pulses through self-similar regime of amplification as described in chapter 3. However this requires the design of a more complicated MOPA configuration where $sech^2$ seed pulses for instance, are first amplified in a fibre amplifier designed to shape the pulse to a parabolic profile, then a negative linear chirp is induced by gratings or a photonic bandgap fibre [19] and finally these pulses are injected in the final fibre amplifier for spectral compression. In this case the quality of the final spectral compression depends mainly on the quality of the generated parabolic pulses. Despite the limitations, the work presented in the previous sections appears more practical than the technique involving spectral compression due to the simplicity of the experimental arrangement and also thanks to the larger tolerance on the design parameters.

5.6 Conclusion

Chapter 5 has described design considerations to achieve efficient frequency doubling of a picosecond fibre laser. This resulted in the demonstration of a laser emitting at 530 nm with an output average power of 80 W which represents the highest power achieved with a frequency doubled fibre laser. This confirms that a properly designed chain of fibre amplifiers combined with an adequate master oscillator provides an alternative technology for efficient harmonic generations.

The high-brightness of the fibre-based source is key in achieving good output beam quality after nonlinear frequency conversion. Furthermore this novel type of high-power green laser based on a highly versatile picosecond fibre laser is also of great interest for the generation of third harmonic and fourth harmonic to produce high average power in the UV region of the spectrum.

The prospect of spectral compression for efficient frequency conversion has also been considered. However, despite the elegance of this technique, it has not shown so far any significant advantage with respect to the generation of high average power in the green. The high repetition rate and low energy regime is nevertheless a distinct advantage for power scaling frequency doubled fibre sources.

References

1. A. Liu, M. A. Norsen, and R. D. Mead, "60-W green output by frequency doubling of a polarized Yb-doped fiber laser," Opt. Lett. **30**, 67-69 (2005).
2. J. K. Wright, "Enhancement of second harmonic power generated by a dielectric crystal inside a laser cavity," Proc. IEEE **51**, 1663 (1963).
3. R. G. Smith, "Theory of Intracavity Optical Second-Harmonic Generation," IEEE J. Quantum Electron. **6**, 215-223 (1970).
4. A. Ashkin, G. D. Boyd, and J. M. ziedzic, "Resonant Optical Second Harmonic Generation and Mixing," IEEE J. Quantum Electron. **2**, 109-124 (1966)
5. G. D. Boyd, and D. A. Kleinman, "Parametric Interaction of Focused Gaussian Light Beams," J. Of Appl. Phys. **19**, 3597-3639 (1968).
6. J. Hald, " Second harmonic generation in an external ring cavity with a Brewster-cut nonlinear crystal: theoretical considerations," Opt. Comm. **197**, 169-173 (2001).
7. H. Wang, A. M. Weiner, "Efficiency of Short-Pulse Type-I Second-Harmonic Generation with Simultaneous Spatial Walk-off, Temporal Walk-off , and Pump Depletion," IEEE J. Quantum Electron. **39**, 1600-1618 (2003)
8. S. V. Popov, S. V. Chernikov, J. R. Taylor, "6-W Average power green light generation using seeded high power ytterbium fibre amplifier and periodically poled KTP," Opt. Comm. **174**, 231, (2000).
9. J. K. Tyminski, "Photorefractive damage in KTP used as second-harmonic generator," J. Appl. Phys. **70**, 5570-5576, (1991).
10. N. Kuzuu, K. Yoshida, H. Yoshida, T. Kamimura, and N. Kamisugi, "Laser-Induced Bulk Damage in Various Types of Vitreous Silica at 1064, 532, 355, and 266 nm: Evidence of Different Damage Mechanisms Between 266-nm and Longer Wavelengths," Appl. Opt. **38**, 2510, (1999).
11. B. Boulanger, I. Rousseau, J.P. Feve, M. Maglione, B. Menaert, and G. Marnier, "Optical studies of laser-induced gray-tracking in KTP," IEEE J. Quantum Electron. **35**, 281, (1999).
12. M. N. Satyanarayan, H. L. Bhat, M. R. Srinivasan, P. Ayyub, and M. S. Multani, "Evidence for the presence of remnant strain in grey-tracked KTiOPO4," Appl. Phys. Lett. **67**, 2810, (1995).

13. SNLO nonlinear optics code available from A. V. Smith, Sandia National Laboratories, Albuquerque, NM 87185-1423.

14. R. G. Smith, "Optical Power Handling Capacity of Low Loss Optical Fibers as Determined by Stimulated Raman and Brillouin Scattering," Appl. Opt. **11**, 2489-2494 (1972).

15. G. P. Agrawal, Nonlinear Fiber Optics, 3rd ed. (Academic, San Diego, Calif. 2001.

16. B. R. Washburn, J. A. Buck, and S. E. Ralph, "Transform-limited spectral compression due to self-phase modulation in fibers ," Opt. Lett. **25**, 445-447 (2000).

17. J. Limpert, N. Deguil-Robin, I. Manek-Hönninger, F. Salin, T. Schreiber, A. Liem, F. Röser, H. Zellmer, A. Tünnermann, A. Courjaud, C. Hönninger, and E. Mottay, "High-power picosecond fiber amplifier based on nonlinear spectral compression," Opt. Lett. **30**, 714-716 (2005).

18. C. Finot, F. Parmigiani, P. Petropoulos, and D. Richardson, "Parabolic pulse evolution in normally dispersive fiber amplifiers preceding the similariton formation regime," Opt. Express **14**, 3161-3170 (2006).

19. M. Rusu and O. G. Okhotnikov, "All-fiber picosecond laser source based on nonlinear spectral compression, " Appl. Phys. Lett. **89**, 091118 (2006).

Chapter 6 Visible sources based on nonlinear frequency conversion in optical fibres

6.1 Introduction

In recent years the outstanding properties of fibre based devices has been exploited by incorporating various rare-earth dopants such as Nd, Yb, Er, Tm in optical fibres to develop sources emitting in the 910-1060 nm, 980/1030-1120 nm, 1530-1600 nm and 1860-2100 nm wavelength ranges respectively [1]. However the development of high-power fibre-based sources in wavelengths outside these spectral bands is quite challenging. Chapter 5 has presented efficient frequency doubling of a fibre source to generate high-power in the green. Nevertheless this technique restricts the operating wavelengths to specific harmonics.

Exploiting nonlinear effects in optical fibres is an attractive alternative to produce fibre sources with various wavelengths. For instance the transfer of energy from an YDFL to longer wavelength via SRS in optical fibres has enabled the development of high-power sources emitting between 1.1 and 1.5 μm for various applications including pumping of EDFA at 1480 nm.

However all these sources are restricted to the near infrared spectral range and operation of a fibre source in the visible region constitutes another challenge. An interesting approach is upconversion lasing which relies on near infrared pumping of a RE doped fibre made of an adequate host material. For instance upconversion from thulium and praseodymium ions have been used to produce high power laser radiation in the blue [2] and from 491nm to 635nm [3] respectively. Another technique is based on the pumping of rare-earth doped fibres with lasers operating at shorter wavelength. Lasing could be obtained at various visible wavelengths by pumping a Pr-doped fibre laser in the blue using an argon ion laser [4] or more recently a semiconductor laser source [5]. Although these techniques are of great technical interest, power scaling is limited either by photodarkening in the fibre or by availability of pump power in the visible.

Therefore in practice external frequency conversion of a fibre based source using nonlinear crystals remains a very attractive method to reach high-power in the visible. High-power

sources emitting in the green and at the edge of the visible spectrum at 780 nm have been demonstrated by frequency doubling Yb [6, 7] and Er/Yb [8] doped fibre lasers, respectively. These novel sources can then pump nonlinear fibres to produce a supercontinuum or to generate specific wavelengths in the visible spectrum through phase-matching occurring in the waveguide. For instance, the first part of this chapter reports on the generation of blue and red components in secondary cores of holey fibres when pumped by green pulses generated by the frequency-doubled pulsed fibre source described in chapter 5. These observations were attributed to phase matching by birefringence within the sub-micrometer sized cores induced by non-symmetric deformation during the fibre drawing.

This method allows wavelength conversion at both short and long sides of the pump wavelength. However some applications require high-power generation in a single wavelength. Therefore another technique to produce visible wavelengths outside the harmonics of a rare-earth doped fibre laser is to frequency double a Raman shifted fibre source. This allows conversion to wavelengths above 515nm. For instance the generation of yellow between 580 and 600 nm is very useful for medical applications such as dermatology and ophthalmology. In addition the development of a fibre-based source emitting at 589 nm has attracted much interest in recent year for Guide star application. The second part of the chapter describes the experimental demonstration of a fibre laser emitting at 589 nm based on the SHG of a picosecond Raman fibre laser emitting at 1178 nm.

6.2 RGB generation in secondary cores of a holey fibre

Due to their wide range of design parameters, photonic crystal fibres are now a well established technology to provide flexible dispersion profiles and exploit specific nonlinear effects. In recent years, supercontinuum generation in such fibres has attracted much interest particularly for its potential to produce white light sources [9-12] for many applications. White light generation from a fibre can be implemented in a simple scheme and its main attraction resides in the remarkable brightness achieved spectrally as well as spatially compared to traditional white light sources [13].

A visible supercontinuum can be produced in a holey fibre from pulsed high-brightness bulk or fibre lasers emitting in the near infrared. Although this technique is very simple as it only involves a pump laser and a nonlinear fibre with adequate dispersion properties, it is relatively inefficient since generation of visible wavelengths is also accompanied by the transfer of a significant fraction of the pump power to longer wavelengths in the infrared. An alternative method consists of employing a visible pump beam centrally located in the visible spectrum to

generate a supercontinuum restricted to the visible wavelengths. This technique requires a zero dispersion wavelength near the pump wavelength which can be achieved with tapered fibres [14, 15] or with phase matching through the excitation of a higher order fibre modes [16].

Some applications such as laser projection displays benefit from higher spectral density at specific wavelengths in the visible. An alternative to supercontinuum generation is therefore to distribute the pump intensity between discrete wavelengths so that the resulting spectral brightness is greatly enhanced. The generation of red, green and blue radiation from a single near infrared source combined with multiple frequency conversion steps has been demonstrated at high-power [17]. Despite its potential for power scaling, this technique involves a large number of components with complex optical arrangements. A simpler approach is to exploit the large nonlinearities of holey fibres and, in particular, phase-matched four-wave mixing to produce specific, narrow wavelength bands.

In this section, the generation of white light in a short length of holey fibre pumped by a green beam from a frequency doubled pulsed fibre laser is reported. Sub-micrometer-scale structures in the cladding of a photonic bandgap fibre are employed as highly nonlinear waveguides. The resulting output beam contains discrete red, green and blue spectral lines, with equal frequency spacing between the green pump and the red and blue sidebands characteristic of phase-matched FWM processes. Birefringence due to asymmetry in the nanofibres is identified to be the cause of this phase-matching. I next present experimental investigations on various fibres and detailed model simulations to interpret these observations. I have carried out the experiments and the numerical simulations were realised by Francesco Poletti and Peter Horak.

6.2.1 Experimental set-up

The experimental set-up is presented in Fig. 6.1. The green pump laser configuration was described in chapter 5. It is based on a fibre MOPA seeded by a gain-switched laser diode producing 80 ps pulses at repetition rates ranging from 32 MHz up to 1 GHz. The lowest frequency of 32 MHz is adopted to achieve maximum peak power with lowest average power. The green output beam is passed through a half wave plate operating at 530 nm to control the polarisation and after collimation is launched into a nonlinear holey fibre as described below. Although the green laser was designed for higher power operation, in this experiment the output average power was restricted to 2 W corresponding to a peak power of 780 W to avoid damaging the holey fibres. The green beam was focused into the holey fibre by an aspheric lens providing high numerical aperture.

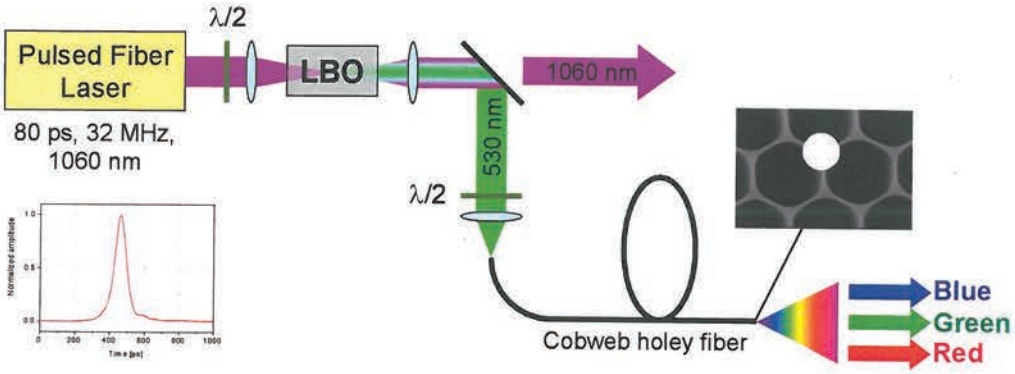

Fig. 6.1. Experimental arrangement for the generation of RGB in cobweb holey fiber. λ/2: half-wave plate at respective wavelengths.

6.2.2 Fibre design

The fibres considered in this study are PBGFs originally designed to achieve guidance in the hollow core in the following wavelength bands: 1070, 1210, 1550, 1800 and 2000 nm (fibres A, B, C, D, and E, respectively). The fibres were drawn from two different preforms: fibres A and B from one, fibres C-E from the other preform. The geometry is similar in all cases and the fibres differ essentially by their overall dimensions. For the work reported here, the fibres are not exploited for their air guiding properties but for the index guiding properties of the holey silica structure surrounding the hollow core. The fibre cladding is shown in Fig. 6.2 and is formed by a periodic arrangement of air holes on a triangular lattice. Each hole can be accurately represented as a hexagon with rounded corners [18] and the entire structure is completely determined by three parameters: the hole-to-hole spacing Λ, the hole diameter d, and the radius of the circles used to round the corners r_c. Our fibres exhibit a relative hole size $d/\Lambda \sim 0.935$ and a $r_c/d = 0.25$, while the pitch Λ scales from 2.5 to 4.7 μm. In this study we are interested in the light-guiding properties of the secondary cores in the cladding (indicated by the green circle in Fig. 6.2) whose dimensions, measured by the radius of an inscribed circle, vary between ~200 and ~400 nm. This corresponds to a nonlinear parameter γ between 394 and 200 $W^{-1}km^{-1}$ for green light.

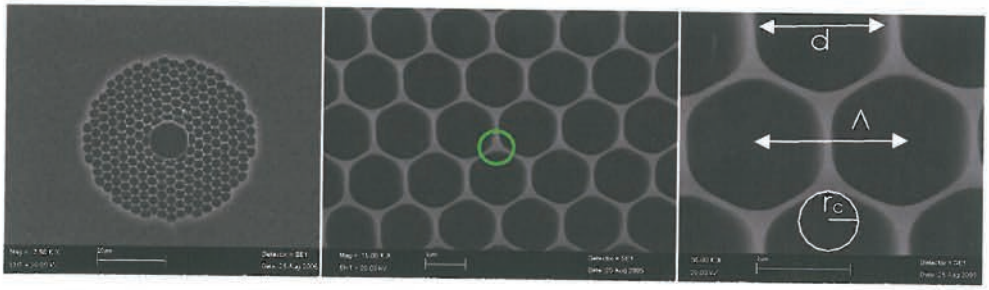

Fig. 6.2. Typical SEM images of fibres used for RGB generation.

6.2.3 Experimental results

The second-harmonic beam at 530 nm was launched into the cladding of the different PBGFs using an objective lens. Specific care was taken to ensure coupling into a single secondary core of the holey fibre structure. After propagation through 1 m in the holey fibres, the output pulse was measured and the spectrum analyzed. The output power typically reached in excess of 300 mW from the 2 W of pump power.

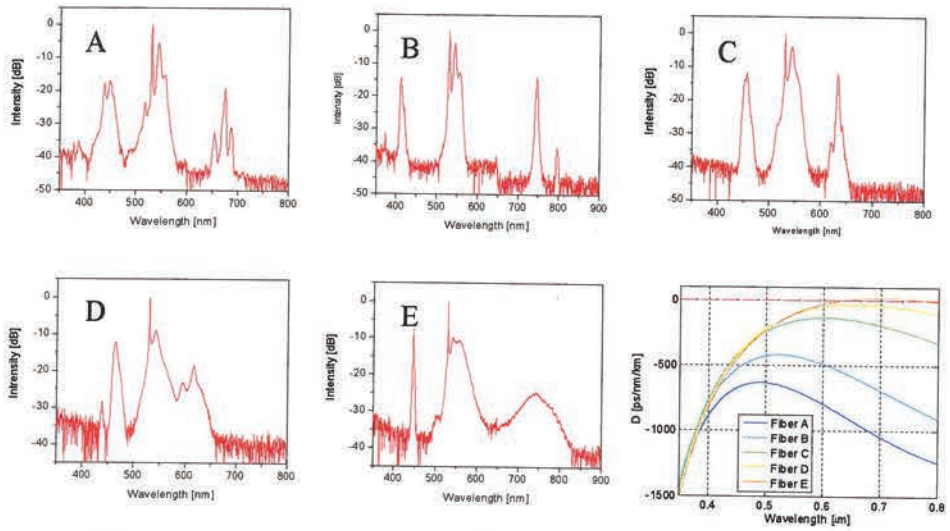

Fig. 6.3. Normalised output spectra obtained from fibres A-E, and corresponding dispersion profiles calculated for a single secondary core as shown in Fig. 6.2.

Typical optical spectra measured directly at the output of the different fibres are presented in Fig. 6.3. Distinct spectral sidebands appearing around the pump wavelength in the blue and red parts of the visible spectrum are observed. The separation between the generated frequencies and the pump frequency satisfies energy conservation, i.e., $2\omega_{green} - \omega_{red} - \omega_{blue} = 0$, which clearly points to a FWM process as the generating mechanism. The output spectra not only vary between different fibre types, but there are also significant differences from core to core within the same fibre. For instance, fibre C could generate blue and red components separated from 100 nm to 300 nm depending on the launch conditions and the choice of excited core. Slight qualitative changes in the spectra of fibre E can be observed, in particular a broadening of the red sidebands. In order to better understand these features, Fig. 6.3 shows the dispersion of light propagating in single secondary cores of fibres A-E, calculated for the idealized fibre structure as outlined in Sec. 6.2.4. For all fibres the green pump is in the normal dispersion regime. However, for fibre E there exists a region of anomalous dispersion, which explains the broadening of the red sideband for this fibre.

Fig. 6.4 depicts the diffracted radiation emitted by the cobweb structure of fibre D. The output mode at the respective wavelengths was imaged using red, green and blue colour filters. It shows that light at all wavelengths is located in a single sub-micron core.

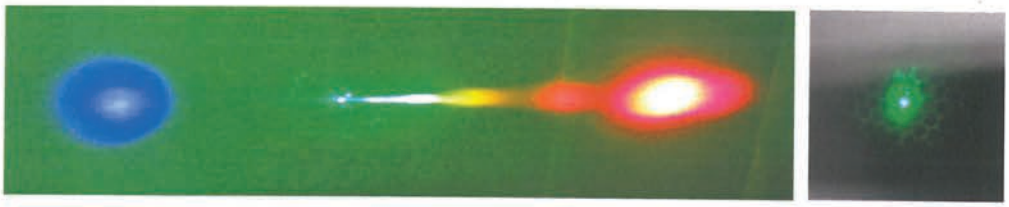

Fig. 6.4. Left: Diffracted picture of the RGB components generated by fibre D. Right: The fibre output observed in the green showing the location of the single excited core.

A cut-back measurement with fibre C revealed that the RGB generation takes place within the first 30 cm of the holey fibre. In fact, compared to the full length of 1 m, a slight improvement in the FWM conversion efficiency at 30 cm is observed, which is attributed to significant losses in the blue due to surface scattering for the longer fibre. At maximum conversion, the blue and red sidebands where less than 10 dB below the residual green pump. In this configuration, a total of 360 mW average output power was reached with 47, 292 and 21 mW of blue, green, and red average power, respectively.

Finally, a strong polarisation dependence of the FWM process was observed. The conversion efficiency to the sidebands was found to depend on the alignment of the input polarisation. In general, only one specific input polarisation resulted in RGB generation. In addition, the output polarisation of each spectral component was analyzed, which showed that the red and blue components were polarized orthogonally to the green pump beam.

6.2.4 Modelling and interpretation

In order to interpret the experimental results and to understand the details of the underlying FWM process, it is important to identify the modes involved and to investigate the phase-matching conditions which determine the exact wavelengths of the red and blue sidebands. To this end, we performed numerical simulations of the fibre cross-section using a fully vectorial mode solver based on hybrid edge-nodal FEM [19]. A portion of the periodic cladding of our fibres, comprising either one or two silica rods with air holes was modelled with anisotropic perfectly matched layers (PMLs) boundary conditions. Propagation constants for the fundamental modes and for all higher order modes were evaluated at different wavelengths and the most relevant phase-matching curves were calculated. We studied four different scenarios, each of which could in principle explain our observations. We will briefly illustrate in the following, where coupling occurs (a) between FM and HOMs within the same rod; (b) between

even and odd supermodes in a system of two adjacent rods; (c) between two modes centered in different rods with small geometrical variations, and finally (d) between the two orthogonal FMs within a single birefringent rod.

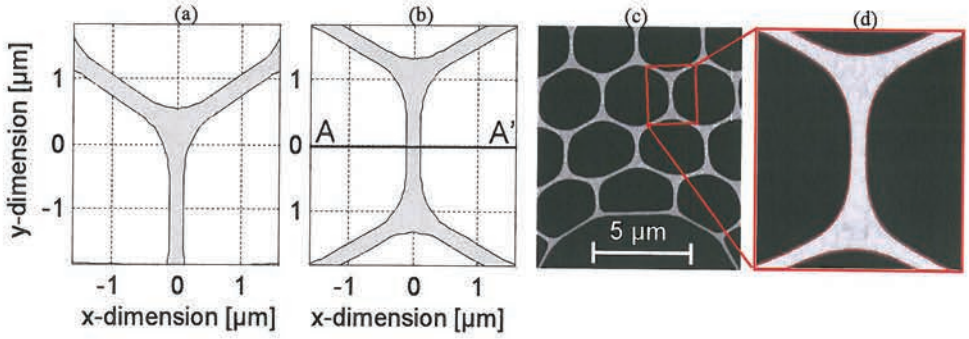

Fig. 6.5. Idealised structure used in the simulations: single rod (a) and double rod (b). In this example Λ = 3.66 µm, d/Λ = 0.935, rc/d = 0.25. (c) High magnification SEM image of fibre C, and (d) detail of the simulated profile.

Because of the apparently large symmetry of the structures under investigation, we initially focused our attention on the idealized, perfectly symmetric, single-rod structure shown in Fig. 6.5(a). The structural parameters were chosen to match the average features of the PBGF air-guiding at 1550 nm (fibre C: Λ = 3.66 µm, d/Λ = 0.935, rc/d = 0.25). Since such an ideal structure possesses a C_{3v} symmetry, its FMs are doubly degenerate [20], and phase-matching is only possible between a fundamental and a higher order mode. The propagation constant mismatch between a FM and any HOM however was too large to generate phase matching between the experimentally observed wavelength bands, and therefore this process cannot be responsible for the observed RGB generation.

The possible interactions between multiple cores was then studied, focusing on the elementary cell consisting of two separate cores, as shown in Fig. 6.5(b). Such a structure possesses inversion symmetry with respect to the AA' axis. Therefore, if the overlap between the modes guided in the two separate cores is not negligible, the structure supports either even or odd "supermodes". The simulations revealed that the splitting in propagation constant between even and odd "fundamental" supermodes was too small to explain the observed phase-matched peaks. On the other hand, good agreement of the sideband wavelengths between measurements and theory could be achieved by a number of specific even and odd higher order supermode pairs. However, simple coupled mode theory considerations suggest that in this case light initially coupled into a single HOM would repeatedly couple into adjacent cores during the propagation and would eventually exit the fibre guided by multiple cores. This contradicts our

experimental observations shown in Fig. 6.4, according to which light at the fibre output was always confined to a single core.

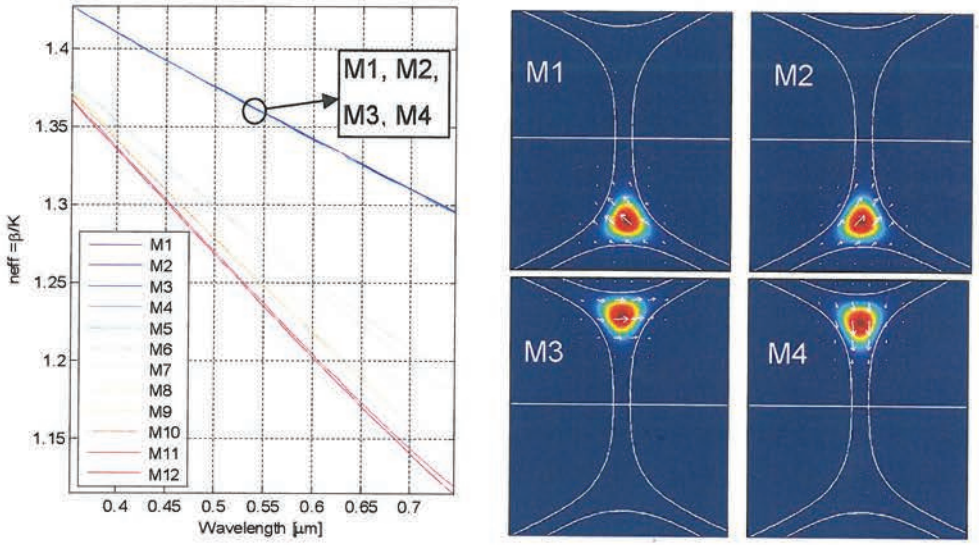

Fig. 6.6. Simulation results for the structure in Fig. 6.5 (d): Effective indices of the first 12 modes (left); Mode intensity and polarisation distribution of the first 4 modes at 530 nm (right).

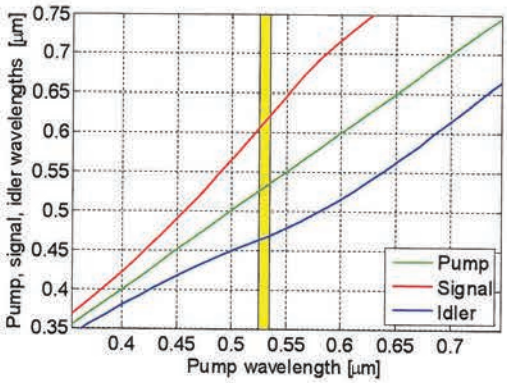

Fig. 6.7. Phase matching curves for the modes of Fig. 6.6: the pump is in mode M1, while signal and idler are in the orthogonally polarised mode M2.

Next, we investigated the effects of the small structural deviations of a real fibre. A pair of rods were isolated from a highly magnified SEM image of the cladding (Fig. 6.5(c)) and through image thresholding and splining we obtained the contour shown in Fig. 6.5(d), which was then meshed and used in the FEM simulations. The effective indices of the first 12 modes of such a structure and the mode fields and polarisations of the two pairs of orthogonal FMs centered in each core are shown in Fig. 6.6. The simulations showed that as a result of minor structural deformations the difference in propagation constant between two modes centered on different rods would produce phase-matched wavelengths approximately in the observed spectral

positions. However, the overlap between modes propagating in different cores is very small, with ~10% of the intensity propagating outside the central core at 700 nm and much less than this in the green and blue, see Fig. 6.6 (right). The nonlinear conversion efficiency by FWM would therefore be extremely small and in particular would be well below the efficiency of Raman conversion within the central cores, in contrast to the spectra shown in Fig. 6.3.

On the other hand, the simulations show that each core exhibits a significant phase modal birefringence B, as large as $2.5\text{x}10^{-4}$ at 530 nm, where $B = |neff_1 - neff_2|$, and $neff_1$ and $neff_2$ are the effective indices of the two orthogonal FMs. Phase matching can thus occur for orthogonal pump and sideband polarisation, in line with the experimentally observed polarisation dependence of RGB generation. The corresponding phase matching curves are shown in Fig. 6.7. The phase-matched wavelengths agree well with the observed sidebands of Fig. 6.3. Repeating the procedure for other rods in the same and in other fibres confirmed a value of modal birefringence in the green between 10^{-4} and $2\text{x}10^{-3}$, with corresponding phase matching curves able to justify the variety of output spectra observed in practice. Moreover, since all contributing modes are propagating within a single secondary core, their spatial overlap is close to 100% and we can expect efficient wavelength conversion. Because of the orthogonal polarisations of the pump and the sidebands required for birefringent phase matching in the normal dispersion regime, the nonlinear gain coefficient is reduced to 1/3 compared to the case of parallel polarisations. The peak gain for FWM processes is thus slightly below, but of the same order of magnitude as the peak Raman gain [21]. This also agrees well with the observed spectra where a Raman shifted peak of the pump is clearly visible and its maximum is comparable to or larger than the FWM sidebands. We thus interpret the mechanism leading to RGB generation in our fibre as a phase-matched FWM process between the polarisation modes of highly birefringent fibre cores. Note that this process has also been termed "polarisation modulation instability" in the literature and has been observed in holey fibres [22, 23], but no such large splitting and high conversion efficiency has been reported in the visible regime before.

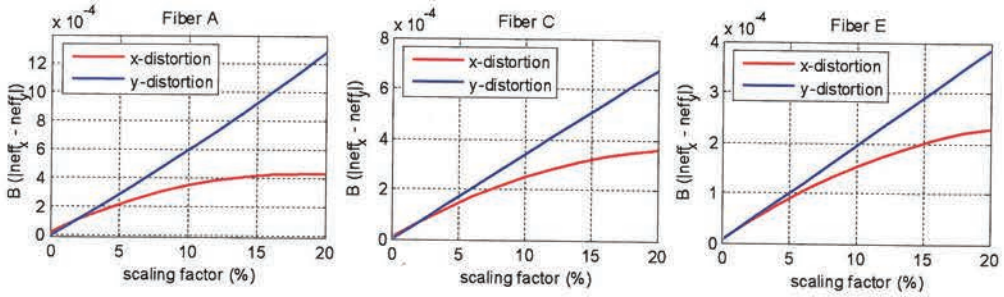

Fig. 6.8. Simulated birefringence at 530 nm when a deformation (linear scaling) is applied along the x and y directions to a single rod with structural parameters corresponding to 3 of the fibres under examination.

In order to investigate the unexpectedly large value of birefringence obtained from simulations on the realistic fibre structure, the ideal single rod was deliberately deformed, Fig. 6.5, and the resulting birefringence was calculated. The results of linear deformation along the x and y axes for fibres A, C and E are presented in Fig. 6.8. As expected, the smallest structure (fibre A) exhibits the largest sensitivity to asymmetric structural variations. However, even for larger structures a scaling factor between 10 and 20% is sufficient to generate $B \sim 5x10^{-4}$, which according to our model produces well spaced sidebands at ~450 and ~600 nm. Note that this analysis is based on longitudinally uniform fibres. For real structures, subject to more random microscopic deformations, an even smaller amount of cladding deformation is probably sufficient to produce the same results. Overall, the required asymmetry of 10-20% seems compatible with the structure of our fibres, see e.g. Fig. 6.5(c), which especially in the first few rings outside the core suffer from small but significant deformations due to expansion of the air core during the fibre drawing process.

FWM can be a very efficient process with, in principle, up to 100% conversion of the pump power into the sidebands. In practice however, several processes can limit the efficiency:

i. Because of the large spectral separation of the sidebands and the large group velocity dispersion in the visible regime, pulses experience considerable walk-off. For example, two pulses at 460 nm and 625 nm, respectively, will be spatially separated by ~14 mm after 1 m of propagation. The length of 80 ps pulses, on the other hand, is ~16 mm. Therefore, efficient nonlinear conversion can only take place over about 114 cm of fibre and the pump power must be high enough to achieve sufficient FWM gain over this length.

ii. Our fibres exhibit relatively large wavelength-dependent losses, in particular fibres A and B with the smallest structures exhibit large losses in the blue. Consequently, we observed slightly larger energy conversion after 30 cm of fibre than after 1 m, as discussed before.

iii. Stimulated Raman scattering forms a competing process to FWM. As already mentioned, for orthogonally polarized pump and sidebands the peak Raman gain and the peak parametric gain are of comparable size. A Raman shifted pump peak will itself create red and blue sidebands albeit at shifted wavelengths according to the modified phase matching condition. However, because of the broader spectral range and thus lower spectral density of the Raman peak compared to the initial pump, the conversion efficiency will be reduced.

iv. Finally, fluctuations of the structural dimensions along the fibre lead to dephasing of pump and sidebands, which limit the maximum energy conversion.

A combination of all these effects is thought to have limited the maximum conversion efficiency in our experiments. Nevertheless, we observed up to ~20% of the output power in the red and blue regions, see Sec. 6.2.3. Improving the coupling of the 530 nm pump light into a single secondary core of the cobweb fibre would increase the pump peak power, which would allow for RGB generation in shorter fibre lengths and thus reduce the effects of spatial walk-off, propagation losses, and dephasing due to structural fluctuations. An optimized laser white light source with approximately equal powers in the red, green, and blue spectral regions seems feasible in this case.

6.3 Picosecond fibre-based laser emitting at 589 nm

In recent years the development of a fibre-based laser guide star system emitting at 589 nm has attracted a lot of interest. Laser guide star systems are based on the emission from sodium in a mesospheric layer and have proved most useful for adaptive corrections of turbulence in the atmosphere [24]. This restricts the laser wavelength to 589 nm. Requirements on the laser source go beyond the wavelength itself. A high-power is needed, typically 10 W or more, and the linewidth must be smaller than the absorption line of 3 GHz.

Conventional guide star systems typically involve high-power bulk solid-state lasers emitting in the near infrared, wavelength conversion schemes such as sum-frequency generation are then employed since high-power lasers emitting directly at 589 nm are at present complex, inefficient and unreliable. The main advantages of fibre lasers are compactness, robustness, and high efficiency. In addition their excellent beam quality and power scalability combined with good thermal management makes them compatible with high-power nonlinear frequency conversion [6, 7] as demonstrated in Chapter 5.

Several fibre-based laser guide star systems have been demonstrated in CW regime mainly based on two methods. A first technique relies on nonlinear down-conversion in an optical fibre to 1178 nm of a pump beam produced by a high-power ytterbium doped fibre laser through stimulated Raman scattering followed by second-harmonic generation in a nonlinear crystal. To date, this configuration enabled the generation of 10 mW using two Stokes shifts [25] and up to 3 W with a single Stokes shift [26]. However spectral broadening inherent to nonlinear frequency conversion in fibre severely degrades the laser linewidth to unacceptable values for the application. The second type of system is based on sum-frequency generation in a nonlinear crystal from two beams emitting at 920 nm and 1530 nm generating by an Nd doped fibre laser and an Er/Yb codoped fibre laser respectively. Since the gain medium relies on rare-earth doped

fibre and not on fibre nonlinearities, this technique appears very promising and demonstration of such sources with powers exceeding 0.5 W have been reported in [27].

Here I present the realisation and characterisation of a high-power pulsed fibre laser producing picosecond pulses at 589 nm based on simultaneous amplification of a pulsed pump beam at 1060 nm and a CW signal beam at 1178 nm in a single ytterbium doped fibre amplifier. Since several hundred watts of power can be generated in fibre amplifiers with picosecond pulses [28], this alternative approach appears attractive for the generation of very high average powers in this spectral range.

6.3.1 Design of the fibre source at 589 nm

The experimental set-up is shown is Fig. 6.9. The main components of the laser source are a CW seed laser, a pulsed pump laser, an Yb doped fibre amplifier that acts also as a Raman fibre amplifier, and a frequency doubler. The seed source for the system is composed of a cascaded Raman fibre laser emitting at 1178 nm pumped by a YDFL emitting at 1070nm. The pump laser is based on a pulsed fibre MOPA source producing picosecond pulses at 1060 nm. Both 1060 and 1178 nm beams are combined using a 980/1060 nm WDM coupler and free-space launched through an isolator designed for 1060 nm into a 23 m long Yb doped fibre. This fibre, pumped by a laser diode stack emitting at 975 nm constitutes the final stage of amplification of the Yb based fibre MOPA which simultaneously amplifies the 1060 nm pulsed beams with the 1178 nm Raman signal. The resulting high-power pulsed Raman signal is then launched into a type-I non-critically phase-matched LBO crystal for frequency doubling at 589 nm. Highly selective dichroic mirrors (DM) are employed at the input and output of the crystal to filter out unwanted pump beams.

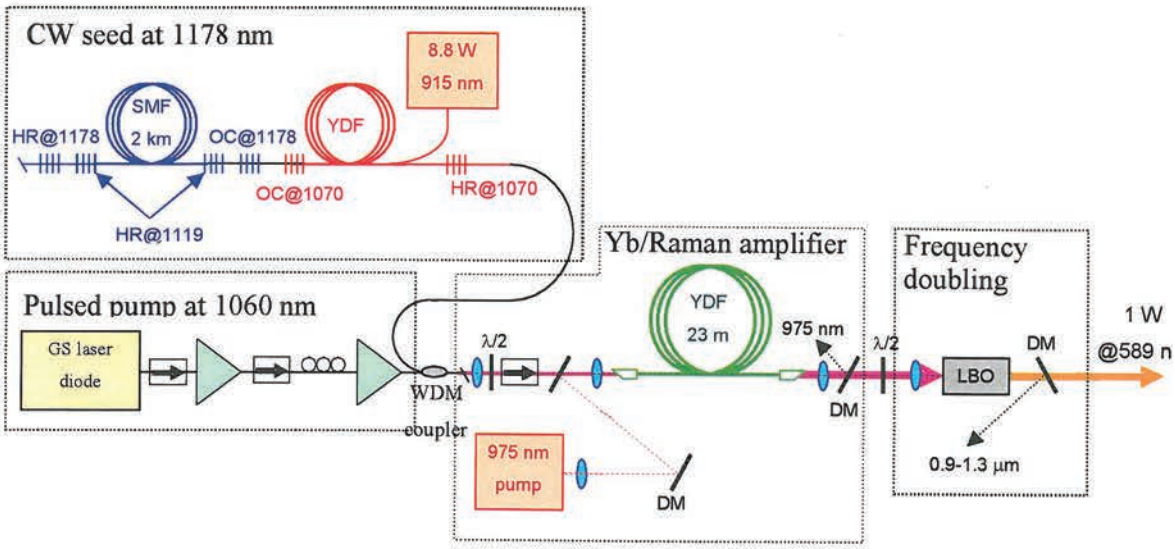

Fig. 6.9. Experimental set-up of the 1 W pulsed fibre based source at 589 nm. HR: high reflection, HT: high transmission, OC: output coupler, DM: dichroic mirror.

6.3.2 Continuous-wave Raman fibre laser at 1178 nm

A cascaded Raman fibre laser (CRFL) was designed and built to constitute the continuous-wave seed source for the fibre based system. In a CRFL, the first Stokes is generated in a fibre producing sufficient Raman gain when pumped by a high-power beam. This radiation is then maintained in a cavity via highly reflective mirrors or FBGs to pump a second Stokes wave, itself generated in a second cavity including an output coupler in the form of a lower reflectivity FBG at the Stokes wavelength. This structure can be repeated via several cavities at various Raman Stokes until the suitable wavelength is reached. Here the CRFL is based on two Stokes waves to produce 1178 nm radiation. The Raman oscillator was composed of a 2 km long dispersion shifted fibre single-mode at 1.5 μm spliced to two pairs of FBGs with reflectivity peaking at 1119 nm and 1178 nm, and bandwidth of 2 and 0.1 nm respectively. The CRFL was pumped in a counter-propagating scheme by a cladding pumped YDFL producing 3.8 W of output power resulting in the generation of 690 mW of total output power of Raman signal. The first Raman Stokes at 1119 nm was not totally depleted in the oscillator as depicted in the spectrum in Fig. 6.10(a). The power produced in the 1119 nm-first and 1178 nm-second Stokes was estimated to be 156 and 534 mW respectively. Although FBGs were designed with a narrow bandwidth, lasing is observed outside the grating and the signal linewidth broadens severely to 0.6 nm (resolution = 0.05 nm) as shown in Fig. 6.10(b). The combination of long fibre length and four-wave mixing between longitudinal modes in the Raman resonator are responsible for this spectral broadening. A narrow linewidth Raman fibre laser can be realized by employing shorter fibre length with higher Raman gain in the Raman cavity [26].

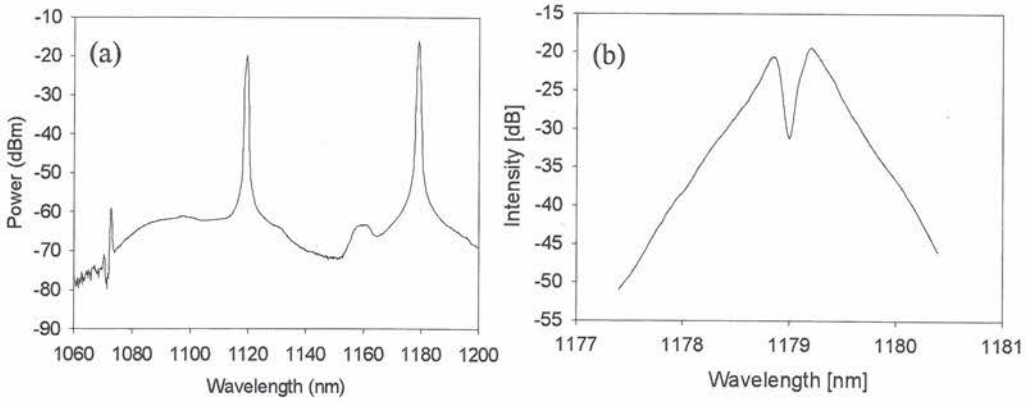

Fig. 6.10. Output spectra of the seed cascaded Raman fibre laser. (a) Spectrum of first and second Raman Stokes signals at 0.69 W total output power (0.5 nm resolution). (b) Spectrum of 1179 nm output at 534 mW output power, linewidth (FWHM) ~ 0.6 nm (0.05 nm resolution).

6.3.3 Pulsed ytterbium doped fibre MOPA system at 1060 nm

As a pump source for the pulsed Raman fibre amplifier, a pulsed YDF MOPA system was utilized. The master oscillator was based on a Fabry-Perot laser diode gain-switched at 32 MHz to produce pulses with 140 ps duration (FWHM) as presented in Fig. 6.11(a). These pulses, with 0.2 mW average power, were then successively amplified by a core-pumped YDFA and a cladding-pumped YDFA separated by isolators to avoid any back reflections, raising the average power to 250 mW. The pulsed signal was finally free-space launched into a final stage high-power amplifier composed of a 23 m long YDF with a core diameter of 8 μm and a D-shaped inner cladding of 400 μm and pumped by a diode stack emitting at 975 nm. This final stage was capable of producing 45 W average power as shown in Fig. 6.11(b). At this power level, two spontaneous Raman Stokes are obtained.

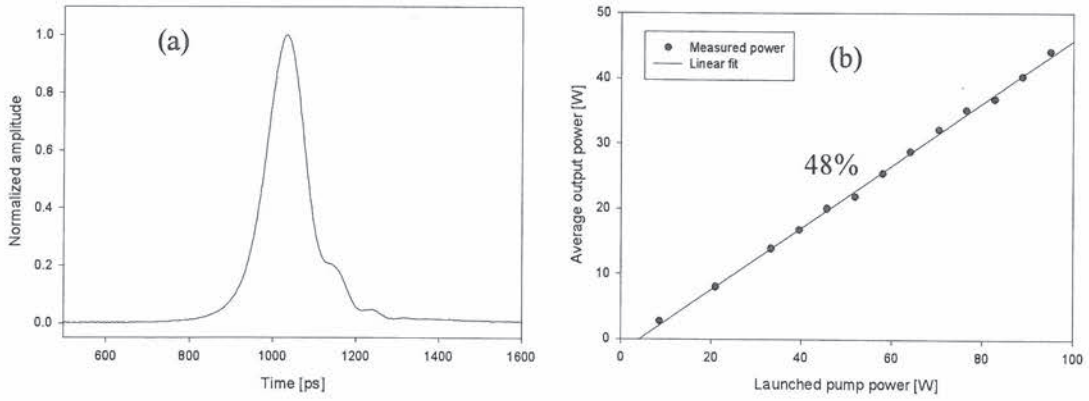

Fig. 6.11. Pulsed fibre MOPA characteristics. (a) Pulse shape from the pulsed laser diode, pulse width (FWHM) ~ 140 ps. (b) Output power characteristics at output of the 23 m Yb-doped fibre.

6.3.4 Pulsed source emitting at 1178 nm

About 120 mW of Raman signal is launched into the high-power final stage YDFA and amplified to 45 W average output power including the remaining pump power. Fig. 6.12(a) shows the evolution of the output spectrum as a function of average power and indicates that although an on-off gain of about 20 dB was reached at 1178 nm, it resulted in a dramatic spectral broadening. In pulse-pumped Raman amplifiers involving short pulses, self-phase modulation and particularly cross-phase modulation induced by simultaneous fibre amplification and propagation of 1060nm, 1119 nm and 1178 nm beams are identified to be the main causes of linewidth degradation. While these detrimental effects can be slightly reduced by adapting adequately the beam polarisation, they remain significant and are in competition with the other nonlinear effect, including the desired stimulated Raman scattering. As expected in pulsed pumping configuration, at maximum output power, a large amount of power remains in the 1060 nm and 1119 nm pump beams as depicted in the optical spectrum. Pulse shapes of the pump and signal beams measured at 25 W output power with a rotating diffraction grating and presented in Fig. 6.12(b) illustrate this partial pump depletion. At this power level, the pulse width of the Raman signal was about 100 ps. Noise was also observed on the output pulse shapes which can also be attributed to the large amount of XPM.

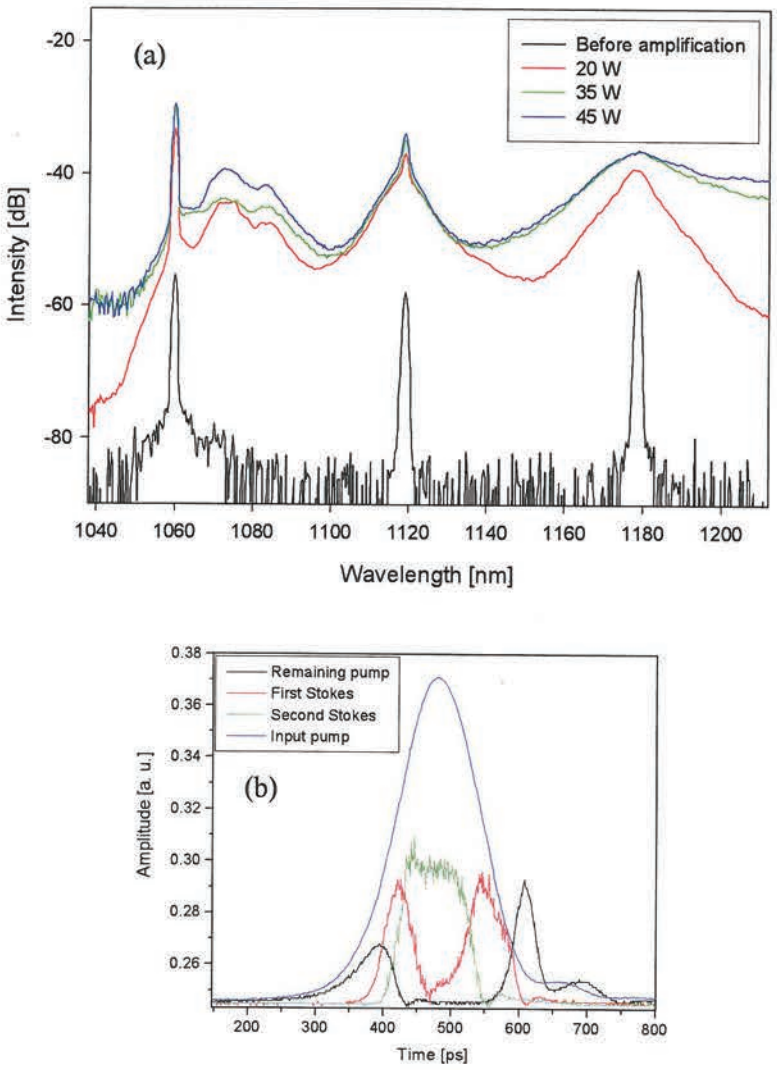

Fig. 6.12. Pulsed Raman fibre amplifier characteristics. (a) Output spectrum at various total average power levels. (b) Pulse shapes at 25 W total average output power, pulse width (FWHM) at 1178 nm ~ 100 ps.

6.3.5 Frequency doubling at 589 nm

The amplified pulsed Raman signal was launched into a 15 mm-long LBO crystal with a combination of lenses. The crystal temperature was optimized for second-harmonic generation at 589 nm and set to 36°C. The state of polarisation was not carefully monitored and controlled after amplification. Nevertheless a half-wave plate was used to rotate the polarisation for best SHG efficiency. Fig. 6.13(a) shows the 2nd Stokes and 589 nm power evolution as a function of total power. With a maximum power of 25 W at 1178 nm, the frequency doubled power reached 1.01 W. The poor conversion efficiency is due to the broad spectral linewidth (FWHM) of 8 nm of the fundamental beam and possibly to a degraded polarisation extinction ratio of the

amplified signal. The output spectrum of the frequency doubled beam at various power levels is shown in Fig. 6.13(b). The spectral linewidth (FWHM) was 3.7 nm at maximum output power.

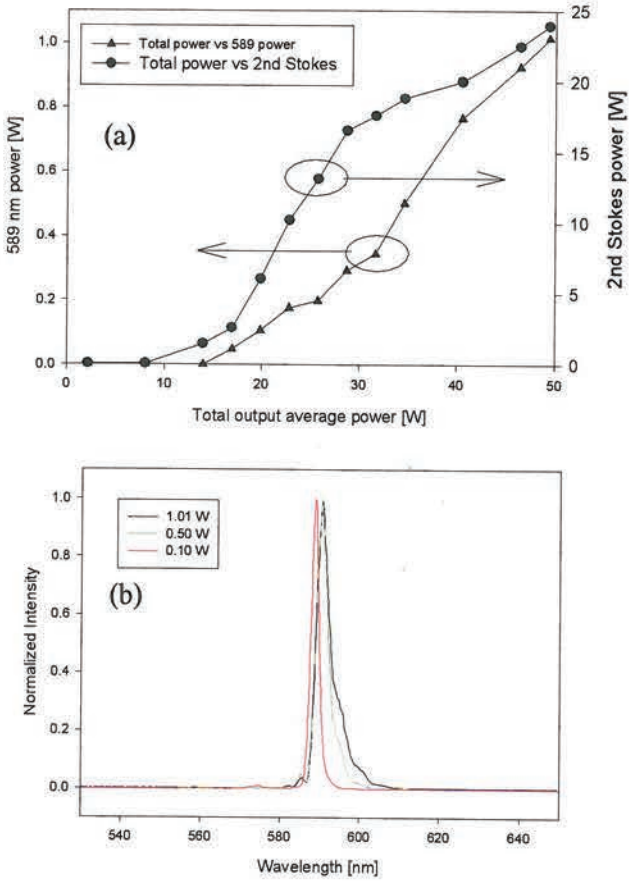

Fig. 6.13. Second-harmonic generation at 589 nm. (a) Average output at 1178 nm and 589 nm versus total average output power. (b) Output spectrum of the frequency doubled pulsed Raman signal at various power levels, linewidth (FWHM) at 1 W ~ 3.7 nm.

6.3.6 Simulated results

Guide star application requires narrow laser linewidth in the order of 3 GHz, which would corresponds to Fourier transform limited pulses with durations of about 200 ps. However the demonstrated laser system produced laser radiation in the near infrared with a linewidth severely broadened to even exceed the acceptance bandwidth of the nonlinear crystal for second-harmonic generation, thus limiting the overall system efficiency. The main mechanism degrading the laser linewidth was identified to be cross-phase modulation between the pump beam and the Raman signals in the fibre amplifier as previously reported and described in the visible in a passive fibre [30]. Self-phase modulation also contributes to the linewidth broadening but is twice less effective than XPM for the same intensity [21].

I simulated the system using a commercial software (VPI TransmissionMaker) where the pump pulsed beam and the two Raman signals were considered co-propagating in a passive single-mode fibre. Although the propagation properties in a passive fibre differ from those in a RE-doped fibre with gain, this analysis helped to study the impact of XPM induced spectral broadening in such a fibre laser system. The fibre length was 40 m with an effective area of 60 μm^2, and the pump beam had a peak power of 2 kW with pulse durations of 140 ps at 32 MHz, power of the seeds was fixed to 100 mW.

The simulated optical spectra after Raman amplification of signals with input linewidths of 1GHz and 50GHz in the 40 m-long fibre were analyzed. Although the initial considered linewidths are narrow with 1 GHz and 50 GHz, simulations shows a dramatic increase of linewidth to 3.5 nm and 7 nm, respectively. The impact of XPM on the output pulses was also investigated and the simulated pulse shapes for the various pump and Raman beams are shown in Fig. 6.14. The simulated output pulse shapes at 1178 nm matched the experimentally measured pulses reported in Fig. 6.12. They also confirm the large intensity distortions induced by strong XPM regime between the co-propagating beams.

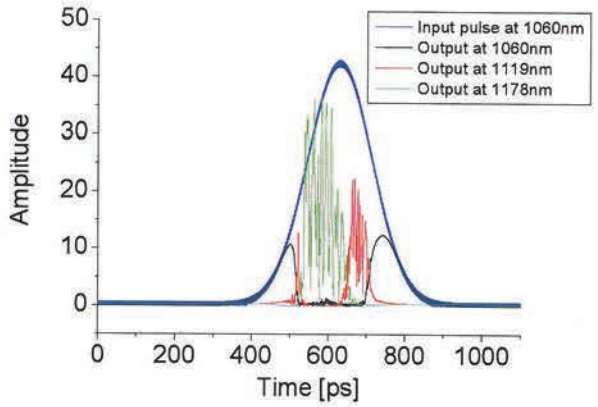

Fig. 6.14. Simulated pulse shape for the pump and Raman beams after co-propagating in a 40 m-long single-mode fibre.

6.3.7 Discussion and prospect

Although this novel approach for the realisation of a pulsed fibre based guide star system seems to offers many benefits including power scalability and potentially an all-fibre configuration, the inherent properties of short pulses implies that Raman amplification is inevitably accompanied by nonlinear spectral broadening. If the pulsed scheme is of interest, longer pulses, for instance in nanosecond regime would allow Raman amplification while mitigating SPM and XPM. In addition shaping pulses to a flat top profile can significantly reduce the impact of phase

modulations [31]. Furthermore the laser system can be simplified by employing a YDFL operating directly at 1120 nm.

From these experimental results, it appears that exploiting nonlinear effects in an optical fibre to produce narrow linewidth radiation is quite challenging. Moreover the peak power requirement for efficient frequency conversion through an LBO crystal constituted a major problem. Therefore an alternative solution based on RE doped fibre amplification and subsequent frequency conversion through periodically-poled crystals providing high nonlinear coefficient looks more promising. Recently there have been several reports on the potential of YDFA for amplification and lasing at wavelengths above 1120nm and particularly at 1178nm either by using high-Q cavity [32] or by heating up the YDF to shift the gain spectrum to longer wavelengths [33]. Another interesting development is based on Bismuth doped fibres. CW and pulsed fibre laser emitting in the 1150-1300nm wavelength region have already been realised with this novel fibre when pumped by a YDFL emitting at 1070 nm for instance [34, 35]. Therefore Bismuth doped fibres appear also very suitable for amplification of 1178nm seed sources and subsequent SHG at 589nm. These technological advances could lead to the development of fibre MOPA systems operating at 1178nm with narrow linewidth ideally suited for SHG. However these novels fibre amplifiers, and particularly Bismuth-based amplifiers, require long devices and the challenge resides then in controlling the onset of stimulated Brillouin scattering that could severely limit power scaling of the narrow linewidth laser. This regime would be in fact very similar to the one obtained with other erbium or ytterbium-based single fibre MOPA systems.

6.4 Conclusion

This chapter has shown through two different experimental demonstrations that nonlinear effects in optical fibres can be very useful to generate visible wavelengths usually difficult to reach with conventional fibre lasers. Both experiments were based on a picosecond Yb-based fibre MOPA at 1060 nm whose design had been presented in chapter 4. In a first set of experiments, the output beam was frequency doubled and launched into the substructures of a PBGF to exploit nonlinearities of these secondary cores. This led to the generation of red and blue spectral sidebands resulting in a white light output beam. A second set of experiments employed this same MOPA system at 1060 nm to pump a cw signal at 1178nm using two Stokes shifts in a high-power YDFA. The resulting amplified signal was then frequency doubled to produce laser radiation 589 nm, a useful wavelength for guide star applications. However the resulting linewidth greatly exceeds the requirement for these applications. This

was partly due to the broad linewidth of the cw seed source and mostly due to the detrimental effects of cross-phase modulations in the Raman fibre amplifier. The use of a narrow linewidth seed source such as a DFB laser emitting at 1178nm would improve the performance of the system; however the amplified signal would still suffer from nonlinear spectral broadening.

Various research laboratories are currently working on the development of fibre-based sources emitting at 589 nm. These types sources are on paper extremely attractive owing to their potential for compactness and robustness, however achieving narrow linewidth with these sources has proved to be very challenging . Alternatively, it should be noted that existing bulk systems can already deliver narrow linewidth at 589 nm with watt level output power in a fairly compact, simple and efficient format [36].

These investigations demonstrate once again the versatility of picosecond fibre lasers. They can produce high average power and sufficient peak power to enhance nonlinear effects in optical fibres. Although the reported experiments were realised in a free-space configuration, the laser design suggests that a quasi all-fibre configuration is possible. This emphasizes the benefit of combining nonlinear optical effects and fibre lasers.

References

1. J. Nilsson, W.A. Clarkson, R. Selvas, J.K. Sahu, P.W. Turner, S.-U. Alam, and A.B. Grudinin, "High-power wavelength-tunable cladding-pumped rare-earth-doped silica fiber lasers," Optical Fiber Technol. **10** , 5-30 (2004).

2. R. Paschotta, N. Moore, W. A. Clarkson, A. C. Tropper, D. C. Hanna, and G. Mazé, "230 mW of Blue Light From a Thulium-Doped Upconversion Fiber Laser," IEEE J. Select. Top. Quantum Electron. **3**, 1100-1102 (1997).

3. R. G. Smart, D. C. Hanna, A. C. Tropper, S. T.Davey, S. F. Carter, and D. Szebesta, "Cw room temperature upconversion lasing at blue, green and red wavelengths in infrared-pumped Pr -doped fluoride fiber," Electron. Lett., **27**, 1307–1308 (1991).

4. J. Y. Allain, M. Monerie, and H. Poignant, "Tunable CW lasing around 610, 635, 695, 715, 885 and 910 nm in praseodymium-doped fluorozirconate fibre", Electron. Lett. **27**, 189–191 (1991).

5. A. Richter, H. Scheife, E. Heumann, G. Huber, W. Seelert, and A. Diening, "Semiconductor laser pumping of continuous-wave Pr^{3+}-doped ZBLAN fibre laser," Electron. Lett. **14**, 794–795 (2005).

6. A. Liu, M. A. Norsen, and R. D. Mead, "60-W green output by frequency doubling of a polarized Yb-doped fiber laser," Opt. Lett. **30**, 67-69 (2005).

7. P. Dupriez, J. K. Sahu, A. Malinowski, Y. Jeong, D. J. Richardson, and J. Nilsson, "80 W green laser based on a frequency doubled, single-mode, linearly polarized fiber laser," in Conference on Lasers and Electro-Optics, paper CThJ1, Long Beach, USA (2006).

8. M. Y. Vyatkin, A. C. Dronov, M. A. Chernikov, S. V. Popov, J. R. Taylor, D. V. Gapontsev, and V. P. Gapontsev, "Multi-watt, 780 nm, single-frequency CW fiber-based by SHG in PPLN and PPKTP," in Proc. Conference on Lasers and Electro-Optics, vol. 3, 1993-1994, Baltimore, USA, 22-27 May 2005.

9. J. C. Travers, S. V. Popov, and J. R. Taylor, "Extended blue supercontinuum generation in cascaded holey fibers," Opt. Lett. **30**, 3132-3134 (2005).

10. S. Coen, A. H. L. Chau, R. Leonhardt, J. D. Harvey, J. C. Knight, W. J. Wadsworth, and P. St. J. Russel, "Supercontinuum generation by stimulated Raman scattering and parametric four-wave mixing in photonic crystal fibers," J. Opt. Soc. Am. B **19**, 753-764 (2002).

11. P. -A. Champert, V. Couderc, P. Leproux, S. Février, V. Tombelaine, L. Labonté, P. Roy, C. Froehly, and P. Nérin, "White-light supercontinuum generation in normally dispersive optical fiber using original multi-wavelength pumping system," Opt. Express **12**, 4366-4371 (2004).

12. V. J. K. Ranka, R. S. Windeler, and A. J. Stentz, "Visible continuum generation in air silica microstructure optical fibers with anomalous dispersion at 800nm ," Opt. Lett. **25**, 25-27 (2000).

13. G. Derra, H. Moench, E. Fischer, H. Giese, U. Hechtfischer, G. Heusler, A. Koerber, U. Niemann, F.-C. Noertemann, P. Pekarski, J. Pollmann-Retsch, A. Ritz, and U. Weichmann, "UHP lamp systems for projection applications," J. Phys. D: Appl. Phys. **38**, 2995-3010 (2005).

14. S. Leon-Saval, T. Birks, W. Wadsworth, P. St. J. Russell, and M. Mason, "Supercontinuum generation in submicron fibre waveguides," Opt. Express **12**, 2864-2869 (2004).

15. M. Rusu, S. Kivistö, C. Gawith, and O. Okhotnikov, "Red-green-blue (RGB) light generator using tapered fiber pumped with a frequency-doubled Yb-fiber laser," Opt. Express **13**, 8547-8554 (2005).

16. J. M. Dudley, L. Provino, N. Grossard, H. Maillotte, R. S. Windeler, B. J. Eggleton, and S. Coen, "Supercontinuum generation in air-silica microstructured fibers with nanosecond and femtosecond pulse pumping ," J. Opt. Soc. Am. B **19**, 765-771 (2002).

17. F. Brunner, E. Innerhofer, S. V. Marchese, T. Südmeyer, R. Paschotta, T. Usami, H. Ito, S. Kurimura, K. Kitamura, G. Arisholm, and U. Keller, "Powerful red-green-blue laser source pumped with a mode-locked thin disk laser," Opt. Lett. **29**, 1921-1923 (2004).

18. N.A. Mortensen and M.D. Nielsen, "Modeling of realistic cladding structures for air-core photonic bandgap fibers," Opt. Lett. **29**, 349-351 (2004).

19. F. Poletti, V. Finazzi, T. M. Monro, N. G. R. Broderick, V. Tse, and D. J. Richardson, "Inverse design and fabrication tolerances of ultra-flattened dispersion holey fibers," Opt. Express **13**, 3728-3736 (2005).

20. P.R. McIsaac, "Symmetry-induced modal characteristics of uniform waveguides. I. Summary of results," IEEE Transactions on Microwave Theory and Techniques MTT-**23**, 421-429 (1975).

21. G. P. Agrawal, *Nonlinear Fiber Oprics*, 3rd ed. (Academic Press, San Diego, CA, USA, 2001).

22. A. Tonello, S. Pitois, S. Wabnitz, G. Millot, T. Martynkien, W. Urbanczyk, J. Wojcik, A. Locatelli, M. Conforti, and C. De Angelis, "Frequency tunable polarization and intermodal modulation instability in high birefringence holey fiber," Opt. Express **14**, 397-404 (2006).

23. R. J. Kruhlak, G. K. L. Wong, J. S. Y. Chen, S. G. Murdoch, R. Leonhardt, J. D. Harvey, N. Y. Joly, and J. C. Knight, "Polarization modulation instability in photonic crystal fibers," Opt. Lett. **31**, 1379-1381 (2006).

24. V. C. Coffey, "Astronomy – Keck laser guide star improves seeing in Hawaii", Laser Focus World, vol. 38 (3), p. 28, March 2002.

25. Y. Feng, S. Huang, A. Shirakawa, and K. Ueda, "589 nm light source based on Raman fiber laser," Jap. J. Appl. Phys. -2, **43**, L722-L724 (2004).

26. D. Georgiev, V. P. Gapontsev, A. G. Dronov, M. Y. Viatkin, A. B. Rulkov, S. V. Popov, and J. R. Taylor, " Watts-level frequency doubling of a narrow line linearly polarized Raman fiber laser to 589nm," Opt. Express **13**, 6772-6776 (2005).

27. D. M. Pennington, J. W. Dawson, A. Drobshoff, Z. Liao, S. Payne, D. Bonaccini, W. Hackenberg, and L. Taylor, "Compact fiber laser approach to 589 nm laser guide stars," in Proc. Conference on Lasers and Electro-Optics 2004, San-Francisco, USA, 16-21 May 2004, paper CFD1.

28. P. Dupriez, A. Piper, A. Malinowski, J. K. Sahu, M. Ibsen, Y. Jeong, L. M. B. Hickey, M. N. Zervas, J. Nilsson, and D. J. Richardson, "321 W average power, 1 GHz, 20 ps, 1060 nm pulsed fiber MOPA source," OFC/NFOEC 2005, Anaheim, USA, 6-11 March 2005, postdeadline paper PDP3.

29. J.-C. Bouteiller, "Spectral Modeling of Raman Fiber Lasers," IEEE Photon. Technol. Lett. 15, 1698-1700 (2003).

30. R. R. Alfano, P. L. Baldeck, P. P. Ho, and G. P. Agrawal, " Cross-phase modulation and induced focusing due to optical nonlinearities in optical fibers and bulk materials," J. Opt. Soc. Am. B **6**, 824-829 (1989).

31. T. Sato, T. Horiguchi, M. Tateda, Y. Koyamada, and H. Izumita, "Spectral-linewidth broadening in synchronous Raman fiber amplification caused by cross-phase modulation effects and its suppression," Opt. Lett. **22**, 880-882 (1997).

32. J. Ota, A. Shirakawa and K.-I. Ueda, "High-Power Yb-Doped Double-Clad Fiber Laser Directly Operating at 1178nm," Jpn. J. Appl. Phys. **4**, L117-L119 (2006).

33. D. A. Grukh, A. S. Kurkov, V. M. Paramonov, and E. M. Dianov, "Effect of heating on the optical properties of Yb3+ -doped fibres and fibre lasers," Quantum Electron. **34**, 579-582 (2004).

34. E. M. Dianov , V. V. Dvoyrin , V. M. Mashinsky , A. A. Umnikov , M. V. Yashkov , A. N. Gur'yanov, "CW bismuth fibre laser," Quantum Electron., **35**, 1083-1084 (2005).

35. V. V. Dvoyrin, V. M. Mashinsky, and E. M. Dianov, " Yb-Bi pulsed fiber lasers," Opt. Lett. **32**, 451-453 (2007).

36. P. Dekker, H. M. Pask, and J. A. Piper, "All-solid-state 704 mW continuous-wave yellow source based on an intracavity, frequency-doubled crystalline Raman laser," Opt. Lett. **32**, 1114-1116 (2007).

Chapter 7 Conclusion and future work

In the following I will summarize the work presented in this thesis and suggest possible improvements and future research directions.

Power scaling of various ultrafast fibre sources has been demonstrated. Important features of these high-power systems are the use of low-power semiconductor lasers producing ultrashort pulses with high repetition rate in combination with large mode area Yb-doped fibre amplifiers. A common challenge in the development of such systems resides in managing fibre nonlinearities to achieve output specifications dictated by the application. Indeed these systems can be designed to minimize nonlinearities such as SRS, SPM and XPM for achieving efficient frequency conversion through a nonlinear crystal. However in other applications nonlinear effects provide a convenient and simple method to produce shorter femtosecond pulses via SPM and pulse compression or new wavelengths via Raman amplification.

For instance, two types of optically pumped passively mode-locked VECSELs were employed as seed sources for a high-power fibre MOPA in which the final LMA fibre amplifier was used to provide high-gain and also induce sufficient SPM for achieving efficient temporal compression down to fs durations. Pulses produced by a first ML-VECSEL with 4.6 ps of duration at 910 MHz and emitted at 1055 nm were amplified up to 200 W of average power. The large amount of SPM accumulated during amplification enabled linear pulse compression down to 430 fs with a typical pedestal causing reduced peak power as confirmed by numerical simulations. Alternatively, the development of a similar system incorporating a ML-VECSEL producing 0.5 ps pulses at 1042 nm with a repetition rate of 1.1 GHz allowed for the self-similar regime of amplification. This resulted in pulse compression down to 170 fs with excellent pulse quality at a maximum average power of 53 W. A mismatch between the Yb gain spectrum and the VECSEL emission wavelength prevented further power scaling. Numerical simulations also confirmed distortion of the SPM-induced chirp caused by this mismatch.
As previously suggested, designing the VECSEL structure to shift its emitting wavelength towards 1060-1070 nm would improve dramatically the performance of the system. In this case, the same MOPA configuration would produce parabolic pulse at average powers exceeding 100 W. The onset of SRS and gain bandwidth limitation would then constitute a limitation for

further improvement. However shifting the wavelength of VECSELs towards 1060 nm is quite challenging. Future research work could consist in investigating various YDFs to shift the peak gain to shorter wavelengths while making sure that requirements for self-similar amplification regime are fulfilled. Moreover, in the experimental demonstration, a fraction of power was extracted to study the potential for efficient pulse compression. Incorporating a pair of bulk gratings designed for high-power in the system would allow pulse compression of the total output power constituting a major improvement. This new femtosecond fibre source could then be utilised for applications. Indeed this novel high-power ultrafast source offers ideal properties for pumping OPOs or highly nonlinear fibre for the generation of high-power supercontinuum and the generation of THz waves.

When only picosecond pulses are required with high average power, it was shown in Chapter 4 that direct amplification of longer pulses allows for further power scaling. Reduced spectral bandwidth is often another important aspect meaning that SPM should be minimised in the fibre amplifier. With these considerations in mind, I have developed a high-power fibre MOPA system based on amplification of 16-20 ps pulses produced by a gain-switched laser diode emitting at 1060 nm. The combination of a high repetition rate of 1 GHz and LMA Yb-doped fibres in the final stage of amplification was key to achieve high-power amplification with reduced SPM-induced spectral bandwidth. Two Yb-doped fibres were investigated for high-power amplification leading to various output characteristics while spectral width was kept below 0.5 nm. A maximum output power of 125 W was produced in a diffraction limited beam by a YDFA comprising a fibre core of 25 μm in diameter and NA<0.05. The average power was further increased to 321 W by employing a fibre with a core diameter of 43 μm and NA~0.09. However these waveguide properties resulted in an output beam quality factor (M^2) of 2.4 meaning that the output beam included higher order modes.
These experimental demonstrations were realised in the early stages of the rapid development in high-power fibre technology. With the outstanding recent developments, these same fibre MOPA systems could be power scaled in a straightforward way towards kilowatt average power in a diffraction-limited output beam. This very high power quasi-CW source would offer high average power, high peak power and microJoule range energy useful for numerous applications such as high-speed micromachining or nonlinear frequency conversion.

In addition to offering highly stable picosecond pulses, a telecom-grade gain-switched semiconductor laser provides unique flexibility in the pulse parameters with selectable repetition rate. This represents an excellent tool to optimise the performance of a high-power fibre sources. Based on these additional considerations, I have developed an improved high-

power fibre MOPA designed for efficient second-harmonic generation through a nonlinear crystal in single-pass configuration. Efficient frequency doubling through a nonlinear crystal requires linearly polarized nearly diffraction limited output beam implying the use of polarisation maintaining LMA YDFs for amplification. In addition high peak power of at least 10 kW and narrow spectral width are important due to limited spectral acceptance bandwidth of conventional crystals. Therefore SPM-induced spectral bandwidth must be minimised. For these reasons, the final stage of amplification includes a LMA PM-YDF with a mode field diameter of 16 μm and the seed source was configured to provide longer pulses with variable repetition rate. These improvements led to the successful experimental demonstration of high-power SHG up to 80 W at 530 nm with a conversion efficiency of 49% and nearly diffraction limited output beam. In this case, the pulses were 80 ps in duration tuned to a repetition rate of 120 MHz allowing reduced spectral bandwidth and negligible level of SRS.

Owing to its outstanding brightness, this fibre based green source offers an excellent alternative to frequency doubled bulk mode-locked lasers. A possible route for future work is the generation of high-power UV radiation via third harmonic or fourth harmonic generation. Assuming standard conversion efficiencies obtained by harmonic generation through LBO and CLBO crystals, 80 W at 530 nm could result in the generation of approximately 30 W at 353 nm and around 8 W at 265 nm, respectively. As suggested in this work, investigating spectral compression as a convenient method to achieve high conversion efficiency despite the high-peak power produced by the amplifier represents another interesting aspect related to harmonic generation from ultrafast fibre-based systems.

The high brightness green laser was also used to pump secondary cores of a holey fibre. We have experimentally observed efficient generation of blue and red components at the fibre output. Based on experimental investigations and numerical calculations, this phenomenon was attributed to high birefringence in the small cores providing support for a phase-matched FWM process.

An efficient and simple scheme for high-power white light generation is of particular interest due to the variety of applications such as laser display and microscopy. Future directions related to this research work include the design of novel fibres with waveguide and nonlinear properties adequately tailored to enhance conversion efficiency via optimal phase matching conditions. Another interesting aspect of white light generation resides in the generation of supercontinuum provided by pumping in the green. Pumping in the visible wavelength ensures more efficient conversion to white light than conventional near IR pumped supercontinuum sources. However this also implies the challenging realisation of novel types of fibres with, for instance, a zero dispersion located near the pump wavelength at 530 nm.

Previously, we have seen that fibre nonlinear effects can be excited externally by employing the high-power beam produced by a fibre MOPA as a pump source. In a final part of this thesis I have developed a fibre based laser guide star system producing 1 W at 589 nm. The unique design consists in using amplified picosecond pulses produced by the versatile gain-switched laser diode to pump radiation at 1178 nm via SRS in an YDFA. In this case nonlinear transfer of power is carried out within the amplifier chain and only nonlinear frequency doubling is achieved externally using a LBO crystal in a single-pass configuration. Despite the simplicity and high degree on integration of such a scheme and the successful realisation of a source with watt level output, the overall conversion process from 1060 nm to 589 nm was quite inefficient. Indeed Raman amplification in this regime is also accompanied by severe SPM and XPM which causes dramatic increase of spectral bandwidth resulting in turn in low conversion efficiency after second-harmonic generation.

This experimental investigation has revealed major limitations due to the high peak power required for efficient frequency doubling and inherent properties of fibre nonlinearities in the picosecond regime. The system performance could be improved by employing ns pulses with rectangular pulse shape. This new pulse format would significantly reduce the impact of phase modulations and ensure satisfactory bandwidth for efficiency frequency conversion. However despite these improvements the final linewidth would most likely exceed the stringent requirements for guide star applications. In fact, the most attractive option to achieve high-power narrow linewidth at 1178 nm, would rely on the realisation of a fibre MOPA source seeded by a CW DFB laser diode emitting at 1178 nm and amplified by new types of fibre amplifiers. Gain at 1178 nm can be offered by bismuth doped fibres or by high temperature YDF for shifting the gain towards longer wavelengths. Subsequent SHG could then be implemented by a periodically poled device for optimal conversion efficiency to 589 nm in the cw regimes, at powers much lower than the (peak) powers required for doubling in LBO.

List of Publications

Conference publications

1. **P.Dupriez**, K.G.Wilcox, C.Finot, A.N.Malinowski, J.K.Sahu, D.J.Richardson, A.C.Tropp, er, J.Nilsson,"Gigahertz parabolic pulse generation in a high-power polarization-maintaining fiber amplifier seeded by a passively mode-locked VECSEL," *ECOC 2006* Cannes 24-28 Sep 2006 We2.3.3.

2. **P. Dupriez**, A. Malinowski, J. K. Sahu, Y. Jeong, J. Nilsson, D. J. Richardson, H.D.Foreman, K.G.Wilcox, A.C.Tropper, F.Morier-Genoud, U.Keller, and J.S.Roberts "High-power single-mode picosecond fiber laser based on amplification of a passively mode-locked 1055-nm VECSEL", *CLEO/QELS 2006* Long Beach, California 21-26 May 2006 CThJ3.

3. **P. Dupriez**, J. K. Sahu, A. Malinowski, Y. Jeong, D. J. Richardson, and J. Nilsson, "80 W green laser based on a frequency-doubled picosecond single-mode linearly-polarized fiber laser", *CLEO/QELS 2006* Long Beach, California 21-26 May 2006 CThJ1.

4. **P. Dupriez**, C. Farrell, M. Ibsen, J. K. Sahu, J. Kim, C. Codemard, Y. Jeong, D. J. Richardson, and J. Nilsson , "1W average power at 589 nm from a frequency doubled pulsed Raman fiber MOPA system", *Photonics West 2006* San Jose, CA 21-16 Jan 2006.

5. **P.Dupriez**, C.Finot, A.Malinowski, J.Nilsson, D.J.Richardson, K.Wilcox, H.Foreman, A.C.Tropper,"Generation d'impulsions ultrabreves de haute puissance et a haut taux de repetition paramplification fibree en regime auto-similaire ou d'auto-modulation de phase,"*25th National Conference on Guided Optics (JNOG)* Metz 7-9 Nov 2006.

6. **P. Dupriez**, A. Piper, C. Farrell, A. Malinowski, J. K. Sahu, Y. Jeong, B.C.Thomsen, J. Nilsson, D. J. Richardson, L.M.B.Hickey, M.N.Zervas, "High average power picosecond pulses from a fiber amplified diode laser at 1060nm", *CLEO/Europe-EQEC 2005* Munich 12-17 Jun 2005 CJ3-1-MON.

7. **P. Dupriez**, A. Piper, A. Malinowski, J. K. Sahu, M. Ibsen, Y. Jeong, L.M.B.Hickey, M.N.Zervas, J. Nilsson, and D. J. Richardson, "321 W average power 1 GHz 20 ps 1060nm pulsed fiber MOPA source", *OFC 2005* Anaheim 6-11 Mar 2005 (Postdeadline).

8. P. Horak, **P. Dupriez**, F. Poletti, M. N. Petrovich, Y. Jeong, J. Nilsson, D. J. Richardson, and D. N. Payne "RGB generation in secondary cores of microstructured fibres," CLEO Europe, Munich 2007 (accepted).

9. J. Kim, **P. Dupriez**, D. B. S. Soh, C. Codemard, S.Yoo, Y. Jeong, and J. Nilsson, and J. K. Sahu, "Depressed clad hollow optical fiber with the fundamental LP_{01} mode cut-off", *Photonics West 2006* San Jose 21-26 Jan 2006 6102-16.

10. C. A. Codemard, **P. Dupriez**, Y. Jeong, J. K. Sahu, M. Ibsen, and J. Nilsson, "High power cladding-pumped Raman fiber laser with true single-mode output at 1660 nm", *OFC 2006* Anaheim 5-10 Mar 2006 OThJ2.

11. H. D. Foreman, K. G. Wilcox, A. C. Tropper, **P. Dupriez**, A. Malinowski, J. K. Sahu, J. Nilsson, D. J. Richardson, F. Morier-Genoud, U. Keller, and J. S. Roberts, "High power femtosecond source based on passively mode-locked 1055-nm VECSEL and Yb-fibre power amplifier", *ASSP 2006* Nevada 29 Jan - 1 Feb 2006.

12. J. K. Sahu, **P. Dupriez**, J. Kim, C. Codemard, J. Nilsson, and D. N. Payne, "Suppression of stimulated Raman scattering in a high-peak-power pulsed 1060 nm fiber MOPA source with purely single-mode output using W-type fiber", *OFC 2006* Anaheim 5-10 Mar 2006 OWD5.

13. C.Finot, **P.Dupriez**, L.Provost, F.Parmigiani, P.Petropoulos, D.J.Richardson, C.Billet, J.Dudley, S.Pitois, G.Millot, "Impulsions paraboliques et similaritons dans les fibres optiques (Parabolic pulses and similaritons in optical fibres)" *PAMO 2006 - Atomic & Molecular Physics Optics* Dijon 5-7 Jul 2006.

14. A.Malinowski, J.H.V.Price, F.He, **P.Dupriez**, H.D. Foreman, A.C.Tropper, J.Nilsson, "Pulsed high power fiber laser systems," *IEEE/LEOS Summer Topical Meeting 2006* Quebec City 17-19 Jul 2006 MC2.2 (Invited).

15. Y.Jeong, J.Nilsson, **P.Dupriez**, C.Codemard, C.Farrell, J.K.Sahu, J.Kim, S.Yoo, D.J.Richardson, D.N.Payne, "High-power master-oscillator power amplifiers based on rare-earth-doped fibres", *Photonics North 2006* Quebec City 5-8 Jun 2006 (Invited).

16. Y. Jeong, J. Nilsson, D. B. S. Soh, C. A. Codemard, **P. Dupriez**, C. Farrell, J. K. Sahu, J. Kim, S.Yoo, D. J. Richardson, and D. N. Payne, "High power single-frequency Yb doped fiber amplifiers", *OFC 2006* Anaheim 5-10 Mar 2006 OThJ7 (Invited).

17. J. Nilsson, Y. Jeong, D. B. S. Soh, C. A. Codemard, **P. Dupriez**, C.Farell, J. K. Sahu, J. Kim, S.Yoo, and D. N. Payne, "High-power fiber lasers: progress and opportunities", *Proc. 14th International Laser Physics Workshop 2005 (LPHYS 2005)* Kyoto 4-8 Jul 2005 PS5 (Plenary).

18. C. Codemard, C. Farrell, **P. Dupriez**, V.Philippov, J. K. Sahu, and J. Nilsson, "Milijoule high-peak power narrow-linewidth sub-hundred nanosecond pulsed fibre MOPA at 1.55 microns", *ONERA Scientific Day* Paris 27-28 Jun 2005.

19. D. B. S. Soh, A.B.Grudinin, J. Nilsson, Y. Jeong, S.Yoo, J. Kim, C. Codemard, and **P. Dupriez**, "Stimulated Raman scattering effect on femtosecond pulse generation using a parabolic amplification and a pulse compressor", *ONERA Scientific Day* Paris 27-28 Jun 2005.

20. Y. Jeong, J. Nilsson, J. K. Sahu, **P. Dupriez**, C. A. Codemard, D. B. S. Soh, C. Farrell, J. Kim, D. J. Richardson, and D. N. Payne, "High power fiber lasers", *CLEO/IQEC-Pacific Rim* Tokyo 11-15 Jul 2005 CWI4-1-INV (Invited).

21. A. Piper, **P. Dupriez**, M. Ibsen, A. Malinowski, J. H. V. Price, D. J. Richardson L. M. B. Hickey, and M. N. Zervas, "A compact 1 GHz, 16 ps pulse source operating at 1060 nm incorporating a high power gain-switched semiconductor laser and fiber grating pulse compressor", *CLEO/Europe-EQEC 2005* Munich 12-17 Jun 2005.

22. Y. Jeong, J. Nilsson, J. K. Sahu, D. B. S. Soh, **P. Dupriez**, C. A. Codemard, C. Farrell, J. Kim, D. J. Richardson, and D. N. Payne, "Beyond 1 kW, the rising power of fibre lasers", *OECC* Seoul 4-8 Jul 2005 8D1-1 (Invited).

23. Y. Jeong, D. B. S. Soh, C. A. Codemard, **P. Dupriez**, C. Farrell, V.Philippov, J. K. Sahu, D. J. Richardson, J. Nilsson, and D. N. Payne, "State of the art of cw fibre lasers", *CLEO/Europe* Munich 12-17 Jun 2005 TFII1-1-WED (Invited).

24. J. K. Sahu, **P. Dupriez**, J. Kim, A. J. Boyland, C. A. Codemard, J. Nilsson, and D. N. Payne, "New Yb:Hf-doped silica fiber for high-power fiber lasers",*CLEO/QELS* Baltimore 22-27 May 2005 CTuK1.

25. J. Nilsson, J. K. Sahu, Y. Jeong, V. Philippov, D. B. S. Soh, C. Codemard, **P. Dupriez**, J. Kim, D. J. Richardson, A. Malinowski, A.N.Piper, J.H.V.Price, K.Furusawa, W.A.Clarkson, D. N. Payne, "High power fiber lasers", *OFC 2005* Anaheim 6-11 Mar 2005 OTuF1 (Invited).

26. C. Codemard, C. Farrell, V. Philippov, **P. Dupriez**, J. K. Sahu, J. Nilsson, "1 mJ narrow-linewidth pulsed fiber MOPA source at 1535 nm", *CLEO/Europe* Munich 12-17 Jun 2005.

27. J. Kim, **P. Dupriez**, D. B. S. Soh, J. K. Sahu, J. Nilsson, and D. N. Payne, "Nd:Al-doped depressed clad hollow fiber laser at 930 nm", *ASSP 2005* Vienna 6-9 Feb 2005.

28. J. H. V. Price, A. Malinowski, A. Piper, F. He, W. Belardi, T. M. Monro, M. Ibsen, B. C. Thomsen, Y. Jeong, C. Codemard, M. A. F. Roelens, **P. Dupriez**, J. K. Sahu, J. Nilsson, D. J. Richardson , "Advances in high power short pulse fiber laser systems and technology", *Photonics West 2005* San Jose 22-27 Jan 2005 5709-30 (Invited).

29. Y. Jeong, **P. Dupriez**, J. K. Sahu, J. Nilsson, D. Y. Shen, W. A. Clarkson, S. D. Jackson , "Thulium-ytterbium co-doped fiber laser with 75W of output power at 2 microns", *SPIE European Symposium on Optics and Photonics for Defence & Security* London 25-28 Oct 2004 Paper 5620-4.

30. Y. Jeong, J. Nilsson, J. K. Sahu, D. B. S. Soh, C. Alegria, **P. Dupriez**, C. A. Codemard, D. N. Payne, R. Horley, L. M. B. Hickey, L. Wanzcyk, C. E. Chryssou, J. Alvarez-Chavez, P. W. Turner, "Single-frequency polarized ytterbium-doped fiber MOPA source with 264W output power", *CLEO/IQEC 2004* San Francisco 16-21 May 2004 CPDD1 (Postdeadline).

31. Y. Jeong, **P. Dupriez**, J. K. Sahu, J. Nilsson, D. Y. Shen, W. A. Clarkson, S. D. Jackson , "Thulium-ytterbium co-doped fiber laser with 32W of output power in the 2 micron wavelength range", *EPS-QEOD Europhoton* Lausanne 29 Aug - 3 Sep 2004 TuB3.

32. J. K. Sahu, V. Philippov, J. Kim, C. Codemard, **P. Dupriez**, J. Nilsson, A. Abdolvand, N. V. Kuleshov, "Passively Q-switched thulium-doped silica fiber laser", *CLEO/IQEC 2004* San Francisco 16-21 May 2004 CThGG.

33. D. B. S. Soh, S. W. Yoo, J. Nilsson, J. K. Sahu, S. Baek, Y. Jeong, L. J. Cooper, C. Codemard, **P. Dupriez**, C. Alegria, V. Philippov, and K. Oh, "Cladding pumped Nd-doped fiber laser tunable from 908 to 938 nm", *CLEO/IQEC 2004* San Francisco 16-21 May 2004 CMK.

34. B. C. Thomsen, Y. Jeong, C. Codemard, M. A. F. Roelens, **P. Dupriez**, J. K. Sahu, J. Nilsson, and D. J. Richardson , "60W 10GHz 4.5ps pulse source at 1.5 microns", *CLEO/IQEC 2004* San Francisco 16-21 May 2004 CMAA.

Invited conferences:

1. **P. Dupriez**, J. K. Sahu, Y. Jeong, A. Malinowski, D. J. Richardson, and J. Nilsson, "High-power, high-brightness green laser based on a frequency doubled picosecond fiber laser", *Photonics West*, San Jose, USA, 2007.

2. **P. Dupriez**, J. Nilsson, Y. Jeong, J. K. Sahu, C. Codemard, D. B. S. Soh, C. Farrell, J. Kim, A. Piper, A. Malinowski, and D. J. Richardson, "Current progress in high-power fiber lasers and amplifiers", *Optical Amplifiers and their Applications (OAA),* Budapest 7-10 Aug 2005.

Journal Publications:

1. **P. Dupriez**, F. Poletti, P. Horak, M. N. Petrovich, Y. Jeong, J. Nilsson, D. J. Richardson, and D. N. Payne, " Efficient white light generation in secondary cores of holey fibers," Opt. Express **15**, 3729-3736 (2007).

2. **P. Dupriez**, C. Finot, A. Malinowski, J. K. Sahu, J. Nilsson, D. J. Richardson, K. G. Wilcox, H. D. Foreman, and A. C. Tropper, "High-power, high repetition rate picosecond and femtosecond sources based on Yb-doped fiber amplification of VECSELs," Opt. Express **14**, 9611-9616 (2006).

3. **P. Dupriez**, A. Piper, A. Malinowski, J. K. Sahu, M. Ibsen, Y. Jeong, L. M. B. Hickey, M. N. Zervas, J. Nilsson, and D. J. Richardson, "High average power high repetition rate picosecond pulsed fiber master oscillator power amplifier source seeded by a gain-switched laser diode at 1060nm," IEEE Photon. Technol. Lett. **18**, 1013-1015 (2006).

4. J. Kim, **P. Dupriez**, D. B. S. Soh, J. Nilsson, and J. K. Sahu, "Core area scaling of Nd:Al-doped silica depressed clad hollow optical fiber and Q-switched laser operation at 0.9 μm," Opt. Lett. **31**, 2833-2835 (2006).

5. C. A. Codemard, **P. Dupriez**, Y. Jeong, J. K. Sahu, M. Ibsen, J. Nilsson, "A High-Power Continuous-Wave Cladding-pumped Raman Fibre Laser", Optics Letters 31(15), 2290-2292 (2006).

6. J. Kim, **P. Dupriez**, C. Codemard, J. Nilsson, and J. K. Sahu, "Suppression of stimulated Raman scattering in a high power Yb-doped fiber amplifier using a W-type core with fundamental mode cut-off", Optics Express **14**, 5103-5113 (2006).

7. Y. Jeong, **P. Dupriez**, J. K. Sahu, J. Nilsson, D. Y. Shen, W. A. Clarkson, S. D. Jackson, "Power-scaling of a 2 micron ytterbium-sensitized thulium-doped silica fibre laser diode-pumped at 975nm", *Electronics Letters* **41,** 173-174 (2005).

8. Y. Jeong, J. Nilsson, J. K. Sahu, D. B. S. Soh, **P. Dupriez**, C. A. Codemard, S. Baek, D. N. Payne, R. Horley, J. A. Alvarez-Chavez, P. W. Turner, "Single-mode plane-polarized ytterbium-doped large-core fiber laser with 633 W continuous-wave output power", *Optics Letters* **30**, 955-957 (2005).

9. Y. Jeong, J. Nilsson, J. K. Sahu, D. B. S. Soh, C.Alegria, **P. Dupriez**, C. A. Codemard, D. N. Payne, R. Horley, L. M. B. Hickey, L. Wanzcyk, J. Chryssou, J. A. Alvarez-Chavez, P. W. Turner, "Single-frequency single-mode plane-polarized ytterbium-doped fiber master-oscillator power amplifier source with 264W output power", *Optics Letters* **30**, 459-461 (2005).

10. D. B. S. Soh, S.Yoo, J. Nilsson, J. K. Sahu, K. Oh, S. Baek, Y. Jeong, C. A. Codemard, **P. Dupriez**, J. Kim, and V. Philippov, "Neodymium-doped cladding pumped aluminosilicate fiber laser tunable in the 0.9 micron wavelength range", *IEEE Journal of Quantum Electronics* **40**, 1275-1282 (2004).

11. C.Codemard, C.Farrell, **P.Dupriez**, V.Philippov, J.K.Sahu, J.Nilsson, "Millijoule high-peak power narrow-linewidth sub-hundred nanosecond pulsed fibre master-oscillator power-amplifier at 1.55 microns," *C.R. Physique* 7, 170-176 (2006).